Design and Implementation of a Low-Cost FMCW Imaging Radar

Prepared by:
Ivan Tchekashkin
TCHIVA001

Supervised by:
Prof. Michael Inggs
Department of Electrical Engineering
University of Cape Town

April 2015

A dissertation submitted to the Department of Electrical Engineering,
University of Cape Town,
in partial fulfilment of the requirements for the degree of
Master of Science in Engineering

Declaration

1. I know the meaning of plagiarism and declare that all the work in the document, save for that which is properly acknowledged, is my own.
2. I have used the IEEE convention for citation and referencing. Each contribution to, and quotation in, this project report from the work(s) of other people, has been attributed and has been cited and referenced.
3. I have not allowed, and will not allow, anyone to copy my work with the intention of passing it off as their own work or part thereof.

Student Name: Ivan Tchekashkin

Signature: ____________________________ **Date:**

Acknowledgements

I would like to thank Professor Michael Inggs and Alan Langman for their guidance, advice and tolerance during the course of this project. It was a very valuable experience. I am also thankful for the financial assistance that was made possible to me through their help.

In addition to this I would like to thank Rodolfo Lima, Justin Coetser, Craig Tong, Samuel Ginsberg, Adrian Stevens, Stephen Paine and Sergey Petrov for their help that brought me closer to finishing this project.

Most importantly, none of this would be possible without the help and support of my parents, they have supported me through all my years of studies and I am very thankful for what I could achieve with their help.

Abstract

Imaging radar systems have been predominantly developed using a coherent pulse radar approach, which is typically associated with expensive and complex hardware that usually requires a large amount of space. Hence, the use of such sensors is reserved to large organizations that can afford to purchase or develop them. This is unfortunate as there are numerous uses for imaging radar sensors in both military and civilian sectors. One of such uses lies in the agricultural sector and entails using imaging radar data to monitor crop development. As a result, a project was initiated at the University of Cape Town (UCT), in collaboration with droneSAR company, which aimed to develop a low-cost, compact, imaging radar that could be mounted on a small Unmanned Aerial Vehicle (UAV). The purpose of this research project is aimed at developing the first system prototype.

The RadioCamera-S is the S-band FMCW radar, that was developed to test the architecture that could be utilised to enable the filtering of the feed-through and nadir components, which are typically the strongest returns in the spectrum. The prototype has two modes of operation that are aimed at shifting the unwanted signals outside of the pass band of the receiver. This is achieved by generating two identical L-FMCW waveforms that are offset by a chosen time period. This enables a shift of the spectrum by the frequency, which corresponds to the time offset.

The capabilities of the proposed hardware were examined and the specifications for the ground based version were developed. The parameters that influence the waveform design were discussed and the optimal values were chosen for the ground based radar system. Verification of the transmitter and receiver operation was carried out, which was followed by system tests that demonstrated that the feed-through signal could be attenuated by employing the first proposed mode of operation. RTI plots were generated and showed that the radar was capable of detecting the movement of a reflector in the observable scene.

Contents

List of Figures

List of Tables

List of Acronyms

ERS-1	European Research Satellite-1
UCT	University of Cape Town
UAV	Unmanned Aerial Vehicle
FMCW	Frequency Modulated Continuous Wave
IF	Intermediate Frequency
SMA	SubMiniature version A
BYU	Brigham Young University
MIT	Massachusetts Institute of Technology
IAP	Independent Activity Period
PRF	Pulse Repetition Frequency
SAR	Synthetic Aperture Radar
PRI	Pulse Repetition Interval
RF	Radio Frequency
PSU	Power Supply Unit
DAC	Digital-to-analog Converter
VCO	Voltage Controlled Oscillator
LNA	Low Noise Amplifier
NF	Noise Figure
LO	Local Oscillator
SPI	Serial Peripheral Interface
DDS	Direct Digital Synthesizer
ADC	Analog-to-digital Converter
STALO	Stable Local Oscillator
FPGA	Field-Programmable Gate Array
TCXO	Temperature Compensated Crystal Oscillator
RCS	Radar Cross Section
PLL	Phase Lock Loop
DVGA	Digitally Controlled Variable Gain Amplifier
DC	Direct Current
LVCMOS	Low Voltage Complementary Metal Oxide Semiconductor
M-LVDS	Multipoint Low Voltage Differential Signalling
LPF	Low Pass Filter
HPF	High Pass Filter

MXR	Mixer
PCB	Printed Circuit Board
BW	Bandwidth
MDS	Minimum Detectable Signal
SNR	Signal to Noise Ratio
CAD	Computer Aided Design
DUT	Device Under Test
RTI	Range Time Intensity
DCR	Direct Conversion Receiver
RAR	Real Aperture Radar

List of Symbols

h	Distance from the radar platform to the ground
ΔY	Swath width
R_{offset}	Distance from the nadir of the radar to the start of the swath
δy	Ground range resolution
δr	Resolution of radar in slant range
r	Range from radar to target of interest
t_{delay}	Time delay between the transmitted and received signals
c	Electromagnetic wave propagation in free space
f_b	Beat Frequency, consists of two frequency components f_{b1} and f_{b2}
Δf	Signal bandwidth
Δf_{az}	Azimuth bandwidth
θ_{az}	3-dB Azimuth beamwidth
v	Platform velocity
λ	Signal wavelength
D_{az}	Antenna Length in azimuth
D_{el}	Antenna width in elevation
T_{obs}	Time of scene observation during which return echos are collected
δx	Azimuth resolution
θ_{el}	3-dB elevation beamwidth
Δt	Waveform period
f_{offset}	Frequency offset between nadir return and the feed-through component
β	Length of the effective free-space path that the feed-through signal takes
R_s	Slant range to target
R_{s_near}	Slant range to the nearest point in the swath
R_{s_far}	Slant range to the furthest point in the swath
R_{ground}	Distance from nadir to the point of interest
S_{t1}	Waveform that is produced by the signal generator S1
S_{t2}	Waveform that is produced by the signal generator S2
t_{offset}	Time delay between waveform S_{t1} and S_{t2}
f_c	Carrier frequency
μ	Chirp rate $\frac{\Delta f}{\Delta t}$
S_{ref}	Product of mixing S_{t1} with S_{t2}
$f_{S_{ref}}$	Frequency of the S_{ref} signal
S_{rx}	Signal received by the Receivers' antenna
$\phi(t)$	Phase of the signal

S_{main}	Product of mixing the received signal with S_{t2}
$f_{S_{main}}$	Frequency of the S_{main}
RF_{out}	Output of the VCO RF port
P_{in}^{sat}	Input power to a device that results in saturation
P_{1dB}	1 dB compression point
G_{amp}	Gain of the amplifier
P_r	Reflected power
P_t	Percentage of transmitted power
k	Boltzmann's constant (1.38×10^{-23} joules/Kelvin
T_0	Standard temperature (290°)
R_u	Maximum unambiguous range of the radar

Chapter 1

Introduction

Imaging radar systems have been predominantly developed using a coherent pulse radar approach, which is typically associated with expensive and complex hardware that usually requires a large amount of space. Hence, the use of such sensors is reserved to large organizations that can afford to purchase or develop them. This is unfortunate as there are numerous uses for imaging radar sensors in both military and civilian sectors. One of such uses lies in the agricultural sector and entails using imaging radar data to monitor crop development. This was successfully demonstrated by analysing data collected by the ERS-1 satellite [9] [10]. As a result, a project was initiated at the University of Cape Town (UCT), in collaboration with droneSAR company, which aimed to develop a low-cost, compact, imaging radar that could be mounted on a small Unmanned Aerial Vehicle (UAV).

As a first step to constructing such a system, a prototype sensor, RadioCamera-S, was developed. The RadioCamera-S utilises available off-the-shelf components in order to keep the costs low. It implements a Frequency Modulated Continuous Wave (FMCW) radar architecture, as it allows a modest amount of power to be used for transmission, which decreases the hardware complexity, lowers the cost and decreases the size of the radar.

Initially it was proposed that the RadioCamera sensor should be a C-band radar in order to match the frequency band that the ERS-1 satellite operated in. However, for the purpose of exploring the architecture that was proposed for the system, a prototype operating in the S-band was developed. This approach was employed, as the components that operate in the S-band region were readily available in packages that had SubMiniature version A (SMA) connectors, thus reducing the assembly time and enabling easy debugging of the final system. A number of similar FMCW imaging radars have already been developed in academic institutions, with some of the systems becoming available commercially.

1.1 Research Motivation

It has been shown that the use of FMCW radar systems for the purpose of imaging is possible and could be done at a fraction of the cost of the pulsed radar systems [1] [11]. Furthermore, it was demonstrated that those sensors could be made compact [3] [4]. However, compact FMCW imaging sensors that are currently available remain relatively expensive and unattainable to the majority of individuals and private entities. Therefore, a niche still exists in the field of low-cost FMCW imaging sensors and due to the current developments in technology it is believed that an FMCW imaging sensor can be made at a low-cost, while still producing high resolution imaging data.

1.2 Research Objectives

The main objective of this research project was based on the development and testing of a prototype FMCW radar using inexpensive, off-the-shelf components. The specification for the radar prototype wasn't well defined at the start of the project, but the following parameters were set as a guideline:

- S-Band operation
- Incorporate the LMX2492, 500 MHz to 14 GHz Low Noise Fractional Phase-locked Loop for ramp/chirp generation
- Utilise the LMH6521 IF amplifier in the receiver
- Employ the Red Pitaya open source platform to acquire data
- Implement a low-cost solution for antenna design

Furthermore, the system parameters had to be chosen in accordance with a predefined operational geometry, as shown in Figure 1.1. The altitude of a small-scale airborne platform (h), was set to be 500 metres, with a propagation velocity of 30 m/s. In this scenario the radar is set to point perpendicularly to the direction of propagation of the platform, which in the case of the figure provided is into the page. The antenna beam is pointed towards the ground, with the requirement that a swath width (ΔY) of a 1000 metres is illuminated and offset (R_{offset}) from nadir by 500 metres. The ground range resolution (δy) is required to be approximately 1 metre mid-swath.

The second objective of this research project is to provide a solution for filtering the feed-through and the nadir return signals. The two signals form a part of the received signal spectrum, which is produced when the received signal is mixed with a portion of the transmitted signal (See Appendix A). As Figure 1.2 shows, these unwanted signals arise from the geometry associated with an imaging radar system

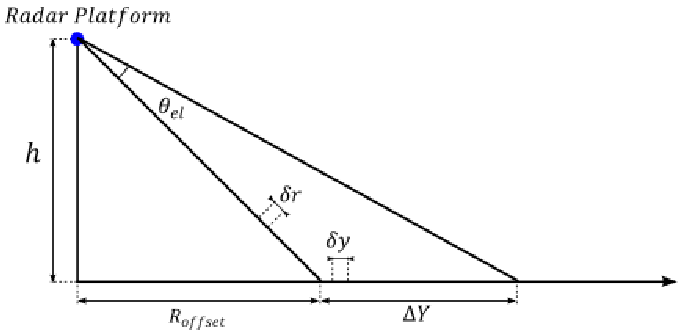

Figure 1.1: Operational geometry of the final system

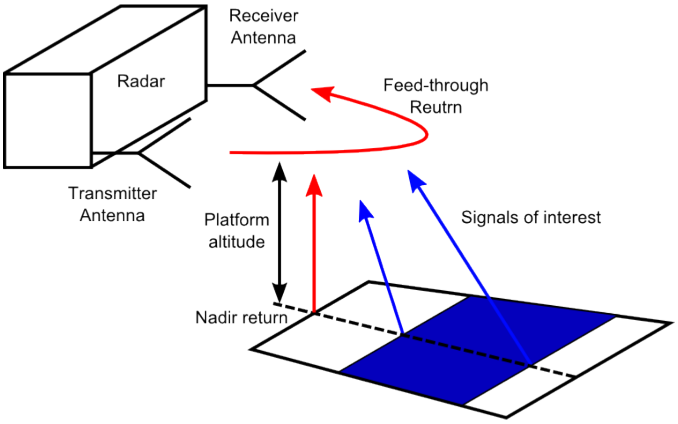

Figure 1.2: Origin of feed-through and nadir signal returns

that utilises dedicated antennas for transmitting and receiving, in conjunction with the fact that the radar is mounted on an airborne platform.

These signals typically have a higher power level than the targets in the range of interest. If they are not filtered, the higher power level associated with their returns places additional requirements on the radar's receiver hardware, as one must increase the dynamic range to accommodate a wider range of power levels. This is shown in Figure 1.3, where the frequency spectrum at the input of the homodyne receiver's signal processor is divided into the unwanted spectrum, marked in red, and the spectrum of interest, marked in blue.

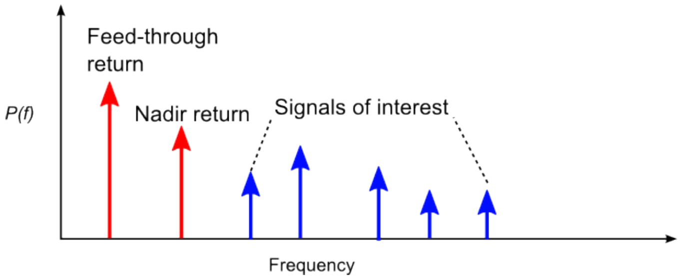

Figure 1.3: Frequency spectrum at the input of the signal processor

1.3 Dissertation Overview

The document begins by presenting an overview of existing FMCW radars which were used for the purpose of synthetic aperture imaging. Four systems were discussed in Chapter 2, in the order in which they were developed starting with the Brigham Young University's (BYU) rail Synthetic Aperture Radar (SAR) and μSAR systems, which are followed by the Artemis MicroASAR and the Massachusetts Institute of Technology (MIT) Independent Activity Period (IAP) Radar course test system.

Despite the fact that all these systems were aimed at producing images based on the SAR principle, the objectives of each one differ. The BYU rail SAR, as discussed in Section 2.1, was developed for the purpose of proving that a radar that utilises an FMCW architecture can indeed be used for the purpose of imaging. This resulted in a system, which was not compact, as it was made to fit a box 430 × 480 × 180 mm in size, however, it did demonstrate that the theoretical range resolution of 0.75 m and the azimuth resolution of 0.1 m, were achievable. It operated in the X-band and successfully utilised a feed-back system to account for the non-linearities in the transmitted signal, which allowed a SAR image to be produced and successfully correlated with an optical image of the test scene.

Then, due to the simplicity of the FMCW architecture and the advances in technology, a smaller version of an imaging radar was made possible. This was realized in the BYU μSAR, which is presented in Section 2.2, while still implementing the same homodyne architecture as in the rail SAR, it was reduced in size to 76.2 × 86.4 × 101.6 mm. Furthermore, it was designed to operate in the C-band, in a continuously recording mode for the entire duration of the flight and could have the Pulse Repetition Frequency (PRF) varied in accordance with the altitude at which the platform was flying. The reduction in size did result in the decrease in range resolution to 1.85 m and a decrease in azimuth resolution to 1.85 m, due to the fact that the storage rate and storage space were limited, which resulted in the necessity to pre-sum the slow-time data.

Whereas the two previous systems were developed by the students at BYU alone, the MicroASAR was developed in collaboration with Artemis and resulted in a system that operated in the C-band, like the μSAR, but had a modified front-end architecture for the purpose of filtering the feed-through signal component from the receiver frequency spectrum. This was implemented using a Surface Acoustic Wave (SAW) bandpass filter and variable PRF which allowed the feed-through component to be shifted to the first null of the filter. In addition, the transmitted signal power was increased in order to increase the operational range of the radar and the signal bandwidth was made variable, which allowed one to vary the range resolution from 1.875 to 0.937 m. The review of MicroASAR can be found in Section 2.3.

The last system of interest was the MIT IAP Radar System which is presented in Section 2.4. The main emphasis of it was placed on its low-cost and ease of assembly aspects. Hence, the MIT IAP Radar System most closely resembled BYU's rail

SAR. It operated in the S-band and consisted of six coaxial microwave parts in the front-end and two metallic cans for the transmitter and receiver antennas. The receiver utilised a homodyne architecture, similar to the rail SAR and the μSAR, with the output of the receiver digitised by a computer sound card, which placed a limit on the beat frequency signal spectrum, which in turn resulted in limiting the range of the radar to 272 m (in accordance with the operational parameters chosen for the practical tests). This system provided a simple framework for a FMCW radar that could be used for Doppler and FMCW ranging, as well as for crude SAR imaging.

Chapter 3 presents the design considerations that had to be accounted for in order to satisfy the limitations of the user required hardware. Some of the more notable constraints are imposed by the LMX2492EVM waveform generator, as it determines the bandwidth of the signal, as well as the minimum and maximum PRI rates, and the Red Pitaya, which was used to digitise the data.

Then the geometry constraints are outlined in Section 3.2. The airborne geometry constraints are explained, with reference to the signal bandwidth requirements, PRI and the antenna elevation beamwidth. Transmitted waveform parameters are then proposed for the use in such an operating geometry. This is followed by a brief description of the ground based radar parameter requirements.

The two-channel filtering method is expanded on in Section 3.3, where two modes of operation are presented and explained graphically. A model is then derived for one of the modes of operation. This is followed by a derivation of a system specification for a RadioCamera-S radar system.

Once the limitations and architecture overview is provided, a look at the hardware implementation is given in Chapter 4. The system was divided into three modules, namely: the transmitter, antenna and the receiver. Each module is examined in a separate section.

The transmitter module is discussed from the point of its two main functionalities, which are to generate a waveform and amplify the modulated waveform to a desired level. The antenna module presents the design procedure that was followed to implement circular waveguide antenna designs, with the return loss and isolation plots demonstrated to verify the produced antennas.

The receiver module is described from the point of view of two channels. The main channel is analysed in more detail, as the input saturation power, the noise figure as well as the receiver sensitivity parameters are derived. Then a brief overview of the housing that is used to hold the three modules together is given. Chapter 5 focuses on the testing procedures, results and discussion of results for the RadioCamera-S radar. First the transmitter module was tested by referring to the waveform generation and the properties of the generated waveforms that allow one to determine if the synthesiser is indeed producing a correct waveform. Then the power level of the two transmitter and the two receiver channels were displayed.

After the two modules were tested separately the system tests were carried out.

First, a delay-line testing procedure demonstrates the frequency components that are produced when two waveforms with a PRI of 2 μs are offset from one another and how the Red Pitaya can be used to sample a particular region. Then the system is completely assembled and tested in a known environment in order to be able to correlate the acquired data with the actual distances to targets.

After a number of tests that examine a single signal return are carried out, a Range-Time-Intensity plot is generated that demonstrates the movement of a single reflector in the scene of interest.

Mode One filtering technique was used successfully to demonstrate the attenuation of the feed-through signal by utilising the properties of the video amplifiers gain response.

Chapter 6 is the last chapter of the dissertation, which draws conclusions by providing a cross examination of the requirements that were set out at the start of the research project with the results that were obtained through theoretical analysis and testing. This is demonstrated in Section 6.1, Section 6.2 is focused on the recommendations for future work that can be carried out on the RadioCamera-S prototype, as well as the future RadioCamera revisions.

There are two Appendices, Appendix A introduces the reader to the architecture of a basic FMCW radar setup and gives a brief outline of the imaging radar operation. This is followed by Appendix B, which aims to provide an overview of the design considerations that one needs to account for when designing an FMCW radar.

Chapter 2

Overview of Existing FMCW Imaging Radar Systems

During the last 14 years, the use of FMCW radar architecture for the purpose of imaging has received close attention in academic circles. A number of research projects showed promising results and in some cases lead to the development of commercial imaging radar systems. This chapter aims to summarise the specifications, design decisions and the performance of a number of those systems starting with the Brigham Young University's (BYU) rail Synthetic Aperture Radar (SAR) and µSAR, in Sections 2.1 and 2.2, respectively. The commercial system that was the successor to the first two BYU systems, the Artemis MicroASAR is discussed in Section 2.3, with the MIT IAP radar course test system examined last in Section 2.4. The chapter ends with a short summary in Section 2.5

2.1 BYU rail SAR

In 2002 a radar rail system was developed by Ryan L.Smith at the Brigham Young University, with the purpose of demonstrating that a radar that utilizes an FMCW architecture, can be used for the purpose of synthetic aperture imaging [1]. The dimensions of the system were tailored to the size of YINSAR, which was a pulsed airborne SAR system developed at BYU and was made to fit a rack-mountable box of 430×480×180 mm in size [12].

2.1.1 Specifications

The specifications of the radar are provided in Table 2.1. The operation frequency range is found in the X-band region and centred on 9.8 GHz, with a bandwidth of 200 MHz. The bandwidth of the transmitted signal as shown in [13] and [6] determines the range resolution of the radar, in accordance with Equation 2.1,

$$\delta r = \frac{c}{2\Delta f}, \qquad (2.1)$$

where Δf is the bandwidth and c is the speed of electromagnetic propagation in freespace. Hence, the maximum range resolution of this system is 0.75 m. As the platform operates at 0 m elevation this corresponds with the effective ground range resolution and no further correction needs to be made.

Table 2.1: BYU rail SAR Specifications

Radar Parameters	
Frequency Band	X-Band
Tx Centre Frequency	9.8 GHz
Tx Power	16 dBm
Chirp Period	1 ms (500 μs for bench tests)
Minimum PRF	700 Hz (2.93 Hz for bench tests)
Bandwidth	200 MHz
Dimensions	430×480×180 mm
Receiver Noise Figure	4 dB
Chirp Generation	VCO
Modulation	Saw-tooth
Antenna Parameters	
Antenna Type	Slotted Waveguide
3-dB Beamwidth	10° azimuth × 45° elevation
Antenna Gain	17 dB
Center Frequency	9.9 GHz
Operating Specifications	
Range Resolution	0.75 m
Theoretical Azimuth Resolution	0.1 m
Platform Velocity	0.327 m/s
Nominal Platform Elevation	0 m

In order for the calculated range resolution to be achieved, one must ensure that the two-way propagation delay that is associated with an illuminated target at a particular range is much smaller than the chirp period (PRI) of the radar. This is shown in [14] and can be expressed as:

$$t_{delay} = \frac{2 \times r}{c} \ll PRI, \qquad (2.2)$$

where t_{delay} is the two-way propagation delay and r is the distance to target. Therefore, with the rail SAR PRI of 500 μs, the two-way propagation delay that will result in a 80 percent overlap of the transmitted waveform with the received waveform is 100 μs. This corresponds to a range of 15 km. However, the true range of the radar will also be limited by the power of the transmitted signal and additional parameters that can be seen in the Radar Range Equation for a FMCW SAR system as derived in [5].

The velocity (v) of the rail SAR platform is 0.327 m/s, this parameter, in conjunction with the wavelength (λ) of the transmitted signal and the antenna azimuth beamwidth (θ_{az}), determines the azimuth bandwidth (Δf_{az}) of the system [1] according to:

$$\Delta f_{az} = \frac{2v\theta_{az}}{\lambda}. \tag{2.3}$$

The azimuth bandwidth can then be used to determine the resolution of the radar in the azimuth direction (δx), according to Equation 2.4, which in this case is 0.1 m. This is partially determined by the 10 degree 3-dB bandwidth of the antennas, which were employed. Two antennas were employed, where one was transmitting and the other receiving. This configuration was realised in order to increase the isolation between the transmitter and receiver. The antennas were of slotted waveguide type with a gain of 17 dB.

$$\delta x = \frac{v}{\Delta f_{az}} = \frac{D_{az}}{2} \tag{2.4}$$

Azimuth resolution of the radar is also used to determine the minimum value of the Pulse Repetition Frequency (PRF), as the bandwidth needs to satisfy the Nyquist criterion, hence the minimum PRF of the radar is [1]:

$$PRF_{min} = 2 \times \frac{2v\theta_{az}}{\lambda}. \tag{2.5}$$

In the case where the above criterion is not accounted for and a lower PRF value is utilised, the antenna mainlobe patterns as transmitted from different locations along the propagation trajectory of the radar, may overlap and cause Doppler ambiguity [15], this is explained in more detail in Appendix B.1.1.

2.1.2 Radar Design

The radar front-end of the rail SAR resembles a homodyne (direct conversion) architecture that mixes a replica of the transmitted signal with the received signal directly to baseband. A simplified block diagram can be seen in Figure 2.1(a), which shows that it has two receiver channels. The two channel design adds the ability to carry out interferometry. A photo of the assembled system can be seen in Figure 2.1(b).

During the design phase, the radar system was divided into seven modules, which are the Main Driver/Power Plane module, Radio Frequency (RF) Transmitter, Low

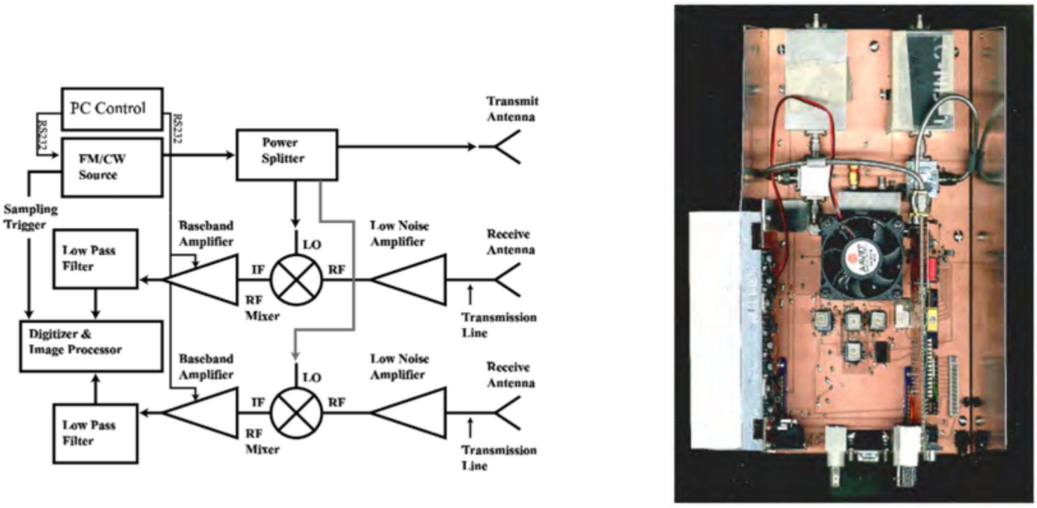

(a) Simplified Block Diagram (b) Assembled System

Figure 2.1: BYU rail SAR System [1]

Noise Amplifier (LNA), RF mixer, Baseband module, Power Supply Unit (PSU) and Digitiser/Image Processor module. The FMCW Source, which is divided between the Driver/Power Plane module and the RF Transmitter module, consists of a PIC16 microcontroller with a 14 bit Digital-to-analogue Converter (DAC), a lowpass filter and a Voltage Controlled Oscillator (VCO).

The microcontroller together with the lowpass filter produces an analogue control signal for the VCO, which outputs a saw-tooth modulated waveform. In order to ensure linearity of the output waveform, a feedback system is implemented that tunes the VCO control signal in order to account for the non-linearities of the VCO (more details on the feedback system can be found in Appendix B.1.2). The linearity of the waveform influences projected range resolution and range ambiguity of the radar, as was shown in [14] and explained in more detail in Appendix B.1.1.

The output of the VCO is fed into a ring coupler, which splits the signal into four, with two ports at 16 dBm and the other two at 26 dBm. One 16 dBm signal is sent directly to the transmitter antenna and the other one is left for testing purposes. The 26 dBm signals are fed to the LO port of the RF mixer.

The LNA module is designed to have a 50 dB Gain and 4 dB Noise Figure (NF). The noise figure of the LNA is required to be low as it is the main component that influences the overall receiver NF. This is explained in more detail in Appendix B.3.1. The module consists of a four stage amplifier, where the first stage is designed for low noise, stage two and three are designed for maximum gain and stage four is designed for maximum gain and maximum output power.

Once the received signal is amplified by the LNA, a HMC220S08 RF mixer is employed for the purpose of de-chirping the received signal in the RF mixer module. The RF and LO ports operating frequency range is 5.9 to 10 GHz, with the output frequency range of DC to 3.5 GHz at the IF port. In order to ensure that the expected performance, as outlined by the documentation, is achieved, the LO port must be driven by a signal with a power level of 10 dBm.

The IF gain module consists of two amplifiers: a 26 dB gain LM7121 video operational amplifier and a variable AD8321 amplifier that has variable gain in range of -28 to 26 dB. The gain of AD8321 amplifier was designed to be set by the PIC16 microcontroller using an SPI interface. The bandwidth of the IF gain stage was 120 MHz, this places a limitation on the beat frequency spectrum that can be analysed and thus on the range of the radar.

Prior to digitisation the output of the gain stage was passed through a lowpass filter. The design of the system allowed the filter to be removed in order to enable the operator to change the cut-off frequency of the spectrum of interest. This allows one to account for the sampling rate of the digitiser without resulting in aliasing.

2.1.3 Performance

The performance analysis of the rail SAR system was initially carried out in the inverse SAR configuration, where a corner reflector was used as a target that was moving with a velocity of 0.327 m/s. The resultant range and azimuth resolution that was obtained corresponded to the theoretically calculated range resolution of 0.75 m and azimuth resolution of 0.1 m.

Then a rail SAR test was carried out, where the sensor was moved along a rail at constant velocity. The collected data was processed to form an image which showed consistency with the optical image of the scene.

2.2 BYU μSAR

BYU μSAR system was developed in 2006 and essentially builds upon the previous system that was designed by R. L. Smith. The radar was designed to fit on a small low-altitude UAV with a wing span of six feet for the purpose of imaging the Arctic sea ice. The use of a FMCW architecture, allowed the costs to be kept low, relative to the costs associated with more traditional pulsed imaging radars[3]. Subsequent sections will cover the specifications of the system, as well as the design aspects of the radar.

2.2.1 Specifications

Table 2.2, shows the specification of the radar system. The frequency band chosen for this design was the C-Band and the center frequency of operation is 5.56 GHz, which falls into the unlicensed Wi-Fi band. The transmitted signal power is 28 dBm, which is higher than the transmitter power of rail SAR (Section 2.1). The increase in transmitted power leads to the increase of the operational range, in accordance with the Radar Range Equation [5].

Table 2.2: BYU μSAR Specifications

Radar Parameters	
Frequency Band	C-Band
Tx Central Frequency	5.56 GHz
Tx Power	28 dBm
PRF	138-2886 Hz (variable)
Bandwidth	80 MHz
Dimensions	76.2 × 86.4 × 101.6 mm
Weight	2 kg
Chirp Generation	DDS
Modulation	Triangular

Antenna Parameters	
Antenna Type	2x8 Patch Array
3-dB Beamwidth	$8.8°$ azimuth $\times 50°$ elevation
Elevation sidelobe level	-17 dB
Azimuth sidelobe level	-18 dB

Operating Specifications	
Range Resolution	1.85 m
Theoretical Azimuth Resolution	0.15 m
Platform Velocity	18-385 m/s (PRF dependent)
Platform Elevation	16-344 m (PRF dependent)
ADC Sampling Rate	328.947 kHz
Data Storage Rate	0.63 MB/s

The PRF value is made variable from 138 to 2886 Hz, which is necessary to allow the system to operate at different heights and speeds [3]. The need to adjust the PRF arises from the relationship that was shown in Equation 2.3, which relates the azimuth bandwidth of the radar to the velocity. As the azimuth bandwidth is related to the minimum PRF by Equation 2.5, one needs to ensure that the PRF value is chosen in accordance to the velocity of the platform, alternatively Doppler ambiguity may occur (a more detailed explanation can be found in Appendix B.1.1).

The bandwidth was chosen to be set at 80 MHz, which leads to a decrease of the range resolution as compared to R.L. Smith's radar and provides the theoretical slant range resolution of 1.875 metres.

The antennas used for this radar are of the patch array type and consist of a 2×8 array. The 3-dB beamwidth is $8.8° \times 50°$, which leads to the maximum theoretical azimuth resolution of 0.15 metres. However, the actual azimuth resolution in the produced images is equal to the range resolution as the data in azimuth is multi-look averaged [3].

2.2.2 Radar Design

The system architecture is divided into five modules, which are the transmitter, receiver, power, digital and the Analogue-to digital converter (ADC).

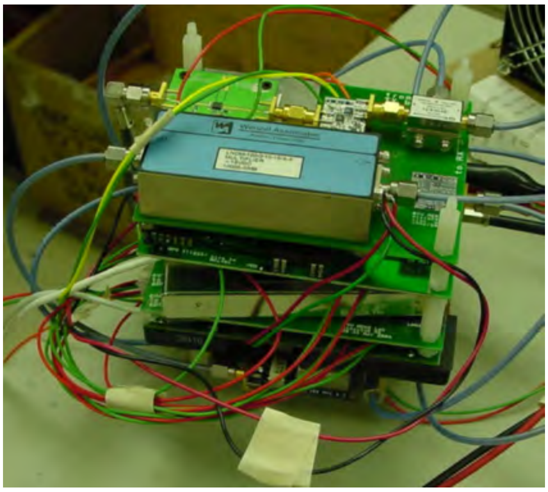

Figure 2.2: Assembled μSAR [2]

Each module is built on a custom microstrip circuit board, which are connected together by wires and coaxial cables. Once completely assembled the system weighs less than 2 kilogramms and occupies a space of 77 ×87 ×102 mm. A photo of the assembled system can be seen in Figure 2.2. μSAR employs a simple homodyne design as the simplified block diagram shows in Figure 2.3. An extra receiver channel can be added if one would like to carry out interferometry.

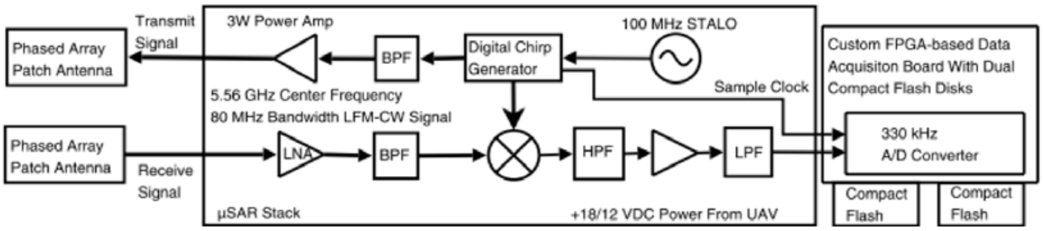

Figure 2.3: BYU μSAR System Block Diagram [3]

The core of the system utilizes a single 100 MHz Stable Local Oscillator (STALO) that is then used to generate the needed frequencies for the system. The chirp waveform is produced by a AD9852 Direct Digital Synthesizer, which is controlled by a microcontroller. The PRF can be set manually using switches. A custom FPGA board is designed to sample the beat frequency signal at a sampling rate of 330 kHz and store the data on two 1 GB flash drives at a rate of 0.63 MB/s. The ADC sampling trigger is not synchronized with the start of the chirp signal for simplification purposes, instead a chirp start detect algorithm is utilised in order to maintain phase continuity and predict azimuth phase.

The system operates on a "turn-on and forget" basis and can record data for approximately half an hour before the flash drives are filled to capacity. μSAR needs a

+12 V or +18 V input from the UAV and utilizes 18 W of power during operation.

2.2.3 Performance

The performance of the radar was tested during a test campaign, which included initial ground testing, where the system was mounted on a side of a car and driven around to record data, as well as further airborne tests, which entailed mounting the radar on a Cessna 185 and flying over the Arctic Ocean. Another test flight was carried out in Provo, Utah region to record images of rural landscapes.

The data which was presented in the available literature did not explicitly state the exact resolution that was achieved by the system. However, the testing campaigns did show that an image of a scene could be reconstructed and the approximate position of the corner reflectors that were set up in the test scene was determined.

The major aspect of the testing campaign for this system was related to evaluating the performance of the chirp start detection, auto-focusing and interference filtering algorithms that are performed after the data was collected, as this dissertation is focused on the development of the hardware for a FMCW radar, the analysis of those algorithms is omitted, but can be found in [2].

2.3 Artemis MicroASAR

Artemis MicroASAR is a successor to the BYU μSAR and was developed in collaboration with Artemis in 2008 [4]. It is more flexible than the previous two systems in that it can vary the signal bandwidth to achieve various range resolutions and can carry out filtering of the feed-through signal by varying the PRF. This filtering technique is of particular interest as the second objective of this dissertation is to carry out filtering of the feed-through and nadir return signals.

2.3.1 Specifications

The specifications of this system are summarised in Table 2.3. MicroASAR is a larger system than the μSAR and requires more power, this is a trade-off that needs to be made as transmission power level is increased to 30 dBm. The transmitted signal is in the C-band region, centred at 5428.76 MHz. The bandwidth of the system can be varied between 80 to 160 MHz, which can provide a maximum range resolution of 0.93 m.

The PRF can be varied between the values of 7 to 14 kHz. This is utilized in order to account for the change in velocity and altitude of the platform, as in the μSAR case. However, the change in PRF is also used to carry out feed-through signal filtering, as will be shown in Section 2.3.3.

Table 2.3: Artemis MicroASAR Specifications

Radar Parameters	
Frequency Band	C-Band
Tx Central Frequency	5.428.76 GHz
Tx Power	30 dBm
PRF	7-14 kHz
Bandwidth	80-160 MHz
Dimensions	221 × 185 × 46 mm
Weight	3.3 kg
Chirp Generation	DDS
Modulation	Saw-tooth

Antenna Parameters	
Antenna Type	2x8 Patch Array
3-dB Beamwidth	8.5° × 50°
Antenna Gain	15.5 dB

Operating Specifications	
Range Resolution	1.25 m (120 MHz bandwidth)
Theoretical Azimuth Resolution	0.15 m
Platform Velocity	10-150 m/s (PRF dependent)
Platform Elevation	100-1500 m (PRF dependent)
Maximum Swath Width	300-2500 m (altitude dependent)
ADC Sampling Rate (Maximum)	500 Mbps
Data Storage Rate	5 MB/s

The antennas that are used are of patch array type and have azimuth 3-dB bandwidth of 8.5 degrees and elevation 3-dB bandwidth of 50 degrees.

The sensor is designed to operate on a small manned or unmanned airborne platform, at the elevation of 100 to 1500 m. The elevation also sets the width of the illuminated swath, which can vary from 300 to 2500 m. Furthermore, the parameters of the system such as PRF are tailored to operate in the velocity range of 10 to 150 m/s, which corresponds with a velocity of a small UAV.

2.3.2 Radar Design

The MicroASAR system is designed to fit into one aluminium enclosure. This enclosure is used in order to minimize spurious emissions, self-interference and interference from outside sources [4]. The complete assembly can be seen in Figure 2.4(a).

The architecture of the MicroASAR differs from the previous two systems and is demonstrated in Figure 2.4(b). The main three processes that take place in the front-end are the upconversion, de-chirping and downconversion, this is in contrast to the more typical homodyne architecture that is encountered in other systems.

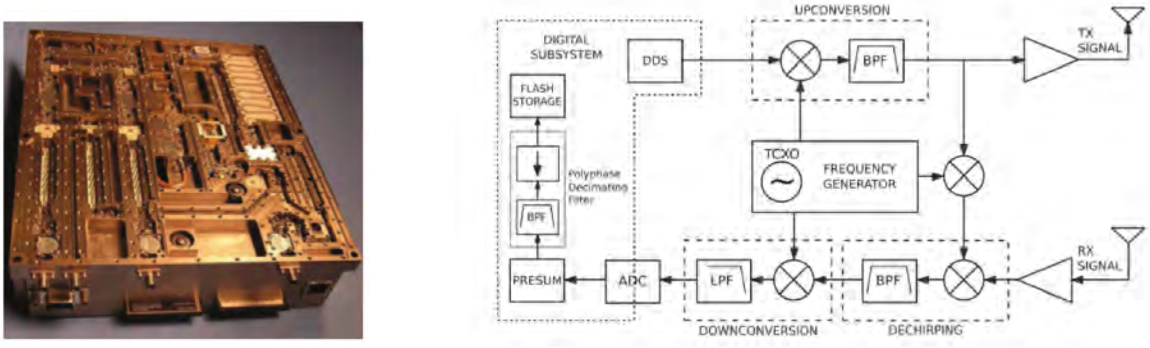

(a) Complete assembly of Artemis microASAR

(b) System block diagram

Figure 2.4: Artemis MicroASAR System [4]

The upconversion process is required as the DDS produces the saw-tooth modulated waveform at baseband and requires it to be stepped up to the carrier frequency, this technique is also used in μSAR. The de-chirping process is carried out in the mixer, where a received signal is mixed with a frequency shifted version of the transmitted signal. The transmitted signal is frequency shifted in order to place the beat frequency spectrum in the bandpass filters pass band, with the feed-through components at the null of the bandpass filter, which is found at 1.1 MHz.

The output of the band pass filter is then downconverted to an offset video frequency where it is sampled by the ADC. In order to synchronise all the signal generation and the sampling at the ADC, a single Temperature Controlled Crystal Oscillator (TCXO) is used.

A Virtex 4 FPGA is used to control the DDS and perform pre-storage processing, that entails pre-summing and filtering of data.

The hardware capabilities of the MicroASAR were extended by improving the maximum sampling rate of the system to 500 Msps and increasing the data storage rate to 5 MB/s. The increase in sampling rate allows to extend the beat frequency bandwidth of the receiver, as ADC hardware must be able to sample at twice the highest frequency present in the beat frequency signal. Hence, an improvement from the sampling rate of 328.947 ksps to 500 Msps, increases the theoretically possible beat frequency band from 164.475 kHz to 250 MHz.

Further considerations have to be made as the width of the beat frequency spectrum will be limited by the PRF and the storage rate. The storage rate places a limitation on the amount of data that can be recorded and thus, increasing the amount of data to improve the quality of the image can only be carried out until the maximum storage rate is not fully utilised.

The multi-look averaging that is employed in μSAR and MicroASAR are the direct result of the fact that the system storage rate is not sufficient to process all the data that is provided by the high PRF rate and requires a set number of consecutive chirp returns in slow-time to be added up, averaged and stored as a single chirp return, thereby degrading the azimuth resolution [4].

2.3.3 Feed-through Signal Filtering

The feed-through signal filtering is carried out using a Surface Acoustic Wave (SAW) bandpass filter, which is centred on 500 MHz. As Figure 2.5 shows the de-chirping of the received signal is carried out in such a manner as to place the received signal in the pass band of the bandpass filter, as opposed to a more conventional de-chirping process, where the received signal is de-chirped to baseband.

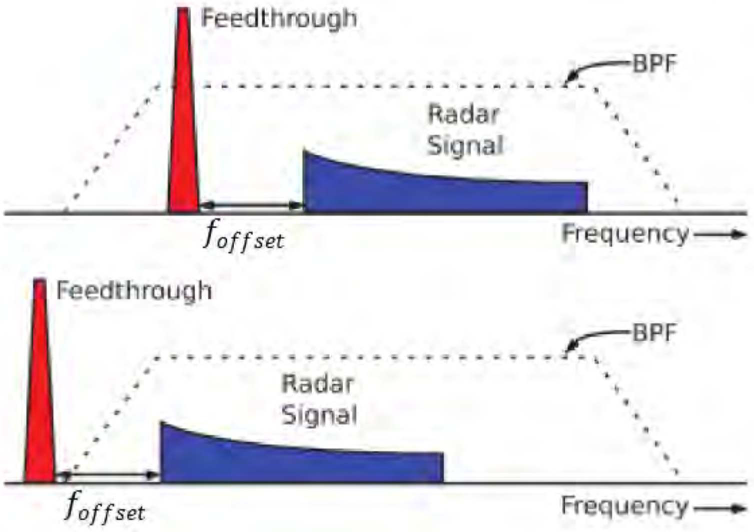

Figure 2.5: Feed-through filtering using a SAW bandpass filter [4]

In order to ensure that the feed-through signal is indeed located at the bandpass filters null, the PRF value must be chosen accordingly, as it determines the spread of the spectrum. This means that depending on the chosen PRF the targets can be brought closer or further in the receivers beat frequency spectrum.

For example, given a two-way propagation delay (t_{delay}) of 60 ns, a chirp bandwidth(Δf) of 100 MHz and a PRF of 10 kHz, the expected beat frequency can be computed according to Equation 2.6 and found to be 60 kHz.

$$f_b = \Delta f \times PRF \times t_{delay} \tag{2.6}$$

If the PRF is increased to 20 kHz, then the beat frequency associated with the time delay of 60 ns is 120 kHz. Therefore, a target that is situated at the range corresponding to the given two-way propagation delay can be located at 60 or 120 kHz in the beat frequency spectrum, based on the PRF value that is chosen.

Artemis MicroASAR, utilises the above principle by computing a minimum PRF value based on the platform altitude, bandwidth and the feed-through path distance. This can be expressed as:

$$PRF_{min} = \frac{cf_{offset}}{2\Delta f(h-\beta)}, \tag{2.7}$$

where f_{offset} is the frequency that corresponds to the range difference between the feed-through path and the nadir return, h is the platform height and β is the length of the effective free-space path that the feed-through signal takes [4].

Therefore, it can be seen that the minimum PRF value will vary, if the altitude of the platform is changing or the bandwidth of the signal is changed.

2.3.4 Performance

The metric that was used to characterise the performance of the MicroASAR system, was the noise equivalent sigma-0 parameter (σ^0), which is the parameter that defines the Signal to Noise Ratio (SNR) of SAR images. As σ^0 depends on the factors such as velocity, PRF and altitude, the operation parameters were as follows:

Velocity: 70 m/s

Altitude: 300 m

PRF: 7.52 kHz

Using the above, σ^0 was calculated for the cross track values and can be seen in Figure 2.6.

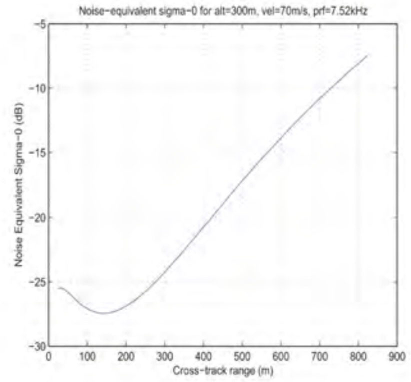

Figure 2.6: Noise-equivalent σ^0 over expected cross-track range for the MicroASAR with reasonable operating parameters [4]

The figure shows that mid-range value for σ^0 is approximately -17 dB, which means that areas that have a higher σ^0 will be discerned above the noise-floor of the SAR image [4]. As -17 dB σ^0 value corresponds to a desert terrain with dry broken soil, the developed areas and areas with more dense vegetation will be displayed more prominently in the image, as the σ^0 that is associated with those areas is typically higher than -17 dB.

2.4 MIT IAP Radar System

The Massachusetts Institute of Technology (MIT) Independent Activity Period (IAP) Radar System was developed for a short course and had to be low-cost in order to be available to the students. The FMCW architecture was employed that used only six coaxial microwave parts in the front-end and two metal cans for the antennas. The assembled system is shown in Figure 2.7 and could be utilised for Doppler and FMCW ranging, as well as crude SAR imaging [5].

Figure 2.7: MIT IAP Radar System complete assembly [5]

2.4.1 Specifications

The specifications of the MIT IAP Radar System can be found in Table 2.4. The frequency of operation is in S-band, centred on 2.4 GHz with a bandwidth of up to 330 MHz. This radar system resembles the rail SAR system that was developed in BYU, as it operates at 0 m elevation using the rail system approach, where the sensor is moved down the straight trajectory while recording the reflected signals.

Another similarity between the two systems is that a VCO is used to directly generate the modulated signal. However, the MIT IAP Radar does not have a feedback system to account for the VCO non-linearities, as the system had to be simple and low-cost.

The PRI of the system can be varied, but for the purpose of the experiments a 20 ms chirp was utilised. This also sets the PRF to a constant value of 50 Hz but due to the fact that the radar's mode of operation involves 0 m elevation, with manual placement of the system along the trajectory to form the synthetic aperture, the PRF does not have the requirement of being variable in real-time to account for the deviation in the platform velocity.

The antennas used in this system are of a circular wave guide type with a 3-dB beamwidth in azimuth and elevation of 72 degrees. They are tuned to a centre frequency of 2.4 GHz, with a 7.2 dBi antenna gain. A major advantage of the circular wave guide antennas is that they can be made of metallic cans, which can be easily procured at a lower-cost than the other antenna types that were mentioned in this chapter.

The MIT IAP Radar System is low-cost and as a result does not aim to achieve very high performance in terms of ranging and image resolution.

Table 2.4: MIT IAP Radar System Specifications

Radar Parameters	
Frequency Band	S-Band
Tx Central Frequency	2.4 GHz
Tx Power	13 dBm
PRI	20 ms
Bandwidth	up to 330 MHz
Receiver Noise Figure	1.2 dB
Chirp Generation	VCO
Modulation	Saw-tooth

Antenna Parameters	
Antenna Type	Circular Waveguide
3-dB Beamwidth	72°
Antennae Coupling	-39 dB
Antenna Gain	7.2 dBi
Center Frequency	2.4 GHz

Operating Specifications	
Estimated Range Resolution	0.41 m
Theoretical Azimuth Resolution	0.35 m
Platform elevation	0 m
Sampling rate	48 kHz

2.4.2 Radar Design

The system block diagram of the MIT IAP Radar System is provided in Figure 2.8, where a homodyne architecture can be seen.

The chirp waveform is generated by a VCO, which is driven by a XR-2206 ramp generator. The signal is amplified by a ZX60-272LN-S+ amplifier, which is also used as the LNA in the receiver due to its low Noise Figure (NF) of 1.1 dB. The output of the amplifier is connected to a ZX10-2-42+ two-way splitter, which feeds the transmitter antenna and the LO port of the ZX-05-43MH+. This is a level 13 mixer, hence the power of the signal at the the LO port is required to be 13 dBm.

The RF port of the mixer is connected to the output of the LNA, which amplifies the signal that is received by the receiver side antenna. The output of the mixer is a signal in the baseband region, which is filtered and amplified prior to digitisation by a computer sound card using the right audio channel of the 3.5 mm audio plug.

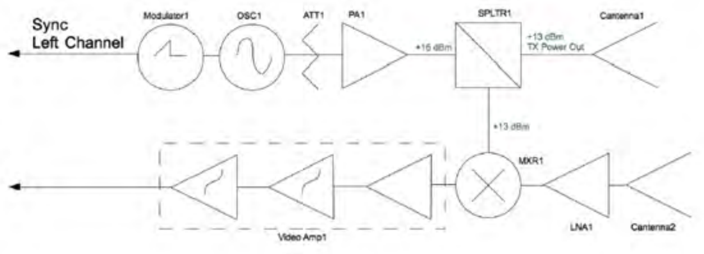

Figure 2.8: MIT IAP Radar System Design [5]

In order to avoid phase errors the transmitted signal is synchronised with the received signal by recording a synchronisation pulse that the ramp generator produces at the start of every ramp. This is implemented using the left audio channel on a 3.5 mm audio plug.

2.4.3 Performance

The performance of the MIT IAP Radar system is characterised by the expected range and imaging resolution. The range was calculated using the Radar Range Equation [5], to yield a maximum range of 829 m for a target with a Radar Cross Section (RCS) of 10 m^2 in the FMCW ranging mode and a maximum range of 2.2 km in the SAR imaging mode for the same target.

The discrepancy between the two ranges can be explained by the fact that the SAR processing adds an additional gain factor that corresponds to the number of profiles recorded in azimuth to synthesise the aperture.

In either case, as the radar system has a limit on the highest beat frequency that it can record, which is set to 15 kHz by the lowpass filter at the output of the video amplifier. Given the PRI of 20 ms and a bandwidth of 330 MHz, the maximum range that can be achieved is 272 m [5].

2.5 Summary

This chapter provided an overview of four distinct systems in the order in which they were developed. All four systems utilised an FMCW architecture for the purpose of imaging, however, each one had a different objective. The rail SAR system aimed at demonstrating that the FMCW architecture can be used for the purpose of imaging, with the μSAR building on the developed framework and realising them in a smaller form factor. The MicroASAR, was a commercial system, that incorporated all the features of the μSAR and implemented a method of feed-through signal removal by modifying the front-end architecture. Lastly, the MIT IAP Radar System was examined due to its emphasis on developing a low-cost FMCW radar that was capable of SAR imaging.

Chapter 3

RadioCamera-S Design Criteria

The design procedure of the RadioCamera-S begins with the analysis of the constraints that are related to the hardware requirements that were user defined. This is explained in Section 3.1. The effects of the operational geometry are discussed in Section 3.2, which is followed by the explanation of the two channel approach that was used to carry out the filtering of the feed-through and nadir return components in Section 3.3. Next, a ground based radar system specification that was developed as the result of the analyses performed in each section of this chapter is provided in Section 3.4, with a brief summary of the contents of the chapter in Section 3.5.

3.1 Hardware Considerations

The user requirements that were defined for this project included the following hardware design considerations:

- S-Band operation
- Incorporate the LMX2492, 500 MHz to 14 GHz Low Noise Fractional Phase-locked Loop for ramp/chirp generation
- Implement a low-cost solution for antenna design
- Utilise the LMH6521 IF amplifier in the receiver
- Employ the Red Pitaya open source platform to acquire data

The reason for the above component selection is that: the LMX2492 ramp generator, LMH6521 IF amplifier and the Red Pitaya were relatively cheap, readily available and came in a development board form factor with SMA connectors at all the required ports. This simplified the testing procedure by reducing the time it took to test different components and configurations, as well as enabled the author to meet the project budget. Unfortunately, this component selection also placed some constraints on the system, which are discussed next.

3.1.1 Frequency of Operation and Waveform Generation

The waveform generator that was employed in the RadioCamera-S design was the LMX2492 evaluation module from *Texas Instruments*. The evaluation module comprises of the LMX2492 Fractional Phase Locked Loop (PLL) with ramp generation capabilities, a loop filter and a RFVC1843DS Voltage Controlled Oscillator.

The characteristics of the VCO essentially define the band of operation. It has three outputs which operate in three distinct bands: the S-band, C-band and X-band. Hence, it satisfies the S-band operation criterion, as it can produce a modulated waveform centred on 2.4125 GHz. An additional advantage is that it can also be integrated into further RadioCamera prototypes, due to the fact that it offers a C-band output.

The evaluation module is restricted to a bandwidth of 175 MHz at the S-band output and has a limit on the length of the PRI. The former is determined by the amplitude of the tuning voltage that the PLL can provide, whereas the latter is determined by a number of factors.

The maximum length of a single repetition of the waveform that can be achieved is determined by the LMX2492 method of programming the modulated waveform. It is capable of generating a configurable piecewise linear FM modulation profile of up to 8 segments [16], each segment can span a maximum of 1.31 ms in length. Hence, the absolute maximum PRI that is achievable is 10.48 ms. This is largely determined by the 100 MHz oscillator that is used to clock both PLL boards. The oscillator defines the frequency of the phase detector in the PLL, which in turn relates to the maximum length of each programmable segment.

Following that, the minimum PRI that can be achieved using the required hardware was determined experimentally to be 75 μs for a triangular ramp that ramps up and down over a 175 MHz bandwidth. If a faster sweep rate is attempted, a loss of lock occurs. The sweep rate of the system depends on the loop filter characteristics. Hence, should a faster ramp rate be desired a different loop filter configuration can be utilised.

The type of modulation that can be produced using the given waveform generator can be varied. However, if a saw-tooth waveform with a direct return from the end to the start frequency is attempted, a loss of lock occurs due to the need to carry out a sweep of 175 MHz in almost no time. As a result a variation of a triangular waveform is required.

3.1.2 Antenna Requirements

The low-cost requirement for the antenna resulted in the consideration of employing the MIT IAP Radar System's circular waveguide antenna design. Those antennas already have defined parameters for the 3-dB elevation and azimuth beamwidth, which are 72 degrees. This leads to further constraints on the design if considered in conjunction with the velocity of the platform and the wavelength of the transmitted signal, which define the azimuth bandwidth of the radar, according to Equation 2.3.

In order to avoid aliasing, the Nyquist criterion needs to be met, therefore the azimuth bandwidth needs to be sampled at twice the highest frequency. This places a limit on the minimum PRF value, which can be calculated by using Equation 2.5.

Given the velocity of the platform to be 30 m/s, as pre-defined by the requirement for the airborne geometry, the wavelength of 0.124 m, which corresponds to the centre frequency of 2.4125 GHz, and the azimuth 3-dB beamwidth to be 72 degrees, the minimum PRF value is 1.216 kHz.

3.1.3 Video Amplifier

The LMH6521 IF amplifier was the video amplifier which was selected for the RadioCamera-S receiver chain. It is a Dual Digitally Controlled Variable Gain Amplifier (DVGA), which is limited to a 26 dB maximum voltage gain. It has a 3 dB Bandwidth of 1200 MHz. However, upon inspection of the Gain versus Frequency plot in the datasheet [17], which can be seen in Figure 3.1, it was found that signals in the frequency range from DC to approximately 1 MHz, are attenuated and the actual gain of the amplifier only reaches the expected value from approximately 10 MHz.

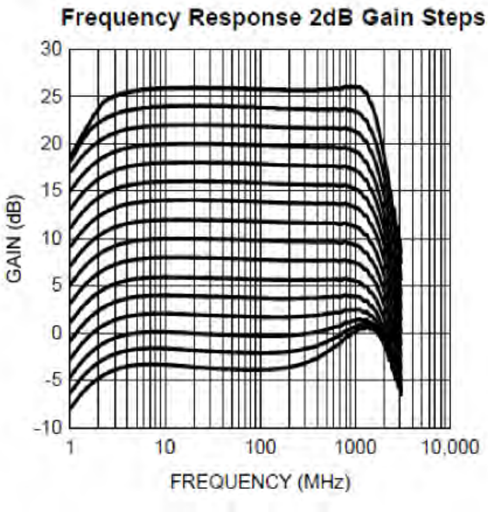

Figure 3.1: Gain versus Frequency plot of the LMH6521

This was also determined experimentally with the results presented in Figure 3.2, where the blue trace is the -20 dBm input and the black trace is the amplifier output. It can be seen that below 500 kHz, the input signal from a signal generator is attenuated by 10 dB, despite the fact that the gain setting of the amplifier is set to 20 dB. This places a limitation on the band of frequencies that can be used in the baseband section of the receiver, as actual target returns that are below the -20 dBm level tend to be filtered in the DC-500 kHz region.

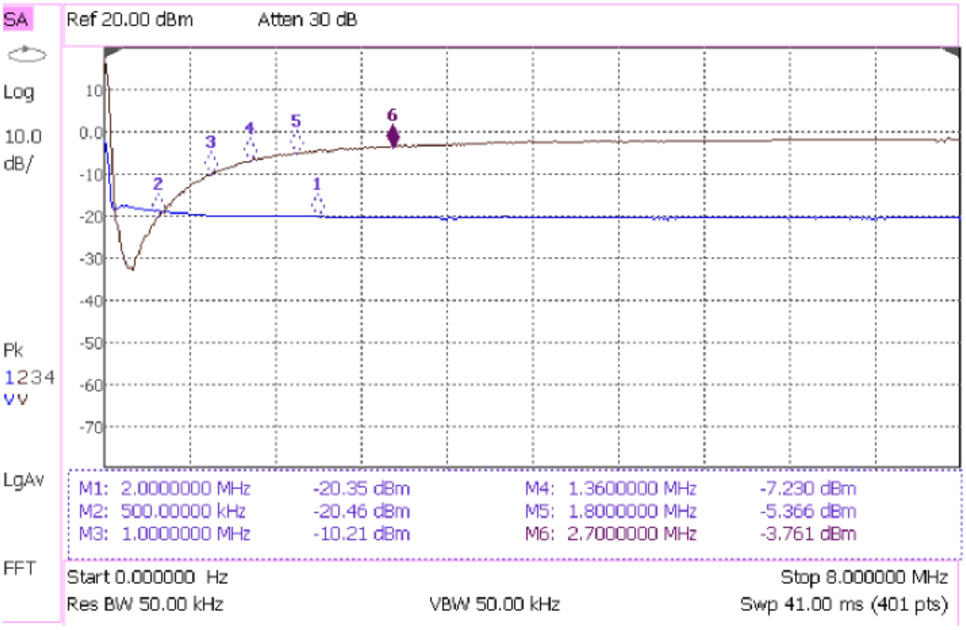

Ref 20.00 dBm Atten 30 dB

M1: 2.0000000 MHz -20.35 dBm
M2: 500.00000 kHz -20.46 dBm
M3: 1.0000000 MHz -10.21 dBm
M4: 1.3600000 MHz -7.230 dBm
M5: 1.8000000 MHz -5.366 dBm
M6: 2.7000000 MHz -3.761 dBm

Start 0.000000 Hz Stop 8.000000 MHz
Res BW 50.00 kHz VBW 50.00 kHz Swp 41.00 ms (401 pts)

Figure 3.2: Magnitude versus Frequency plot of the LMH6521

3.1.4 Signal Digitisation

The Red Pitaya open source platform is based around a Xilinx Zynq 7010 SoC and is required to perform the function of a signal digitiser. It has two fast analogue channels that can have a maximum sample rate of 125 Msps. This limits the beat frequency spectrum to 62.5 MHz. Should one wish to reduce the sample rate, one can set a decimation factor of 8, 64, 1024, 8192, 65536, which will lead to a proportional reduction of the maximum frequency that can be sampled.

The ADC resolution is 14 bits, which determines the maximum theoretical ADC dynamic range (DR) to be 86.7 dB, as calculated using Equation 3.1, where N corresponds to the ADC resolution in bits. The actual usable dynamic range will be lower due to the fact that one needs to ensure that there is headroom between the maximum signal at the input and the maximum signal that the ADC can process. This is required in order to avoid saturating the ADC.

$$DR = 6.021N + 1.763, \tag{3.1}$$

The ADC is clocked by an on-board oscillator at a frequency of 125 MHz. The oscillator utilises the LVDS standard, as opposed to the single ended LVCMOS, which is used to clock the two synthesiser boards. An attempt was made to synchronise the Red Pitaya with the 100 MHz LVCMOS clock, by using the NB3N201S Low-Voltage M-LVDS Driver Receiver, however, due to the converter malfunction, the units were not synchronised.

This malfunction was predominantly attributed to the fact that the PCB for the converter had to be made by hand, due to insufficient time to procure the PCB from the manufacturer. As a result the track width and spacing that is required by the LVDS standard were not achieved, which resulted in signal degradation to the point where the ADC could not be clocked effectively.

The system could still operate asynchronously when a single shot FMCW ranging radar setup is employed. However, problems will arise if the system will operate in an imaging mode due to pulse to pulse phase errors.

The available data acquisition routines limit the number of samples that can be recorded continuously to 16384 samples. This places limitations on the time frame that can be sampled, as if 16384 samples are sampled at 125 Msps, then a maximum of 131 μs can be recorded. If the sample rate is decimated by a factor of 8, to 15.6 Msps, this can be extended to a time period of 1.05 ms at the expense of the bandwidth. This time period will essentially be referred to as the maximum PRI, as the Red Pitaya is currently unable to digitise a longer PRI.

Lastly, as the Red Pitaya is a new system, which does not have a large user community supporting it, the application development time is extended, due to the lack of documentation and previous user expertise. The above limitation of the number of samples that can be acquired at any one time is a fitting example, as it will require time and resources to modify the existing routines.

3.2 System Geometry Considerations

As was mentioned in Chapter 1, the RadioCamera project is aimed at designing a radar that will be compact enough to fit on a small UAV and operate in the C-band. The RadioCamera-S prototype on the other hand is a ground based system, that is utilised to test the hardware and the architecture for the future revision that will be implemented in a small form factor. As a result there will be differences in the expected operational range, waveform design criteria and the beat frequency spectra of the airborne and ground based systems. This section aims to address both of the operational geometries and provide a framework for understanding the parameter variations due to the difference in operational conditions.

3.2.1 Airborne System Geometry Considerations

The geometry of the airborne system that was utilised to define the radar parameters can be seen in Figure 3.3. The elevation of a small-scale airborne platform (h), was set to be 500 metres. In this scenario the radar is set to point perpendicularly to the direction of propagation of the platform, which in the case of the provided figure is into the page and has a velocity equal to 30 m/s. The antenna beam is pointed towards the ground, with the requirement that a swath width (ΔY) of a 1000 metres needs to be illuminated and offset (R_{offset}) from nadir by 500 metres. The ground range resolution (δy) is required to be approximately 1 metre mid-swath.

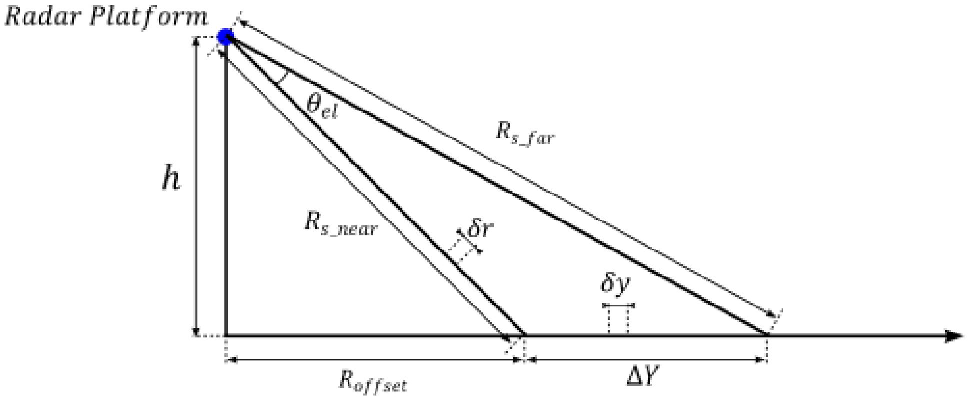

Figure 3.3: Operational geometry of the final system

The terms R_{s_near} and R_{s_far} correspond to the distance from the radar to the nearest point in the swath and to the furthest point in the swath in meters, respectively. Given the geometrical dimensions of the system, the range can be computed using the following equation:

$$R_s = \sqrt{h^2 + R_{ground}^2}, \tag{3.2}$$

where h is the height (elevation) of the platform and R_{ground} is the distance from the nadir to the point of intersection of the slant range with the ground plane. Using this equation the two ranges can be computed:

$$R_{s\_near} = \sqrt{500^2 + 500^2} = 707.1 \tag{3.3}$$

$$R_{s\_far} = \sqrt{500^2 + 1500^2} = 1581.1 \tag{3.4}$$

Hence, the range profile that will be seen at the receiver can be illustrated by Figure 3.4, where the length (β) of the effective free space path that the feed-through signal takes is approximately 2 m (in accordance with [4]) and the radar elevation (h) is equal to 500 m.

The range values in the range profile are related to the frequency components of the beat frequency spectrum through the two-way propagation delay that they produce. The associated time delays can be computed by using Equation 2.2. The results are presented in Table 3.1.

Once the two-way propagation delay for the targets of interest was computed it can be related to the frequency components of the beat frequency spectrum by the following relationship [18]:

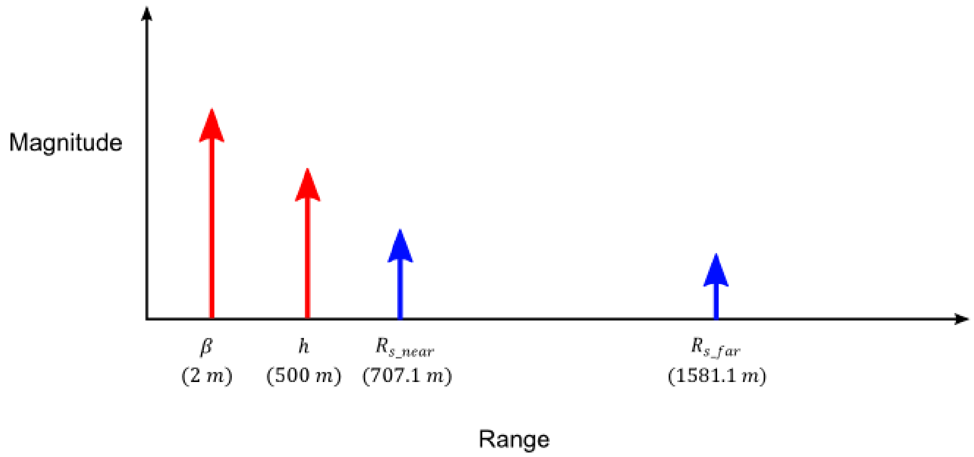

Figure 3.4: RadioCamera-S typical range profile

Table 3.1: Relationship between range and two-way propagation delay of the returns of interest

Return	**Range**	**Time Delay**
	m	μs
Feed-through	2	0.0013
Nadir return	500	3.333
Near Swath	707.1	4.714
Far Swath	1581.1	10.541

$$f_{beat} = \frac{\Delta f}{\Delta t} t_{delay}, \tag{3.5}$$

where Δf is the bandwidth of the signal and Δt is the duration of the ramp (PRI). As the two-way propagation delay is constant for the target at the given range, the beat frequency signal can be varied by changing the values of the bandwidth of the transmitted signal and the ramp duration (PRI) of the waveform. However, those parameters are also responsible for additional factors that affect the performance of the radar:

- Bandwidth of the signal needs to be high enough to satisfy the range resolution condition
- Two-way propagation delay of the furthest target must be much smaller than the PRI [14]

Furthermore, the geometry of the system also places a minimum requirement on the elevation beamwidth of the antenna. The above mentioned design considerations will now be explained in more detail.

Signal Bandwidth

As the resolution requirements of the system dictate that the range resolution should be approximately 1 m mid-swath, the slant resolution can be computed by using the following expression [1]:

$$\delta r = \frac{\delta y}{\sqrt{1 + \frac{h^2}{R_{ground}^2}}}, \tag{3.6}$$

where δr is the slant range, δy is the ground range, h is the elevation of the platform and R_{ground} is the ground range distance from nadir to the point of intersection of the slant range line of sight with the ground plane.

Given the geometry, the mid-swath point is located 1000 m away from nadir, taking into account the 1 m ground resolution, the slant resolution is equal to 0.89 m. Hence, the minimum bandwidth (Δf_{min}) of the transmitted signal that can be used to satisfy this slant range resolution can be computed by the following equation:

$$\Delta f_{min} = \frac{c}{2\delta r}, \tag{3.7}$$

which results in Δf_{min} equal to 168.5 MHz. As the maximum bandwidth of the transmitter is 175 MHz, this criterion is satisfied.

Two-way Propagation Delay and PRI

According to [14], the two-way propagation delay of the furthest target needs to be much smaller than the PRI of the chirp signal. The exact ratio between the two is not specified in literature, hence for the purpose of this dissertation, an assumption will be made that the two-way propagation delay must not be longer than 20% of the PRI.

Due to the fact that the furthest target that is to be illuminated by the radar is located at 1581.1 m, with the corresponding two-way propagation delay of 10.541 μs. The minimum PRI that can be employed by the system is computed by using the following equation:

$$PRI_{min} = \frac{max(t_{delay}) \times 100\%}{20\%}, \tag{3.8}$$

and is equal to 52.66 μs. However, this is below the minimum PRI that the LMX2492EVM can generate, as it limits the PRI value at 75 μs. Hence, the minimu system PRI is 75 μ. Furthermore, as the PRI and PRF are related according to the expression:

$$PRF = \frac{1}{PRI}, \tag{3.9}$$

the maximum PRF value will be the inverse of minimum PRI value and equal to 13.33 kHz.

Elevation Beamwidth

The near and far points of the swath and the platform elevation are used to determine the minimum elevation 3-dB beamwidth of the antenna, this can be expressed by the following relationship:

$$min(\theta_{el}) = arctan\left(\frac{R_{s\_near}}{h}\right) - arctan\left(\frac{R_{s\_far}}{h}\right). \tag{3.10}$$

As the elevation is set at 500 m, R_{s_near} point is 500 m away from nadir and R_{s_far} point is 1500 m away from nadir, than the minimum 3-dB elevation beamwidth of the antenna is 26.6 degrees.

It has to be noted that it is critical to consider the instability of the airborne platform during the design of the airborne radar antennas. The beamwidth, as computed previously, is suitable for the ideal case, where the platform maintains a constant height, pitch, roll and yaw. In a real world scenario, a small UAV will be subjected to weather conditions which will result in changes to the trajectory and altitude. Hence, if one is required to observe a 1000 m swath from a real airborne platform, an elevation beamwidth that exceeds 26.6 degrees would be needed. The extent to which this beamwidth will be increased is directly linked to the degree of stability that a chosen platform will show.

Waveform Parameters

As a result of the above parameter analysis a suitable waveform for the airborne system, would have a 175 MHz bandwidth and a triangular modulated wave, with the up ramp having a longer duration than the down ramp in order to maximise the PRF and ensure that the PLL does not lose lock during operation.

A suitable up ramp duration would be 100 μs, as it provides a good balance between the target overlap, spectral spread and satisfies the minimum PRI together with the minimum PRF criteria. The down ramp can be set to 25 μs as it is the maximum frequency sweep that results in PLL staying phase locked.

The beat frequency spectrum that is occupied when a 100 μs up ramp is used in conjunction with a requirement to illuminate a 1000 m swath at a 500 m offset from nadir is 18.5 MHz, which can be accommodated by the Red Pitaya.

3.2.2 Ground Based System Geometry Considerations

The ground based system geometry differs from the airborne case in that it is located at 0 m elevation. It is pointed down range, with the range of interest being from 0 to 40 m. Figure 3.5 demonstrates a typical range profile of a system.

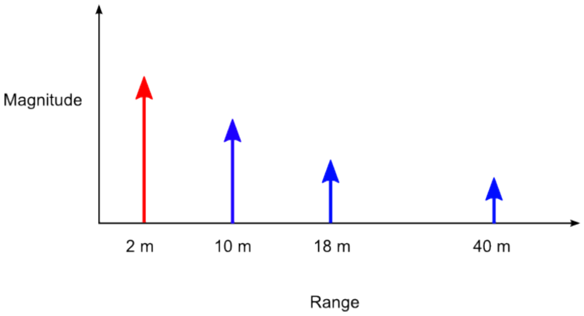

Figure 3.5: Ground based radar range profile

Due to the fact that the distance to targets was reduced, the time delay associated with them is also significantly less, Table 3.2, shows the relationship. This also results in the reduction of the minimum PRI value as the furthest target corresponds to a shorter delay of 0.26 μs, and in accordance to Equation 3.8, the minimum PRI value for the bench system is 1.33 μs.

Table 3.2: Relationship between range and two-way propagation delay of the returns of interest for the ground based radar

Return	**Range**	**Time Delay**
	m	ns
Feed-through	2	13.3
Target 1	10	66.7
Target 2	18	120
Max Range	40	266

Additional requirements for the ground based system would be to minimize the PRI in order to spread the spectrum as wide as possible. This can be justified by the fact that the targets are situated at close proximity and the wider the spectral spread the better the targets will be demonstrated in the beat frequency spectrum. However, this does come with a trade-off, as the short ramping time decreases the overlap time between the transmitted signal and the target, which will decrease the strength of the returned signal.

3.3 The Two-Channel Filtering Approach

The proposed two channel filtering architecture is illustrated in Figure 3.6. The waveform generators S1 and S2 produce identical L-FMCW waveforms but have a time offset (t_{offset}) between them. The "S1" with its respective signal S_{t1} and "S2", which produces the signal S_{t2}, is the notation that is employed in this dissertation to refer to the respective waveform generators when discussing the precedence of waveforms in the radar transmitter.

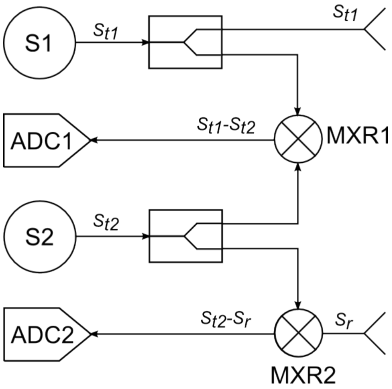

Figure 3.6: Simplified signal block diagram that demonstrates the main signal paths associated with the two channel filtering approach

The offset time can be related to a shift in frequency in the beat frequency spectrum at the output of the mixers. Based on the precedence of waveforms, two modes of operation can be identified:

Mode One - Signal S_{t1} from waveform generator S1 is lagging signal S_{t2}

Mode Two - Signal S_{t1} from waveform generator S1 is leading signal S_{t2}

Once the spectrum is shifted a high pass filter can be used to filter the unwanted signals in the case of Mode One and a low pass filter can be used to filter the unwanted signals in Mode Two. The exact description of the two modes and how they can be used to aid the filtering of the unwanted echoes is demonstrated using a graphical approach and then followed by a mathematical model derivation.

3.3.1 Graphical Description

Figure 3.7 illustrates the two modes of operation as they were described above.

Mode One

In the main receiver channel the signal that contains the target information is mixed together in MXR2 with a copy of the signal produced in waveform generator S2,

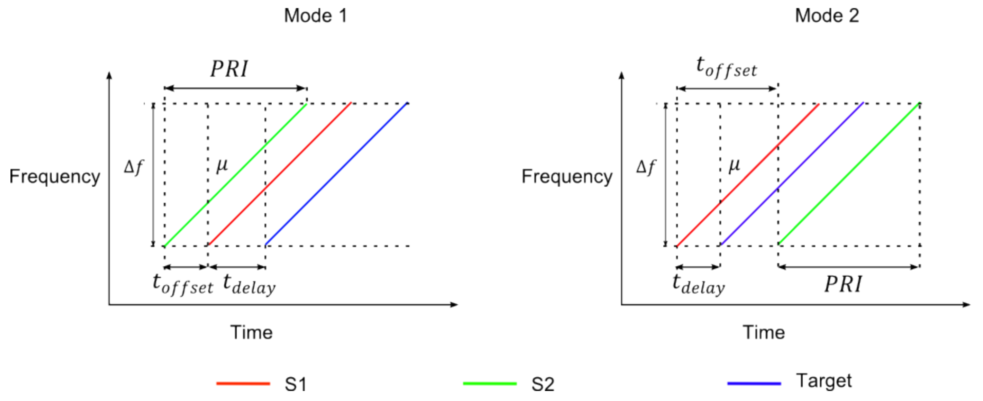

Figure 3.7: Two modes of operation of RadioCamera-S radar system

hence the time delay to target increases from the the value of t_{delay} to a value of $t_{delay} + t_{offset}$. Hence, the frequency components that usually associate with the t_{delay}, will be translated in the frequency spectrum by a factor that is proportional to t_{offset} in the frequency domain. The conversion from the time to frequency domain can be carried out using Equation 2.6 or 3.5. This process is illustrated in Figure 3.8.

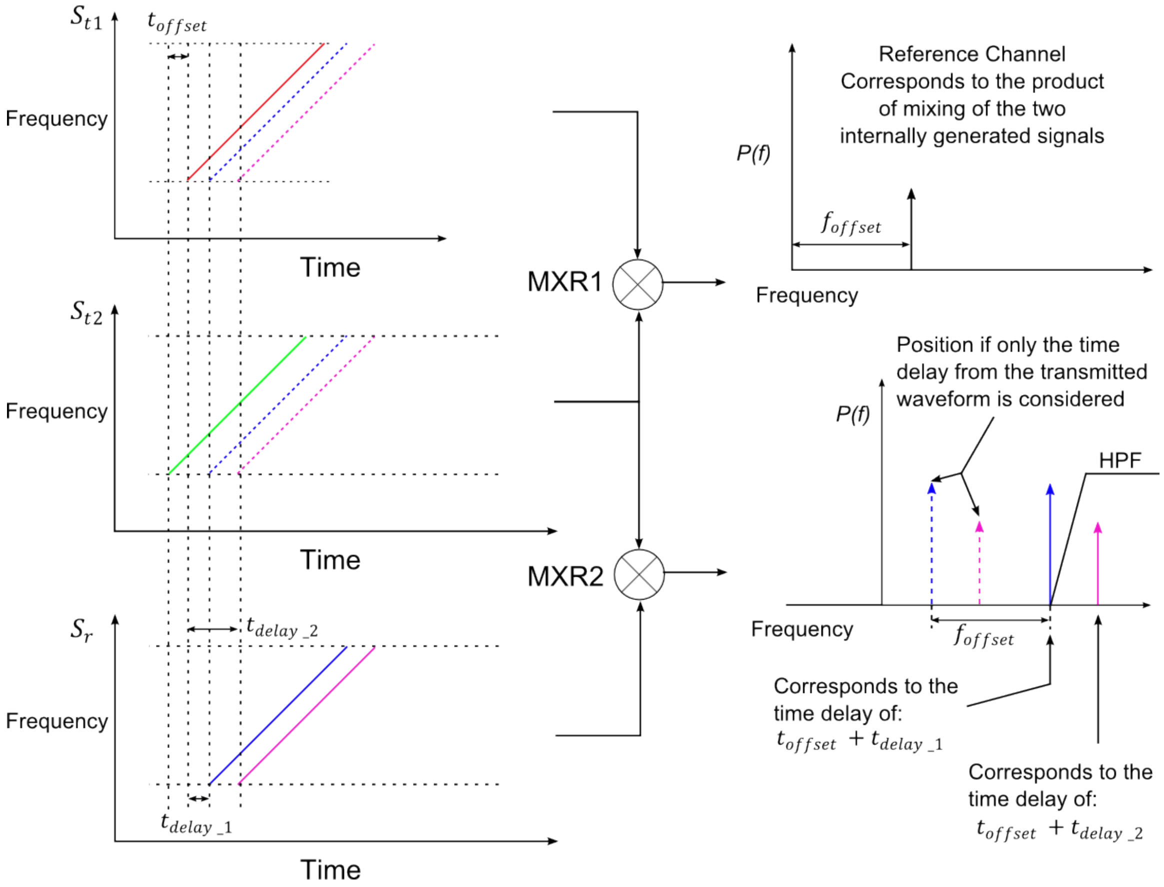

Figure 3.8: Graphical representation of Mode One

Meanwhile, in the reference channel of the receiver, the two waveforms that were generated by S1 and S2 are mixed together in mixer, MXR1, to produce a reference signal. The frequency of the reference signal is directly proportional to t_{offset} in the frequency domain. Once, the location of the reference signal is known in the frequency domain, the information in the main channel can be modified to represent true range.

This mode is useful, when a high pass filter is present in the receiver chain, it does not invert the spectrum, which makes it easier to interpret the data. Furthermore, the PRI value can be varied to account for different airborne platform elevations in order to position the feed-through and nadir returns outside of the filter pass band.

Mode Two

Figure 3.9 shows the second mode of operation of the RadioCamera-S, prototype. It needs to be used with a low pass filter, as the feed-through and the nadir return signals become inverted, due to the fact that signal S_{t2} is offset by a time coefficient that is greater than the time delays from the target, with respect to the transmitted signal. Hence, further targets will appear closer in the beat frequency spectrum.

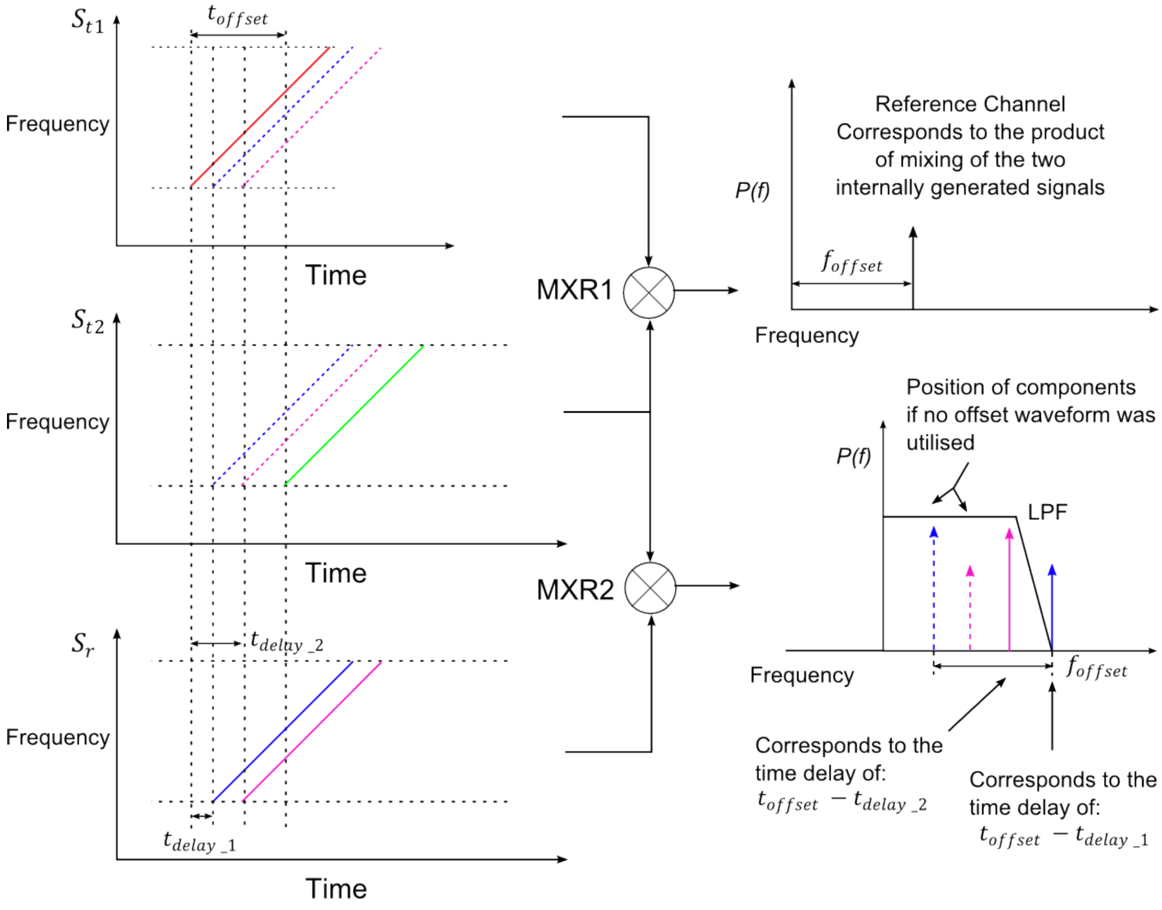

Figure 3.9: Graphical representation of Mode Two

Care must be taken when implementing this method, because if additional target returns are received with a time delay that is greater than the offset value, they will fold over the targets that are located at a time delay, which is less than the offset value by the same margin.

3.3.2 Model Derivation

The method of filtering the signals which are located at a known range can also be expressed mathematically. This will be demonstrated by deriving the model for Mode One. If the waveform that is produced by waveform generator S1 is represented as:

$$S_{t1} = e^{j(2\pi f_c t + \frac{\mu t^2}{2})}, \tag{3.11}$$

where f_c is the carrier frequency, t is the variation in time and μ is the chirp rate $(\frac{\Delta f}{\Delta t})$. Then the waveform that is generated by waveform generator S2 and triggered at a time offset of t_{offset} from S_{t1} can be expressed as:

$$S_{t2} = e^{j(2\pi f_c (t + t_{offset}) + \frac{\mu (t + t_{offset})^2}{2})}. \tag{3.12}$$

The amplitude coefficients of the waveforms are left out of this analysis for the purpose of simplification. Those two waveforms are mixed together to produce a reference channel of the receiver. The mixing process can be modelled as the multiplication of signal S_{t1} by the complex conjugate of the time offset signal S_{t2}, the result of the mixing process is shown in Equation 3.13.

$$S_{ref} = e^{j(-2\pi f_c t_{offset} - \mu \times t \times t_{offset} - \frac{\mu t_{offset}^2}{2})}. \tag{3.13}$$

The derivative of the phase corresponds to the frequency value of the signal, hence, the derivative of the S_{ref} signal will yield the following:

$$f_{S_{ref}} = -\mu t_{offset}. \tag{3.14}$$

This can be used at a later stage to derive the range to target, once the beat frequency of the target signal from the main receiver channel is known.

The signal at the receiver can be expressed as:

$$S_{rx} = e^{j(2\pi f_c (t - t_{delay}) + \frac{\mu (t - t_{delay})^2}{2})}. \tag{3.15}$$

where t_{delay} is the two-way propagation delay that corresponds to range to target. S_{rx} signal contains the information from one target, if multiple targets were present, one would require to add all the exponential terms that correspond to each target.

The signal at the main receiver channel is a result of mixing operation of signals S_{t2} and signal S_{rx}. Only the phase information of the output signal is presented in Equation 3.16 for ease of presentation:

$$\phi(t) = 2\pi f_c(t_{delay} - t_{offset}) + \mu t(t_{delay} - t_{offset}) - \frac{\mu}{2}(t_{delay}^2 - \mu t_{offset}) \tag{3.16}$$

In order to determine what the resultant beat frequency component is, a derivative with respect to time of the phase can be found:

$$f_{S_{main}} = \mu(t_{delay} + t_{offset}). \tag{3.17}$$

Equation 3.17 shows that the relationship between t_{offset} and t_{delay} determines the beat frequency of the target in the beat frequency spectrum of the main receiver channel.

In order to obtain the true beat frequency value that corresponds to the actual range to target the beat frequency components need to be added, this is shown in Equation 3.18.

$$f_{beat} = f_{S_{main}} + f_{S_{ref}}, \tag{3.18}$$

if the values for the two beat frequencies are substituted from Equations 3.17 and 3.14, Equation 3.18 becomes:

$$f_{beat} = \mu(t_{delay} + t_{offset}) - \mu t_{offset} = \mu t_{delay}. \tag{3.19}$$

This essentially allows one to derive the true two-way propagation delay that corresponds to the target position using a reference and a main receiver channel, while filtering the unwanted signals out. Mode Two operates on the similar premise, however, the signs change in the above equation as the spectrum is inverted due to the fact that signal S_{t2} is offset by a factor of $-t_{offset}$ from the target return and by the factor of $-t_{delay} - t_{offset}$ from the transmitted signal.

3.4 System Specification

After the analysis of the hardware limitations, as well as the predefined geometry, a system specification can be proposed for the RadioCamera-S prototype that will be refined after the practical testing is carried out. Table 3.3 demonstrates the radar, antenna and operational parameters for the ground based system.

Table 3.3: RadioCamera-S ground based system specifications

Radar Parameters	
Frequency Band	S-Band
Tx Central Frequency	2.4125 GHz
PRI_{min}	75 μs
PRI_{max}	1.05 ms
PRF_{max}	13.33 kHz
PRF_{min}	0.952 kHz
Bandwidth_{min}	175 MHz
Chirp Generation	VCO

Antenna Parameters	
Elevation Beamwidth	72°

Operating Specifications	
Range Resolution	0.89 m
Sampling Rate	125 MHz

It is problematic to provide a specification for the airborne version, as the change from S-band to C-band will result in changes to antenna dimensions, the minimum PRF value, azimuth beamwidth and, if the LMX2492EVM's C-band channel is used, the bandwidth of the system will also increase to 350 MHz, which will redefine the maximum range resolution. As a result those changes that will be required, the airborne C-band system specification is left out of this discussion.

3.5 Summary

This chapter presented the design considerations that had to be accounted for in order to satisfy the hardware limitations, as well as the predefined operational geometry requirements. Characteristics of the transmitted waveform was provided for the airborne and the ground based systems. Then, the two channel filtering technique was explained graphically and mathematically through the derivation of the process model. Finally, the system specification for RadioCamera-S was presented. The airborne specification was not derived due to the inconsistencies between a S-band and C-band system implementation, however, the insight into the factors that should be considered when developing a specification for the airborne system were presented.

Chapter 4

Hardware Implementation

The specification that was developed in Section 3.4 predominantly relates to the waveform design aspect. The limitations that were related to the pre-defined hardware components were also discussed. However, not all of the components that form the RF front-end were mentioned.

The RF front-end design for the prototype was flexible, as the main objective of the prototype is to demonstrate the implementation of the two channel filtering scheme utilising low-cost, readily available components. Therefore, the components that were used to assemble the RadioCamera-S prototype were similar to the components employed by the MIT IAP Radar System, which was reviewed in Section 2.4.

RadioCamera-S system was divided into three modules: transmitter, antenna and receiver, which are examined in Sections 4.1, 4.2 and 4.3,respectively. Then a description of the complete system assembly is provided in Section 4.4. The chapter closes with a brief summary in Section 4.5.

4.1 Transmitter

Figure 4.1 illustrates the transmitter module of the RadioCamera-S. It consists of two channels. Channel one is connected to the antenna, meanwhile the second channel is used in conjunction with channel one to provide a zero range reference when the radar is operated in feed-through filtering mode. A detailed description of this mode of operation can be found in Section 3.3. Additionally, the second channel is used to de-ramp the signal which comes from the receiver side antenna.

The transmitter module is powered by a 5 Volt power supply and can be divided into two distinct sub-modules, based on functionality:

- Waveform Generator
- Amplification Stage

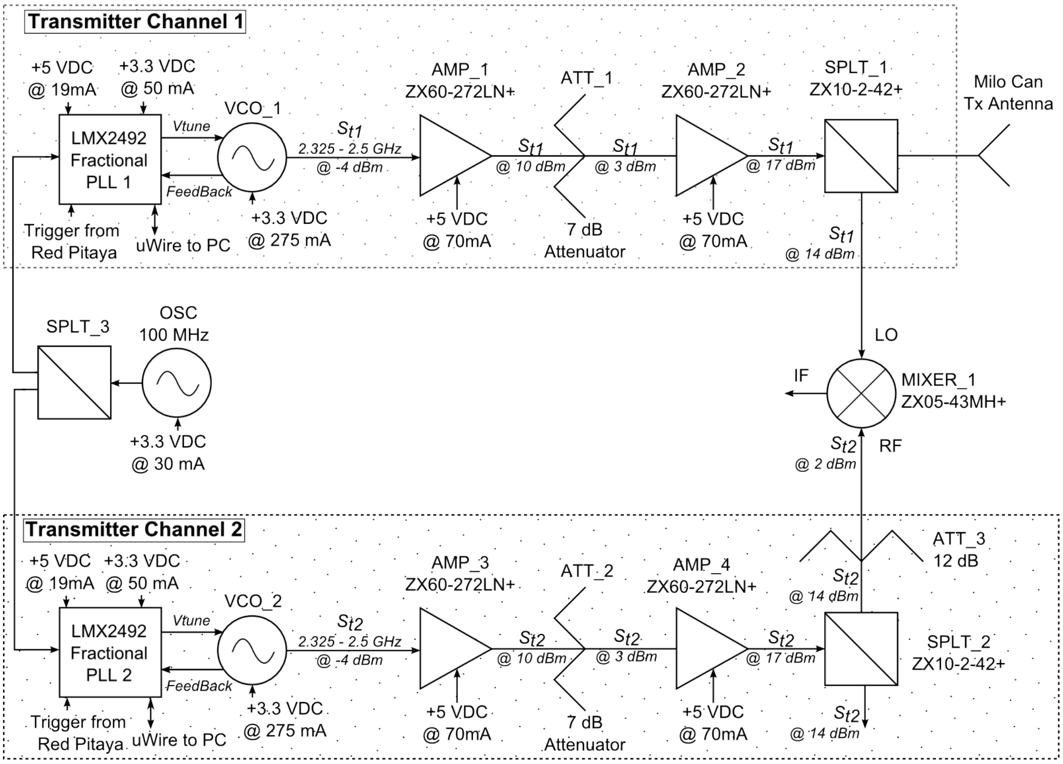

Figure 4.1: Two channel transmitter signal block diagram

4.1.1 Waveform Generation

The hardware requirements dictate that the LMX2492EVM should be used to generate the L-FMCW signal. It is a evaluation module for the LMX2492 Low Noise Fractional N PLL that has chirp generation capability [16] and is utilised in conjunction with a RFVC1843 MMIC VCO. This VCO has a frequency range of 9.8 to 11.3 GHz and additional outputs, where the frequency output (RF_{out}) is divided by two ($\frac{RF_{out}}{2}$) and four ($\frac{RF_{out}}{4}$) [19]. Therefore, the operating frequency of the RFVC1843 VCO determines the operating frequency of the transmitter.

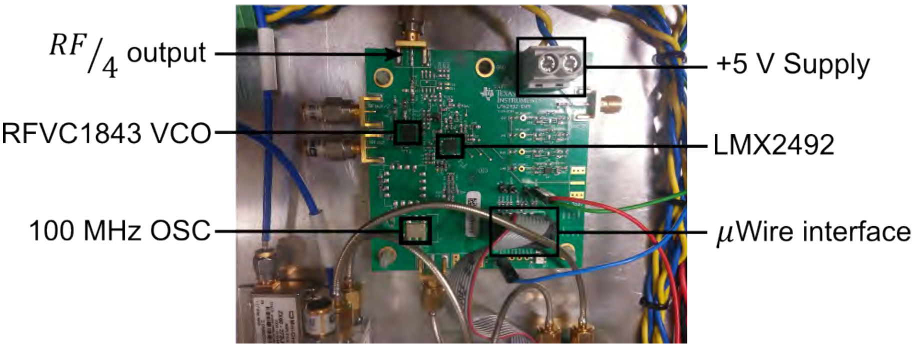

Figure 4.2: LMX2492 Evaluation module for the Low Noise Fractional N PLL that has chirp generation capability

Figure 4.2 shows the main components of the evaluation module. The LMX2492 controls the output of the VCO by providing a tuning voltage that is in range of 0 to 4.8 Volts. However, the VCO tuning voltage has a range of 0 to 15 Volts, hence the full range that the VCO can provide is not accessible.

Furthermore, the specified frequency range of the LMX2492EVM is in the range of 9.4 to 10.1 GHz [20] for the undivided output channel, 4.7 to 5.05 GHz for the $\frac{RF_{out}}{2}$ output and 2.35 to 2.525 GHz for the $\frac{RF_{out}}{4}$ output. As the system is specified to operate at S-Band, the output of interest is the $\frac{RF_{out}}{4}$. The maximum signal bandwidth of that output channel is 175 MHz, which satisfies the bandwidth requirements, as stated in Section 3.2.1.

It has to be noted that the specified operating frequency ranges for the evaluation boards and the VCO differ, this can be explained by referring to Figure 4.3(a), where the Frequency versus Tuning voltage of the undivided VCO output is shown. It can be seen that the frequency range from 9.8 to 11.3 GHz has a linear response to the tuning voltage, where as the region in the frequency band below including the proposed 9.4 to 10.1 GHz, is non-linear. The same applies to the divide by four, $\frac{RF_{out}}{4}$, output, as shown in Figure 4.3(b). Hence, the evaluation module operates in the non-linear region of the VCO.

In order to compensate for the non-linearity, the PLL and VCO are connected in a closed loop configuration. This configuration allows a tuning voltage, which is produced by the PLL, to be varied in accordance with the non-linear frequency-voltage response of the VCO and ensure that the output frequency ramp is linear, as described in Appendix B.1.1.

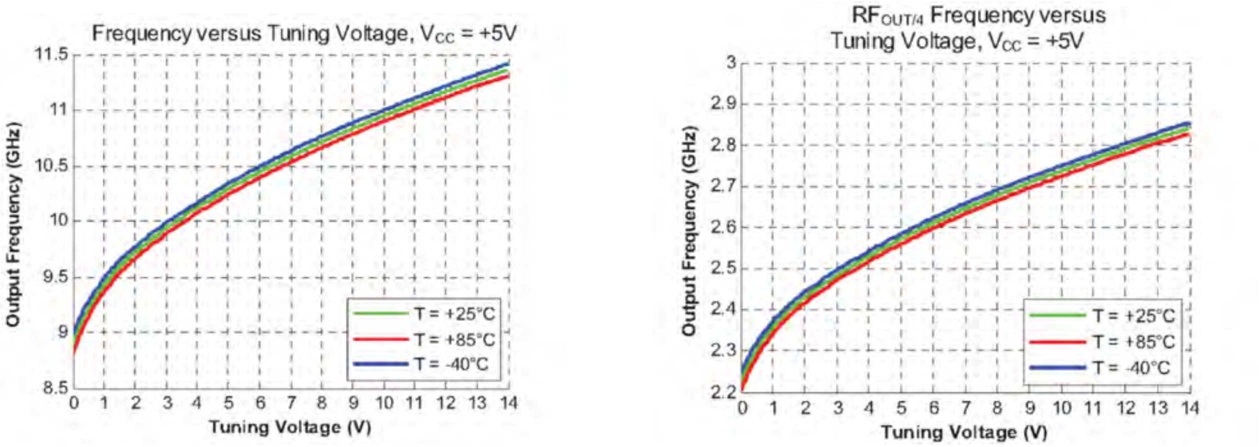

(a) Frequency versus Tuning voltage relationship for the undivided (RF_{out}) VCO output

(b) Frequency versus Tuning voltage relationship for the divided by four ($\frac{RF_{out}}{4}$) VCO output

Figure 4.3: Frequency versus Tuning voltage relationship of the RFVC1843 VCO [19]

The power output of the VCO at the $\frac{RF_{out}}{4}$ channel, is defined to be -2 dBm, however, one also needs to consider the possible losses that may occur in the transmission line that connect the given output to the SMA connector at the edge of the Printed Circuit Board (PCB).

In addition to that, the default configuration of the evaluation board has a 6 dB

T attenuator at the VCO output ports. Therefore, those attenuators should be removed in order to obtain the power level that is specified in the VCO datasheet.

The evaluation board was programmed from the PC by utilising the *Texas Instrument's Codeloader 4 software*, in conjunction with the *USB2ANY Programmer*, that served as the interface between the PC and the board. The waveforms that were programmed were of the saw-tooth and triangular modulation type and were designed to span the entire available 175 MHz bandwidth, centred as close as possible to 2.4 GHz.

LMX2492 has an operational bandwidth of 500 MHz to 14 GHz, hence the next revision of RadioCamera series of radars can be upgraded to C-band, without the need to change the primary method of ramp generation. Instead, only the VCO can be substituted to satisfy the new frequency range of operation.

4.1.2 Amplifier Stage

The ZX60-272LN+ low noise amplifiers with a frequency range of operation of 2300 MHz to 2700 MHz were used in the transmitter amplification stage. Those amplifiers were utilised by the MIT IAP Radar System and chosen due to their low-cost and availability. Figure 4.4 demonstrates a single amplification channel that consists of two amplifiers with an attenuator in between.

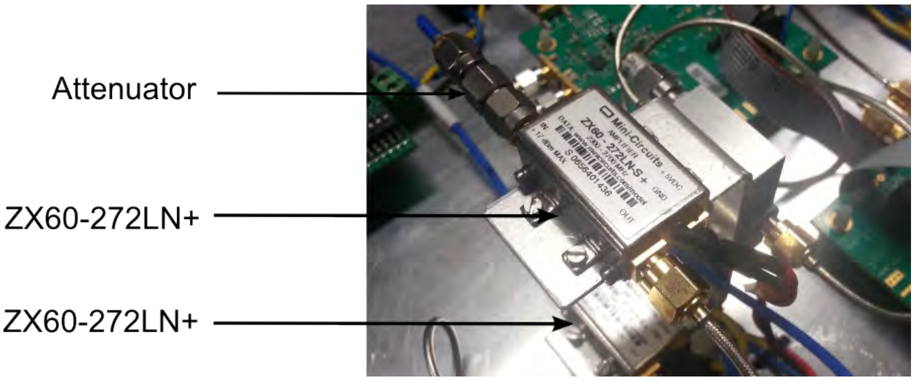

Figure 4.4: RadioCamera-S transmitter amplification chain

Two amplifiers had to be cascaded for each transmitter channel, as the output power of the waveform generator was significantly lower than the output power of the VCO in the MIT IAP Radar System, which only required a single amplifier. An attenuator had to be used between the two amplifiers in order to attenuate the output of the first amplifier to a level that will not saturate the second amplifier. This level can be calculated using the information provided in the datasheet [21], where the parameters of interest are the 1 dB compression point and the gain of the amplifier. The input power which results in saturation can be found using the following expression:

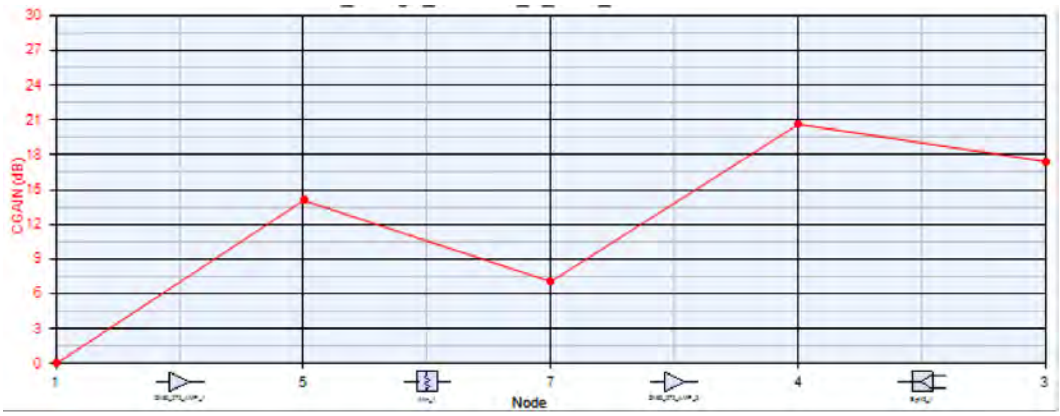

Figure 4.5: Cascaded gain of the transmitter channel

$$P_{in}^{sat} = P_{1dB} - G_{amp}, \tag{4.1}$$

where P_{1dB} corresponds to the 1 dB compression point of the amplifier, G_{amp} is the gain of the amplifier and P_{in}^{sat} is the input power level that results in saturation.

Given the gain of 14.19 dB at 2400 MHz and the 1 dB compression point of 18.24 dBm, the input power that will result in saturation is 4.05 dBm. Therefore, one needs to ensure that the input to the amplifier is not higher than that power level.

Using the *SystemVue* software package the cascaded gain plot was produced and can be seen in Figure 4.5. It demonstrates the signal gain at the input and output of all the devices in the chain. The gain of the whole amplification stage is 20.6 dB prior to the, ZX10-2-42+, splitter and 17.6 dB after the splitter at the input of the antenna, due to the total loss of 3 dB during the signal splitting process.

In an ideal case a single amplifier with a gain of around 21 dB could have been used, however, the ZX60-272LN+ amplifiers are low cost and require a 5 Volt power supply which is the voltage level of the PSU that was utilised to power the system. Alternative amplifiers ([22], [23], [24]) were considered, however, higher gain is typically related to a higher supply voltage requirement, as well as higher cost. Therefore, in an effort to save time and money the available amplifiers were utilised in a cascaded configuration.

4.2 Antenna

The antenna design was based on the MIT IAP Radar System's metallic can circular wave guide antenna. This allowed the costs of the system to be kept low. Furthermore, by following the detailed design outline provided in [5] and [11], the antenna parameters from the documentation could be used. This was useful as specialised facilities like the anechoic chamber were not available, hence, the antenna gain and 3-dB beamwidth could not be determined through testing.

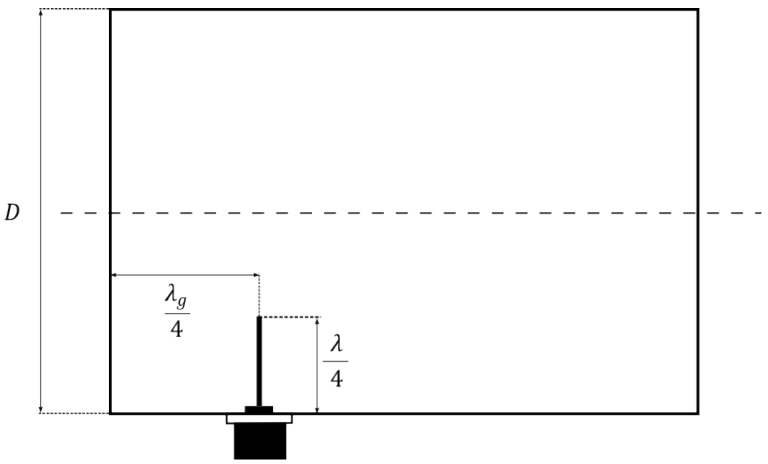

Figure 4.6: Circular waveguide antenna design parameters

4.2.1 Design Procedure

In order to successfully implement a circular wave guide antenna design, the parameters shown in Figure 4.6 need to be chosen based on the required frequency band of operation and a suitable mode of electromagnetic propagation.

The mode of signal propagation through the waveguide that was chosen is the TE11 circular waveguide mode. In order for other modes of propagation to not interfere, a 100 mm diameter (D) is chosen for the circular waveguide. Given the diameter, the TE11 circular waveguide mode cut-off wavelength is found to be 170 mm, which corresponds to a cut-off frequency of 1.8 GHz [11]. TE21 and TE01 modes of propagation have cut-off frequencies at 2.9 and 3.6 GHz, respectively, which makes the above mentioned waveguide diameter suitable for operation in the 2.4 GHz range.

As RadioCamera-S transmits a signal that is centred at the frequency of 2.4125 GHz, which corresponds to the wavelength (λ) of 124 mm, the antenna's probe needs to be one quarter wavelength in order to excite the TE11 mode, which is approximately 31 mm.

Another important parameter that places a requirement on the antenna design is impedance matching, which determines the amount of power that is transferred. In order to achieve a satisfactory impedance match the position of the probe needs to be a quarter of the guide wavelength from the back wall of the waveguide [25]. Therefore, given a guide wavelength (λ_g) of 185 mm at 2.4 GHz, the probe needs to be positioned 46 mm from the back wall of the waveguide.

Figure 4.7 shows the RadioCamera-S antennas, that were produced according to the above requirements.

Figure 4.7: RadioCamera-S antenna assembly

4.2.2 Antenna Characteristics

Based on the tests that were done during the design of the MIT IAP Radar System, an antenna that follows the design requirements that were outlined in the previous section can be expected to have the following characteristics:

- Peak gain of 7.2 dBi (decibel isotropic)
- 3-dB beamwidth of 72° in azimuth and elevation

Those two parameters can be derived from the far-field radiation patterns that are shown in Figure 4.8. The beamwidth parameter is greater than the required minimum elevation beamwidth of 26.6°, which was derived in Section 3.2.1.

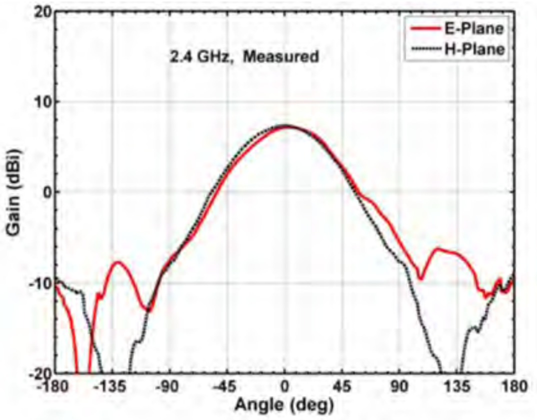

Figure 4.8: Measured far-field gain radiation patterns for the designed circular waveguide antenna [11]

In order to ensure that the transmitter antenna radiates more than 90 percent of the input power, the return loss (S11) parameter was measured using the Agilent

E5071B Network Analyser that was calibrated using Agilent's 85033E Calibration Kit. The band of interest is 2.3 GHz to 2.5 GHz, where the return loss should be less or equal to -10 dB in order to ensure that the required amount of power is transmitted. This can be shown by first calculating the reflected power (P_r) using the following equation:

$$P_r = 10^{\frac{\text{Return Loss}}{10}}, \tag{4.2}$$

where if a return loss of -10 dB is achieved P_r is equal to 0.1. The percentage of transmitted power (P_{tx})can then be calculated using Equation 4.3 [26].

$$P_t = 1 - P_r, \tag{4.3}$$

which results in P_t equal to 0.9 or 90 percent. The return loss measurement of the transmitter antenna can be seen in Figure 4.9, which also shows that the bandwidth of the antenna is 2.31 GHz to 2.76 GHz.

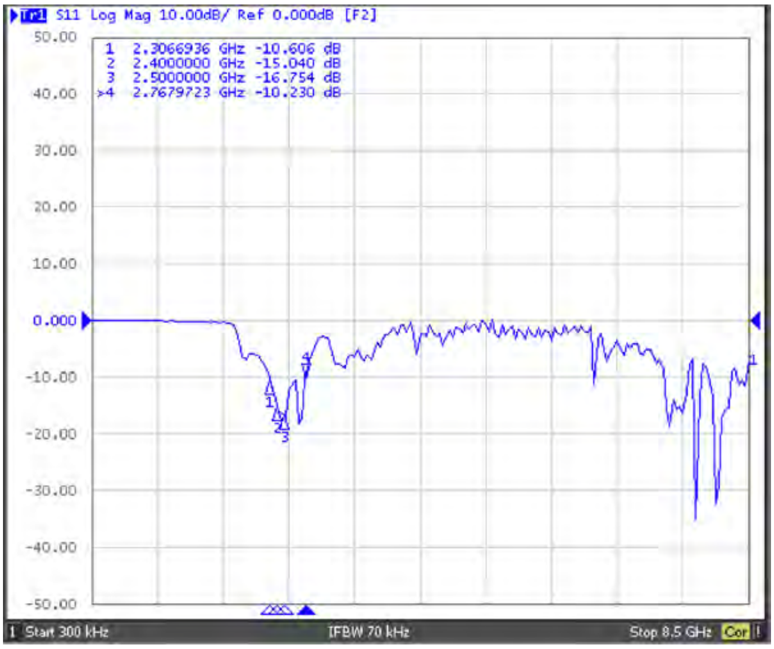
```
 1   2.3066936 GHz -10.606 dB
 2   2.4000000 GHz -15.040 dB
 3   2.5000000 GHz -16.754 dB
>4   2.7679723 GHz -10.230 dB
```

Figure 4.9: Transmitter antenna return loss measurement

The return loss of the receiver antenna was also measured and utilised for the purpose of tuning the antenna to the correct frequency band. The return loss plot for the receiver antenna can be seen in Figure 4.10, which shows that the bandwidth of the receiver's antenna is 2.18 GHz to 2.52 GHz wide.

Due to the fact that a dedicated antenna is used for the transmitter and for the receiver, the isolation between the antennas in this configuration, determines the isolation between the transmitter and the receiver channels of the radar, as well

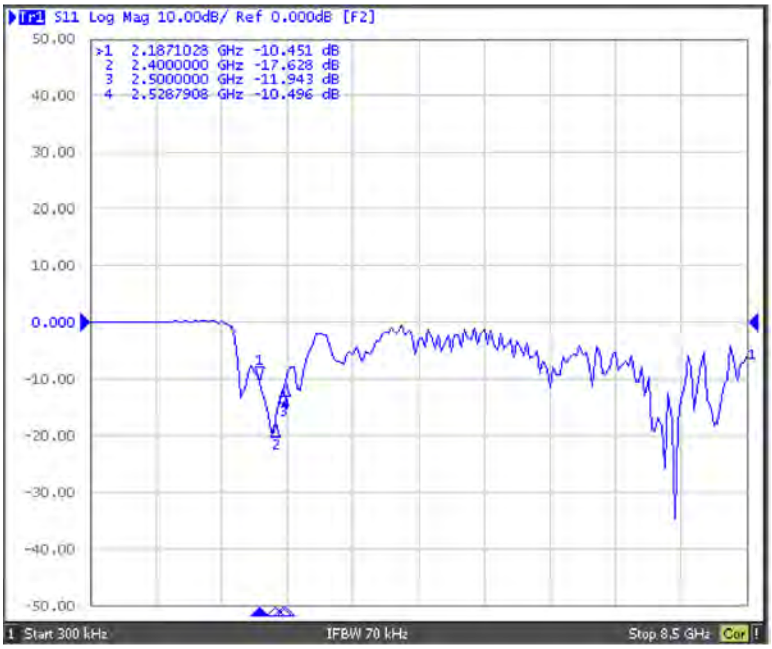

```
Tr1 S11 Log Mag 10.00dB/ Ref 0.000dB [F2]
>1  2.1871028 GHz -10.451 dB
 2  2.4000000 GHz -17.628 dB
 3  2.5000000 GHz -11.943 dB
 4  2.5287908 GHz -10.496 dB
```

Figure 4.10: Receiver antenna return loss measurement

as the level of the feed-through signal. In the MIT IAP Radar system the separation between the antennas was chosen to be 200 mm (probe-to-probe), which corresponded to an isolation of -39 dB.

The RadioCamera-S system assembly allows one to vary the probe-to-probe separation from 100 mm to 340 mm. In particular the isolation was measured at 200 mm and 340 mm probe-to-probe separations. Figure 4.11, demonstrates the S12-parameter plot of the transmitter and receiver antennas that are separated by 200 mm distance in order to achieve an isolation of -39 dB. This matches the MIT IAP Radar System parameter.

Then, the maximum separation of 340 mm is set and measured to provide an isolation of approximately -44 dB. This is shown in Figure 4.12. As a result, the maximum separation was employed.

4.3 Receiver

The receiver module consists of a reference channel and the main receiver channel. Both receiver channels employ the homodyne architecture, as they rely on mixers to shift the signals from the microwave frequency, down to baseband frequency range. The reference channel mixes the two offset transmitter side chirp signals to generate a reference beat frequency signal. The main receiver channel mixes one of the chirp signals with the received signal. A detailed description of each channel is provided below.

Figure 4.11: Antenna isolation with a 200 mm probe-to-probe separation

Figure 4.12: Antenna isolation with a 340 mm probe-to-probe separation

4.3.1 Receiver Reference Channel

The reference channel is a product of the two offset ramp signals and consists of a ZX05-43MH+ mixer and a VLFX-105 lowpass filter, with the Red Pitaya which is used to digitise the signal. Those components, as well as the signal levels can be seen in Figure 4.13.

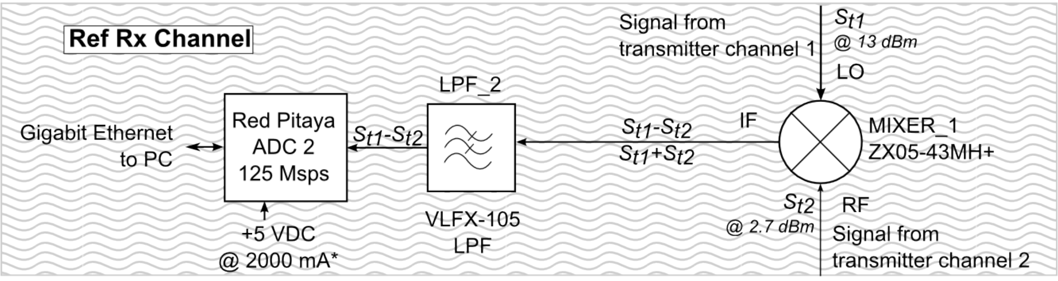

Figure 4.13: Receiver reference channel signal block diagram

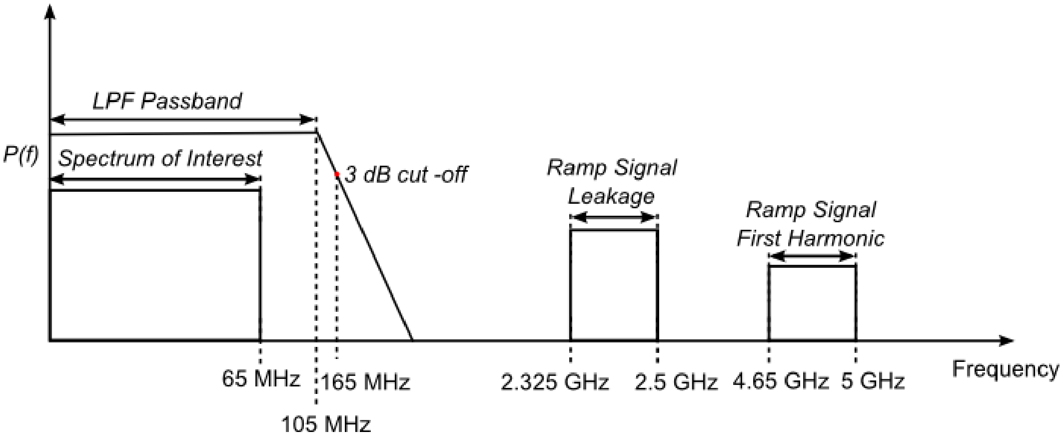

Figure 4.14: The effect of the VLFX-105 low pass filter on the receiver spectrum

The ZX05-43MH+ is a wideband, level 13 mixer [27]. This means that it requires a signal with a power level of +13 dBm to drive its LO port and has a wide operational frequency range of 824 MHz to 4200 MHz. This satisfies the requirements for the RadioCamera-S signals as the proposed operating frequency is in range of 2300 MHz to 2500 MHz.

The VLFX-105 is a lowpass filter that has a passband of DC-105 MHz, with a gentle roll off. Due to this, it is used for filtering out the high frequency components from the baseband spectrum, as the mixer has a LO-IF isolation of 24 dB, which results in the presence of the attenuated ramp signals present in the range of 2.325 to 2.5 GHz, with a harmonic at 4.65 to 5 GHz. This is demonstrated in Figure 4.14.

The gentle roll off and the high cut-off frequency of 105 MHz, render this current filter incapable of being utilised for the Mode Two operation of the radar. A suitable filter for the implementation of Mode Two will have a cut-off of around 30 MHz to 40 MHz and a steep roll off. Such a filter was unavailable at the time and the author was unable to procure one due to the time constraints.

Hence, the sole reason for incorporating the VLFX-105 filter in to the design was to filter the high frequency components from the baseband spectrum. This ensures that the high frequency harmonics, that were produced by the VCO and leaked into the RF port of the mixer from the LO port, do not fold over into the frequency

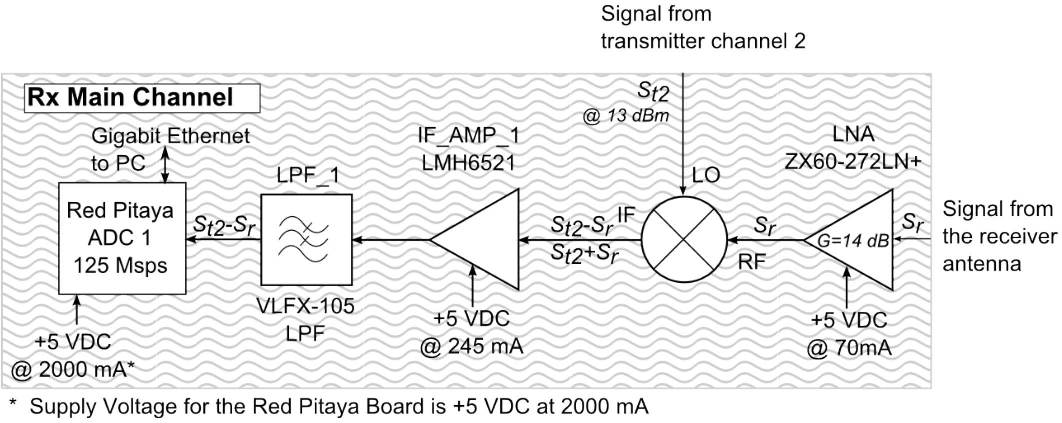

Figure 4.15: Receiver main channel signal block diagram

spectrum of interest when the ADC samples the received signal.

As the reference receiver channel only consists of two components, the input saturation point is determined by the mixer. Hence, the RF input of the mixer must not be higher than 9 dBm in order to avoid saturating the channel.

It has to be noted that it is good practice to operate atleast 5 dB below this point. Hence, if an input of about 4 dBm is fed to the RF port, the output at the IF port should be approximately -2.3 dBm, as the mixer has a typical conversion loss of 6.3 dB.

4.3.2 Receiver Main Channel

The main receiver channel, consists of a ZX60-272LN+ LNA, ZX05-43MH+ mixer, LMH6521 IF amplifier, VLFX-105 lowpass filter and the Red Pitaya board for digitising the signal. Figure 4.15 demonstrates the signal block diagram.

The analysis of the main receiver channel entails the derivation of the input saturation point, the cascaded Noise Figure (NF), sensitivity and the dynamic range, which are carried out in following sections.

Main Channel Input Saturation Analysis

In order to ensure that the receiver is not saturated, an analysis of the receiver component properties needs to be carried out and the saturation power of each component needs to be determined. Table 4.1 summarises the gain, conversion losses, insertion losses, as well as the 1 dB compression points of the main receiver channel components, which will be used to determine the receiver saturation point.

Table 4.1: Main receiver channel component parameters

Device	**Gain**	**1 dB compression**
	dB	dBm
ZX60-272LN+ LNA	14.19	18.24
ZX05-43MH+	-6.3	9
LMH6521	20	17
VLFX-105	-1.2	-

Given the current receiver structure, one is required to compute the saturation points for each of the two amplifiers, as well as the mixer. The lowest power level that will cause saturation of any of the aforementioned components will be effectively the receiver saturation input power.

The saturation power was already computed for the ZX60-272LN+ amplifier in Section 4.1.2 and found to be 4.05 dBm. The input saturation power (P^{sat}_{mixer}) for the ZX05-43MH+ mixer can be found to be equal to -5.19 dBm using the following equation:

$$P^{sat}_{mixer} = P^{1dB}_{mixer} - G_{LNA} \tag{4.4}$$

where P^{1dB}_{mixer} is the compression point of the mixer and G_{LNA} is the gain of the LNA.

Lastly, the input saturation of the video amplifier (P^{sat}_{IF}) can be calculated to be -10.89 dBm using Equation 4.5

$$P^{sat}_{IF} = P^{1dB}_{IF} - G_{IF} - G_{mixer} - G_{LNA} \tag{4.5}$$

where P^{1dB}_{IF} is the compression point of the video amplifier, G_{IF} is the gain of the video amplifier and G_{mixer} is the conversion loss of the mixer.

On the basis of the three saturation points that were computed above, the main receiver channel saturation power is -10.89 dBm, as if a higher power value is fed into the input of the receiver, the video amplifier will saturate.

Main Channel Noise Figure Analysis

A noise figure of the receiver measures the degradation of the signal-to-noise ratio (SNR) of a input signal. Sources of noise include thermal noise, shot noise and other effects due to physics of various types of transistors, all of which are combined into the noise factor (F) [5]. The noise factor can be expressed in decibels and is then known as the noise figure.

To compute the noise figure of the receiver, the gain, as well as the noise factor of each component in the receiver chain needs to be known. The main receiver channel component parameters are shown in Table 4.2. This analysis does not include the losses associated with the cable that connects the receiver antenna to the receiver itself. Hence, the following analysis determines the noise figure of the radar receiver and not that of the whole radar system.

Table 4.2: Main receiver channel component parameters

Device	**Gain**	**Noise Figure**
	dB	dB
ZX60-272LN+	14.19	1.1
ZX05-43MH+	-6.3	6.3
LMH6521	20	7.3
VLFX-105	-1.2	1.2

The noise figure of the receiver can be calculated using Equation 4.6, where F_{LNA}, F_{mixer}, F_{IF}, F_{LPF} are the noise factors of the LNA, mixer, IF amplifier and the low pass filter respectively. G_{LNA} corresponds to the gain of the LNA, G_{mixer} is the conversion loss that is associated with the mixer and G_{IF} is the gain of the video amplifier. Those values are all required to be expressed in linear units. Hence, taking into considerations the component parameters and by utilising the provided equation, the main receiver channel noise figure is found to be 5.14 dB.

$$NF = 10 \times \left(F_{LNA} + \frac{F_{mixer} - 1}{G_{LNA}} + \frac{F_{IF} - 1}{G_{LNA} G_{mixer}} + \frac{F_{LPF} - 1}{G_{LNA} G_{mixer} G_{IF}} \right) \tag{4.6}$$

A more detailed description of the noise figure is provided in Appendix B.3.1.

Receiver Sensitivity

Receiver sensitivity defines the weakest signal that can be detected by the radar receiver. This is also known as the Minimum Detectable Signal (MDS) and is measured in dBm [13] [5]. The noise that is associated with the radar receiver essentially sets the limit on the MDS, as is shown by Equation B.20.

$$MDS = 10log_{10}\left(\frac{kT_0}{1mW}\right) + NF_{sys} + 10log(BW_{rec}) + SNR_{out}, \tag{4.7}$$

where k is the Boltzmann's constant (1.38×10^{-23} joules/Kelvin), T_0 is the standard temperature equal to 290°, BW_{rec} is the receiver bandwidth (Hz) and SNR_{out} is the minimum required SNR for detection.

Hence, in order to calculate the MDS, the receiver bandwidth can be approximated to be 62.5 MHz, based on the sampling rate of the Red Pitaya and a signal-to-noise ratio that can be set to 13.4 dB, which corresponds to the gold standard of radar performance providing the probability of detection of 95 percent and a probability of false alarm of 10^{-6} [5]. Finally, given the noise figure of 5.14 dB, the MDS of the RadioCamera-S receiver can be approximated to be -77.5 dBm. Similarly to the noise figure analysis, this receiver sensitivity analysis derives the MDS for the RadioCamera-S receiver and not the radar system. This occurs because the power loss of the cable that attaches the receiver antenna to the RadioCamera-S receiver is not taken into consideration in this analysis.

Receiver Dynamic Range

The dynamic range of the receiver is defined to be the difference between the peak signal that can be processed by the receiver without the receiver saturating and the MDS. Additionally, this dynamic range should be facilitated by the ADC that was used to digitise the signal.

The maximum signal that the receiver can process was computed for the RadioCamera-S receiver and found to be approximately -10.89 dBm. The MDS of the receiver was found to be -77.48 dBm. Therefore, the dynamic range of the receiver is 66.59 dB. This dynamic range should be able to be processed by the receiver as it is less than the expected theoretical maximum dynamic range of Red Pitaya's ADC (86.7 dB, as mentioned in Section 3.1.4).

4.4 System Housing

The system housing that was required to provide a base for the three system modules was designed in accordance with the following requirements:

- Enable easy access to the components for debugging
- Provide a neat layout and wiring distribution
- Portable housing that can be easily transported
- Neat front panel design for external connections
- Aluminium body in order to provide a common ground for the components

All the above requirements were implemented in a system housing, which was designed using *SolidWorks* CAD software package. The complete system assembly is shown in Figure 4.16, which demonstrates the placement of the main system components.

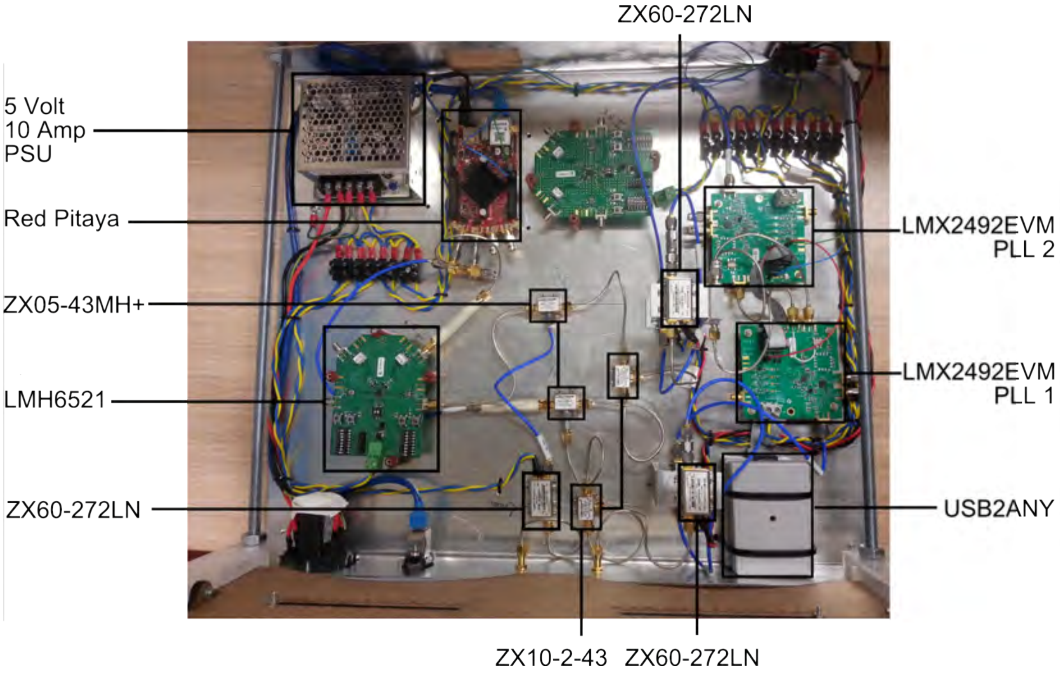

Figure 4.16: RadioCamera-S systema assembly

4.5 Summary

This chapter introduced the reader to the hardware implementation of the RadioCamera-S prototype by providing a detailed description of each of the three modules. The transmitter module was discussed from the point of the two main functions that it performs, which are waveform generation and signal amplification. Then a description of antenna design requirements is provided in conjunction with the performance characteristics, which are achieved if those requirements are fulfilled. The receiver module is described next by analysing each channel separately.

Together the three modules form a complete radar system, the signal block diagram of which is shown in Figure B.1.

Chapter 5

RadioCamera-S Testing and Results

The test procedures that are outlined in this chapter relate to the performance analysis of the transmitter and the receiver modules, as well as, the performance of the completely integrated system. The transmitter tests can be seen in Section 5.1, with the receiver module testing provided in Section 5.2. The system tests are divided into delay-line tests in Section 5.3 and the fully integrated system tests as described in Section 5.4.

Each section aims to describe the testing procedures, demonstrate the results and provide a brief discussion.

5.1 Transmitter Testing

The transmitter tests are divided into the waveform generation tests and the amplification stage power level verification.

5.1.1 Waveform Generation

In order for RadioCamera-S to operate as a FMCW ranging and imaging radar, the output of the waveform generator is required to span the bandwidth of interest and follow a correct modulation scheme. As was proposed in Section 3.2.1 and 3.2.2, the two waveforms that will be examined are:

Waveform 1 - 175 MHz bandwidth, 50 μs up ramp with a 25 μs down ramp

Waveform 2 - 175 MHz bandwidth, 100 μs up ramp with a 25 μs down ramp

The output of the LMX2492EVM module is connected to the Agilent Technologies Field Fox Spectrum Analyser in order to examine the spectrum of the output waveform. In addition to that, the Agilent Infiniium MS09104 Oscilloscope is used to examine the tuning voltage of the waveform, as well as, the state of the PLL in order to determine if the PLL is in the phase locked state for the entire duration of the frequency sweep.

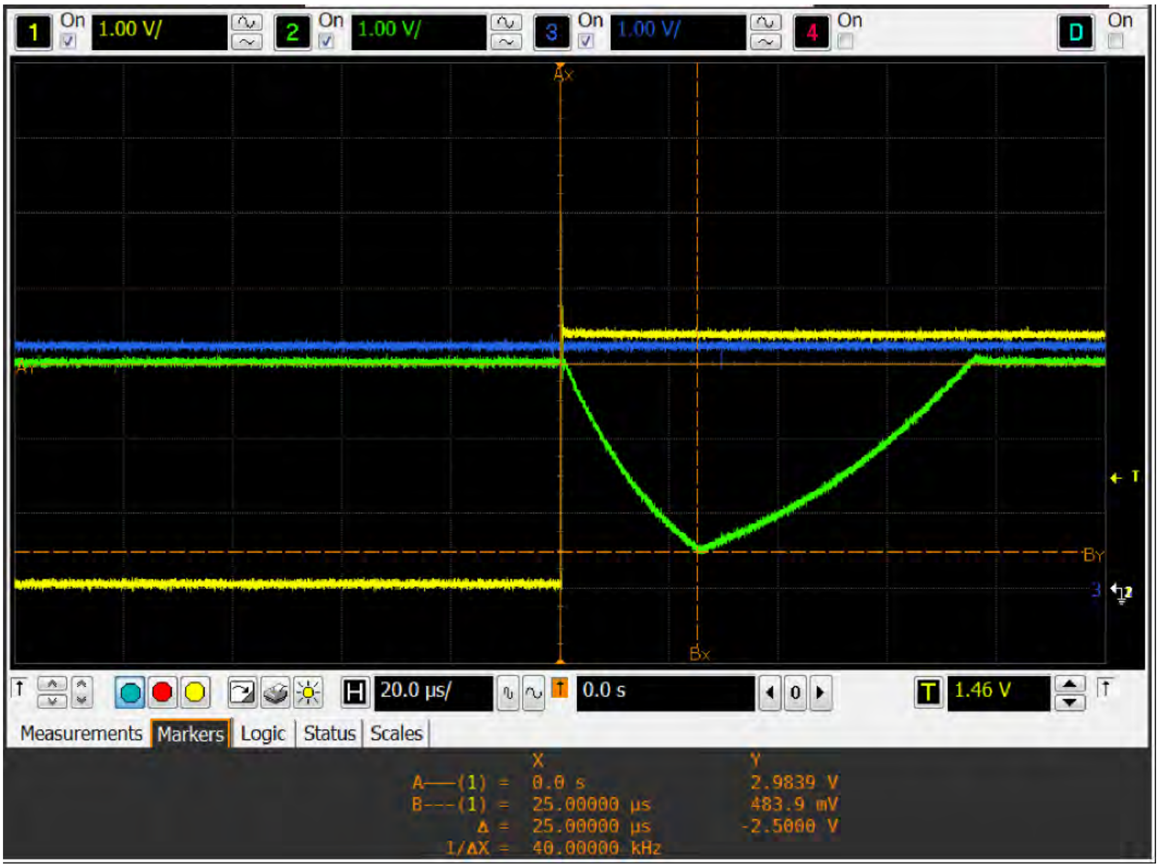

```
                  X                    Y
A——(1) =   0.0 s               2.9839 V
B---(1) =  25.00000 µs         483.9 mV
      Δ =  25.00000 µs        -2.5000 V
   1/ΔX =  40.00000 kHz
```

Figure 5.1: Tuning voltage and phase lock indicator for the waveform that sweeps through a 175 MHz bandwidth with a 75 μs PRI

Figure 5.1 demonstrates signals that are associated with **waveform 1**, the tuning voltage is shown by the green trace, the phase lock indicator is represented by the blue trace and the trigger signal, which is the yellow trace. The fact that the phase lock indicator is always high, means that the phase is locked for the duration of the modulated waveform sweep, which is required in order to ensure that the output of the VCO corresponds to the programmed waveform. Markers demonstrate that the up ramp is indeed 100 μs and the peak-to-peak amplitude of the tuning voltage is 2.5 Volts, which corresponds to a frequency excursion of 175 MHz.

Signals that characterise **Waveform 2** can be seen in Figure 5.2 and demonstrate that the voltage excursion is 2.5 Volts, which results in a 175 MHz sweep. The phase lock indicator is also in a logic high state, meaning that phase lock is maintained for the duration of the waveform.

The spectrum of both of the above waveforms was observed using the Field Fox Spectrum Analyser and can be seen in Figure 5.3.

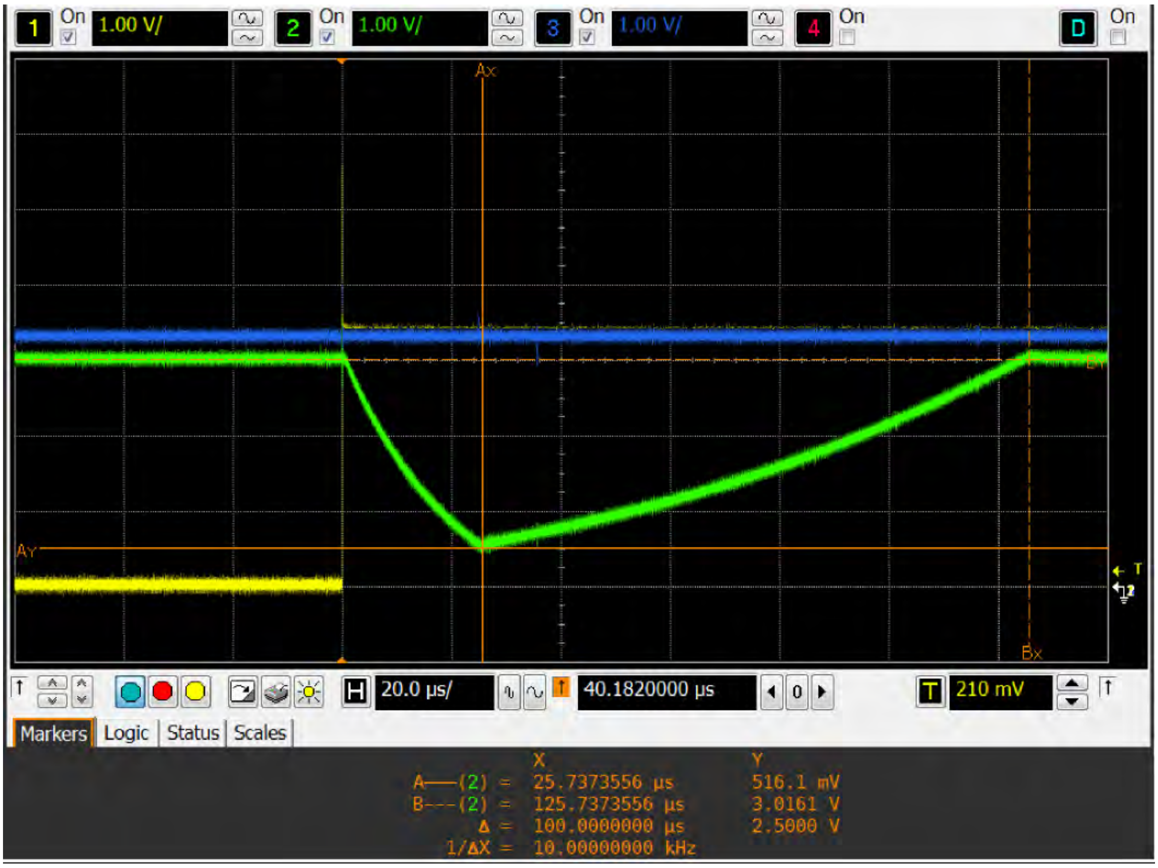

```
              X                     Y
A——(2) =  25.7373556 µs         516.1 mV
B---(2) =  125.7373556 µs        3.0161 V
      Δ =  100.0000000 µs        2.5000 V
   1/ΔX =  10.00000000 kHz
```

Figure 5.2: Tuning voltage and phase lock indicator for the waveform that sweeps through a 175 MHz bandwidth with a 125 μs PRI

5.1.2 Power Levels

To ensure that the output power of the two transmitted channels does indeed correspond to the values projected using the information from the component datasheets one is required to step through the signal chain and verify the power levels.

This is accomplished by using the Field Fox spectrum Analyser to measure the power levels on the segments of interest. To produce accurate measurements, the loss in the cable that was used to interface between the Device Under Test (DUT) and the spectrum analyser was accounted for in the measurements. The cables that were used to connect the components also need to be considered in the calculations, as the frequency of operation is in the range of 2.4 GHz and cable losses typically increase as the frequency is increased.

Figure 5.4 demonstrates the projected values together with the measured values. The plot demonstrates that the initial value at the output of the LMX2492EVM varies from the expected value by a margin of 7.6 dB, this error could possibly be explained by a faulty connector on the board or a bad solder joint. It was decided not to attempt to resolder the SMA connector, as that would require a large amount of heat applied to the board, which could result in permanent damage to other components. Given that the gain of the transmitter stage is sufficient to overcome

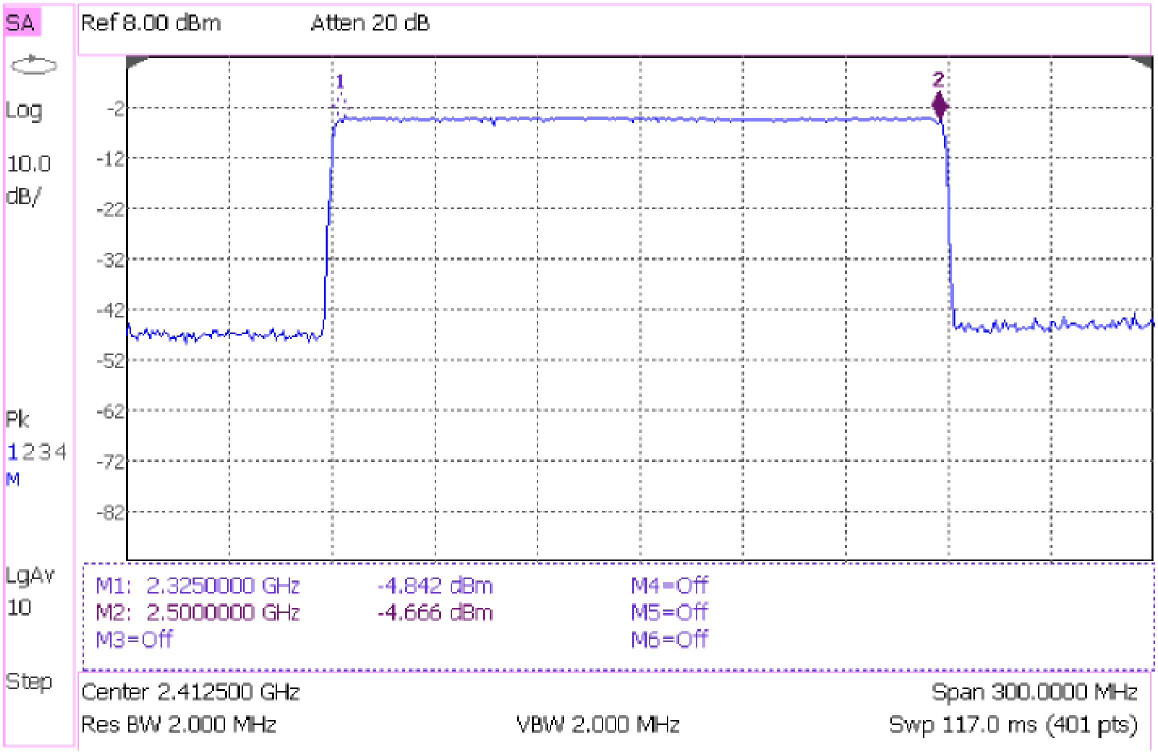

SA

Ref 8.00 dBm Atten 20 dB

Log 10.0 dB/

Pk 1 2 3 4 M

LgAv 10

Step

M1: 2.3250000 GHz -4.842 dBm M4=Off
M2: 2.5000000 GHz -4.666 dBm M5=Off
M3=Off M6=Off

Center 2.412500 GHz Span 300.0000 MHz
Res BW 2.000 MHz VBW 2.000 MHz Swp 117.0 ms (401 pts)

Figure 5.3: Spectrum of the waveform that sweeps through the 175 MHz, which is applicable to **waveform 1** and **waveform 2**

the low power level at the LMX2492EVM output, the problem does not cause a detrimental effect on the performance of the system.

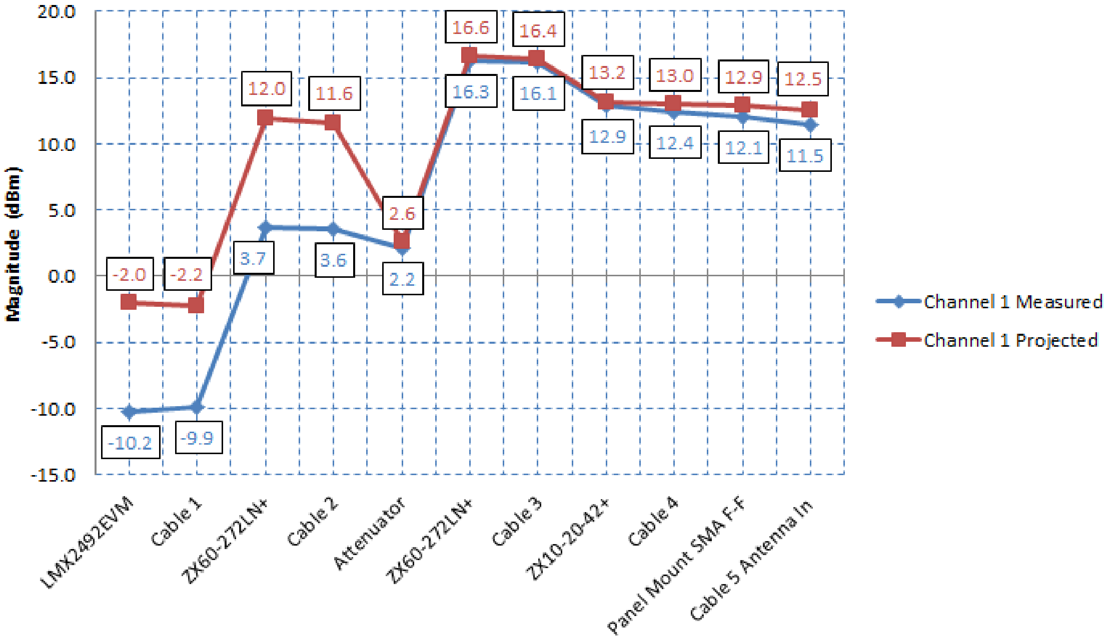

Figure 5.4: Transmitter channel 1 power levels

The rest of the power levels are sufficiently close to the projected values, except for the output of the front-panel connector and the cable connecting the antenna to the output port. These two values are down by approximately 1 dB, which can be attributed to measurement error, as the Spectrum Analyser typically has a +/- 0.5 dB amplitude accuracy. Another possible cause for this fault could be damage to the cable, that was caused by excessive bending.

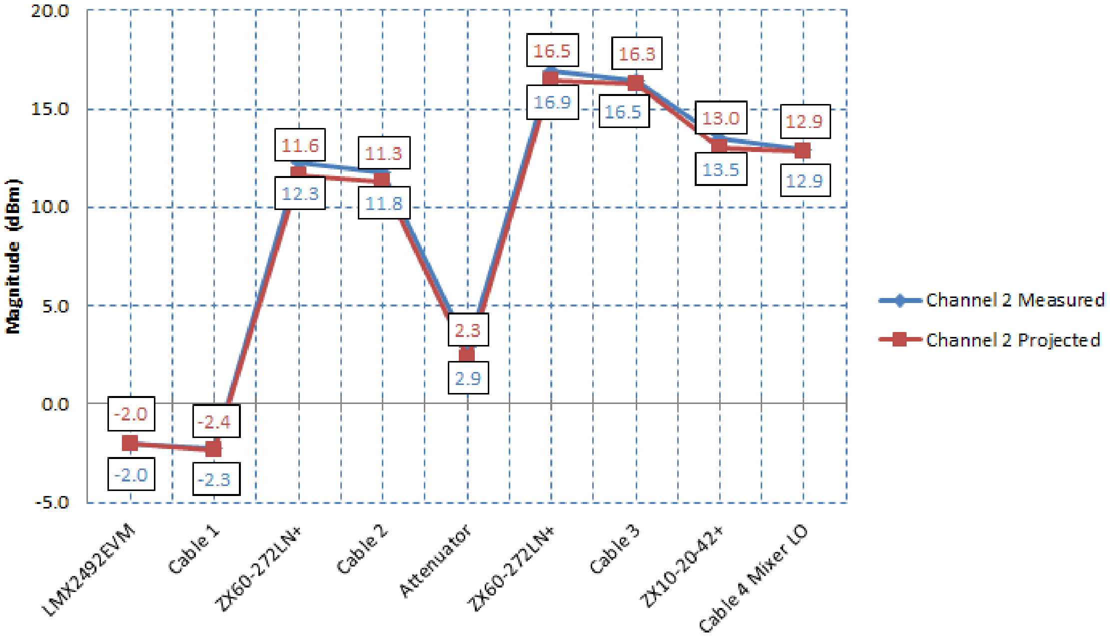

Figure 5.5: Transmitter channel 2 power levels

Transmitter channel 2 power levels can be examined in Figure 5.5, where the worst disparity is equal to 0.7 dB, which occurs at the output of the first amplifier. This can be explained by the fact that the gain of the amplifier is not flat across the whole band and the projected value could be off by a small amount. That, in conjunction with the measurement uncertainty of the equipment could be the result of the disparity.

Overall the power levels conform with the expected values and the outputs are sufficiently high to drive the LO ports of the mixers and provide the needed power to the transmitter antenna.

5.2 Receiver Power Level Verification

The power levels of the two receiver channels were analysed using a similar procedure to that outlined in Section 5.1.2.

The input power to the receiver was set to a power level of -26.2 dBm. This corresponds to the maximum output power of the transmitter with the antenna isolation added to it, which is the power level of the direct coupling, or feed-through signal.

The actual calculation determined the maximum signal to be at a level of -27.5 dBm, however, as the attenuators that were used, had a +/- 0.5 dB variance the resultant input signal was higher than expected. This explains the disparity in the projected and measured values in Figure 5.6.

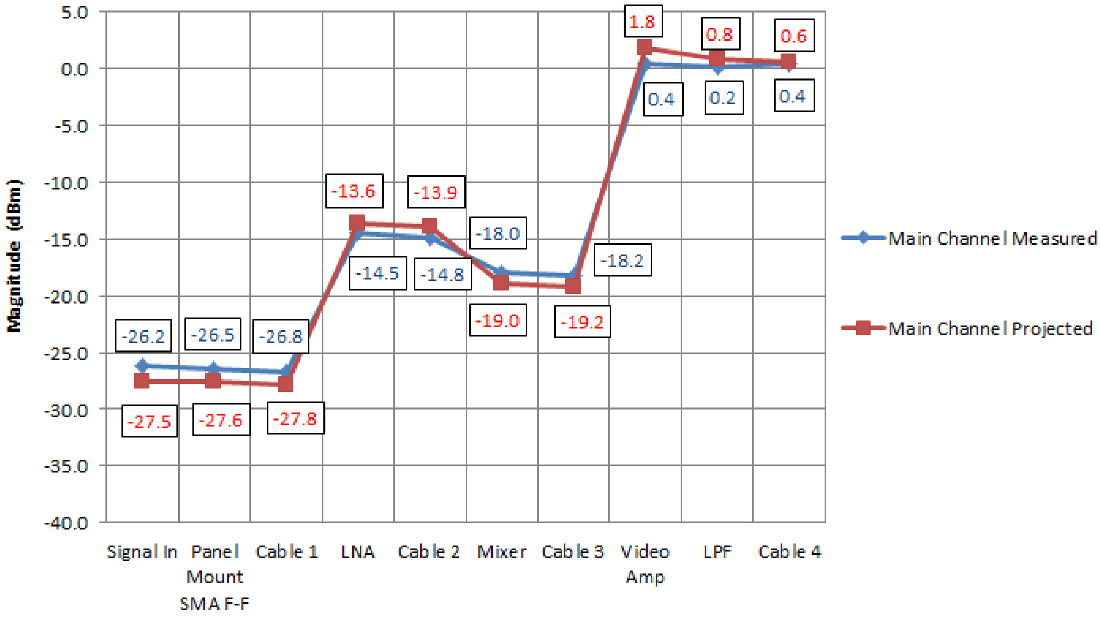

Figure 5.6: Main receiver channel power levels

The power levels associated with the reference channel of the receiver can be examined in Figure 5.7. The projected values conform to that of the measured ones, it should be noted that the loss associated with the cable that connects the spectrum analyser with the DUT reduces greatly at baseband frequencies, this was accounted for, for components at the IF output port of the mixer.

The projected values conform to the measured values for the receiver channels. The expected power levels at the input of the signal digitiser are 0.4 dBm for the main channel and -3.3 for the reference channel. The lower power level of the reference channel can be tolerated, as there are no signal returns that can interfere with it, as the reference channel is a product of two internally generated waveforms.

5.3 Delay-Line Tests

The delay-line test makes use of two LMR400 cables that have a 50 ohm impedance, with the associated delays of:

Cable 1 - 59.96 ns

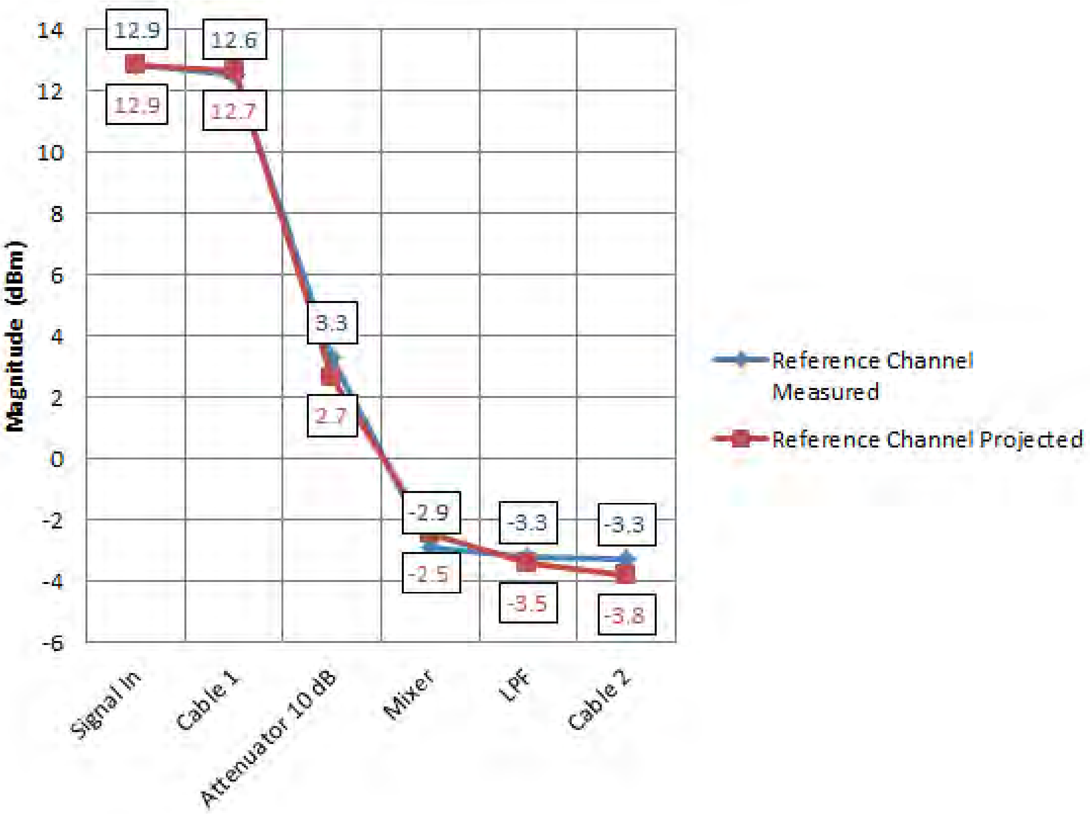

Figure 5.7: Reference receiver channel power levels

Cable 2 - 49.57 ns

This adds up to a total of 109.53 ns. The cable adds an additional 6.45 dB of attenuation. In order to simulate a feed-through signal return, the input to the receiver is required to be lowered to -27.54 dBm. To achieve this, given an output signal of 12.5 dBm, approximately 33 dB of attenuation is required, which was realised by utilising three 10 dB attenuators and a single 3 dB attenuator. This resulted in an input of -27.8 dBm, which is sufficiently close to the expected feed-through power.

The test procedure entails the following: first set up the two waveform generators to produce waveforms that have a 50 μs up ramp and a 25 μs down ramp. The two waveforms must be offset and operated in mode one, as described in Section 3.3.1, where the transmitting waveform is leading the internal transmitter channel by a time delay of 2 μs. This is expected to produce two components at the reference channel of the receiver, one at 7 MHz and the second at 14 MHz. The reference channel signal spectrum at the input to the Red Pitaya was observed using the Field Fox Spectrum Analyser, with the beat frequency spectrum shown in Figure 5.8.

The spectrum of the main receiver channel is shown in Figure 5.9. The two peaks now appear at approximately 7.381 MHz and 14.763 MHz. This is due to the additional 109.53 ns delay, as the total time offset between transmitter channel two waveform and the delayed return is 2 μs $+0.109$ μs $= 2.109$ μs. This time delay can

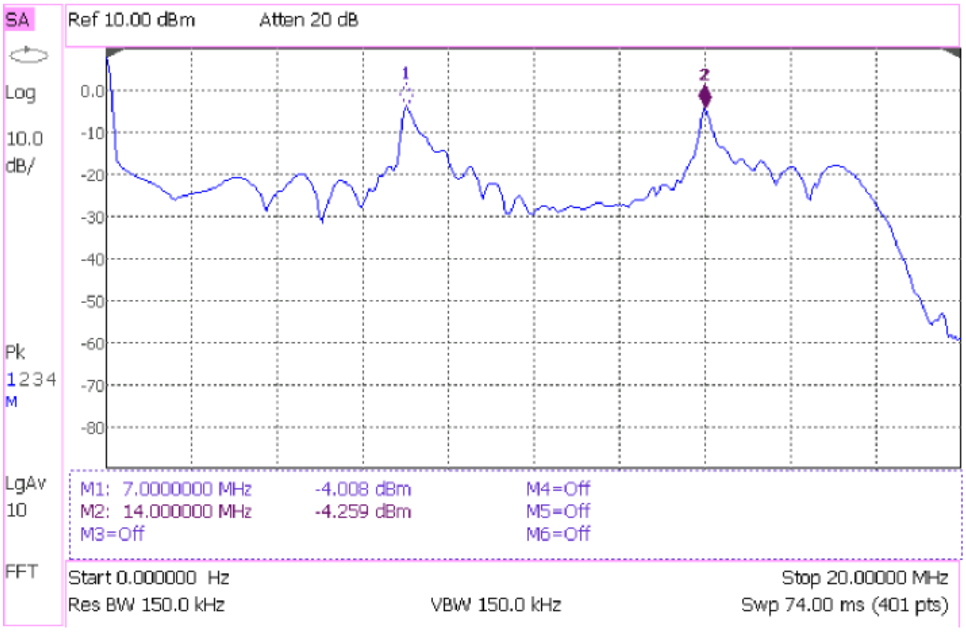

Ref 10.00 dBm Atten 20 dB

M1: 7.0000000 MHz -4.008 dBm M4=Off
M2: 14.000000 MHz -4.259 dBm M5=Off
M3=Off M6=Off

Start 0.000000 Hz Stop 20.00000 MHz
Res BW 150.0 kHz VBW 150.0 kHz Swp 74.00 ms (401 pts)

Figure 5.8: Receiver Reference Channel Spectrum during the Delay Line Test, where two waveform with a bandwidth of 175 MHz, 50 μs up ramp and a 25 μs down ramp were offset by a time delay of 2 μs

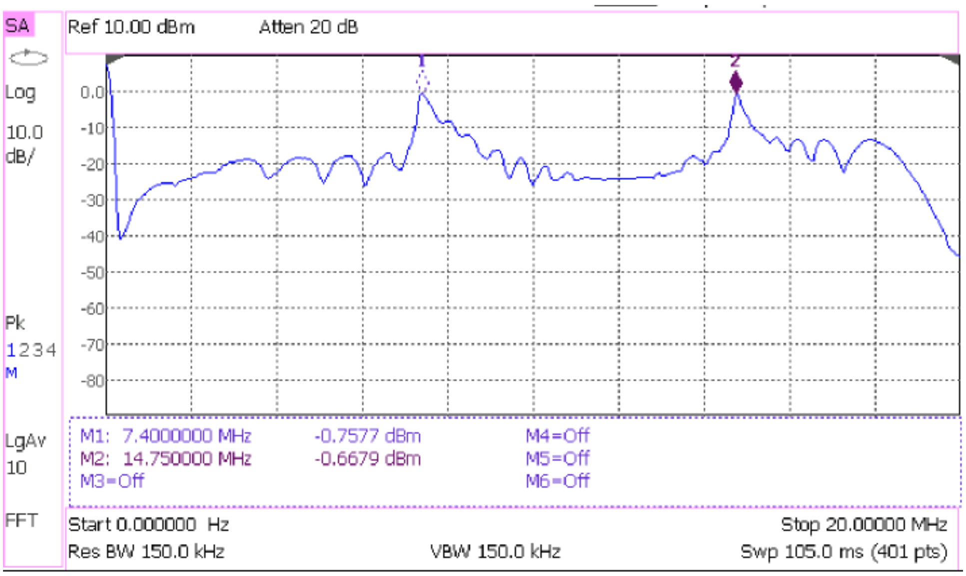

Ref 10.00 dBm Atten 20 dB

M1: 7.4000000 MHz -0.7577 dBm M4=Off
M2: 14.750000 MHz -0.6679 dBm M5=Off
M3=Off M6=Off

Start 0.000000 Hz Stop 20.00000 MHz
Res BW 150.0 kHz VBW 150.0 kHz Swp 105.0 ms (401 pts)

Figure 5.9: Receiver Main Channel Spectrum during the Delay Line Test, where two waveform with a bandwidth of 175 MHz, 50 μs up ramp and a 25 μs down ramp were offset by a time delay of 2 μs

be related to frequency by using Equation 3.5 to derive the aforementioned 7.381 MHz beat frequency that is associated with the 50 μs up ramps of the waveform and the 14.763 MHz beat frequency component that is associated with the 25 μs down ramp. This occurs as the spectrum analyser is sampling both the up ramp and the down ramp. In order for useful measurements to be taken, either the up ramp or the down ramp must be sampled. This can be achieved with the Red Pitaya, as is shown in Figure 5.10, where only the 50 μs up ramp is sampled, which results in the absence of 14 and 14.763 MHz components from the spectrum.

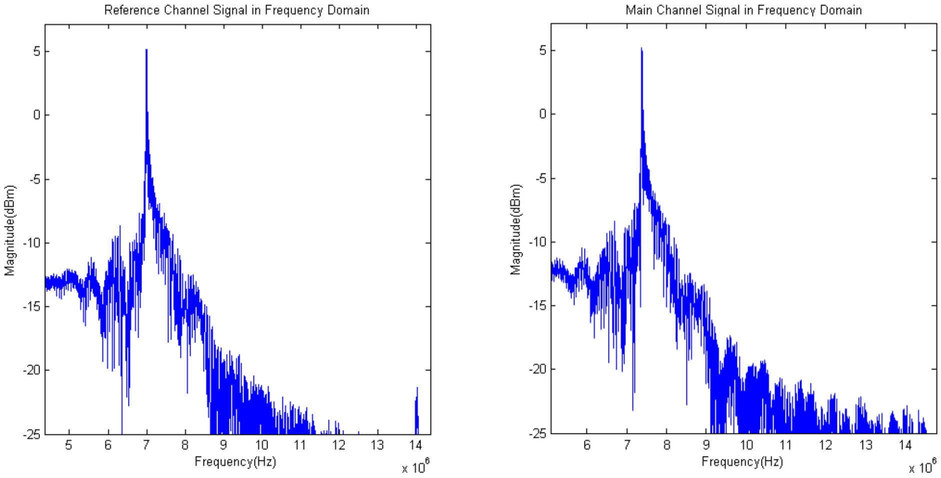

Figure 5.10: Reference and Main Receiver Spectrums Acquired by the Red Pitaya, where two waveform with a bandwidth of 175 MHz, 50 μs up ramp and a 25 μs down ramp were offset by a time delay of 2 μs and only the 50 μs up ramp was sampled

5.4 Integrated System Tests

The tests in this section aim to demonstrate that the radar can be operated in the FMCW ranging mode, as well as implement operation mode number one for the purpose of the feed-through signal filtering.

The waveform that was used for the purpose of the tests has a bandwidth of 175 MHz and a total PRI of 75 μs, with a up ramp of 50 μs and a down ramp of 25 μs. The part of the waveform that was digitised by the Red Pitaya is the down ramp. This was utilised due to the fact that a shorter sweep corresponds to a greater spectral spread and as the scene is limited to 40 m, it is advantageous to spread the targets as broadly as possible across the beat frequency spectrum.

The series of tests starts by obtaining a return from a scene without the presence of a reference reflector. The scene is shown in Figure 5.11, which is a 40 m corridor. The transmitter is setup in a way that the transmitter channel 2 is lagging the waveform at channel 1 by 560 ns. This places the feed-through component at 4 MHz in the main receiver channel, with the reference channel having a peak of 3.93 MHz. The raw signal returns can be seen in Figure 5.12.

A Matlab program is implemented to search for the peak in the reference channel and use it to determine the true range of the targets in the scene. The output of this process is demonstrated in Figure 5.13, where the feed-through is the component

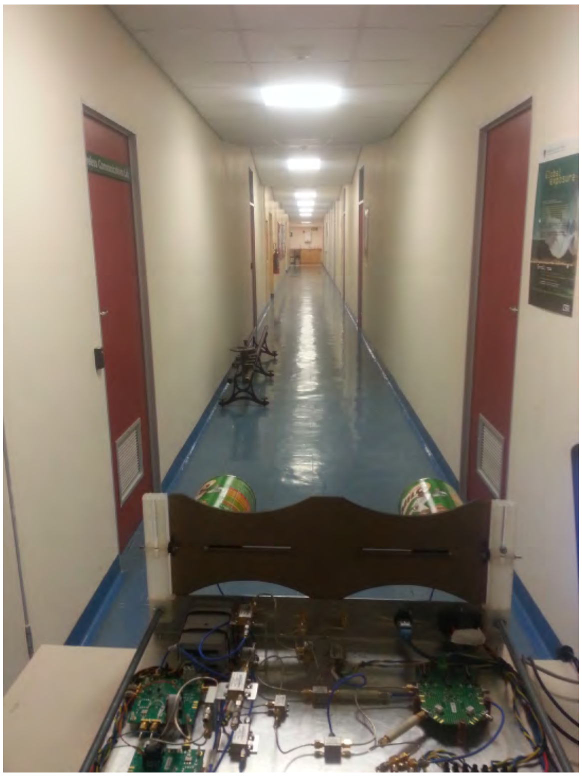

Figure 5.11: Test scene for the RadioCamera-S integration tests

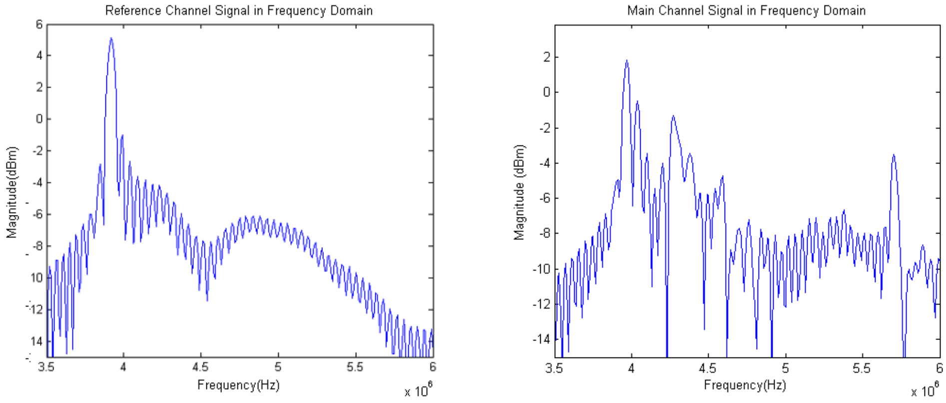

Figure 5.12: The two receiver channels in the frequency domain

that has the highest power and a return from the far wall of the corridor can be seen at approximately 39 m.

Next, a trolley with a reflector, which can be seen in Figure 5.14, was placed at 4.5 m, 16 m and 28.8 m away from the radar. The return signals were recorded and overlaid on a same graph, which can be seen in Figure 5.15, where the red plot shows the reflection when the trolley was placed at 4.5 m, the black plot shows the return when the trolley was located 16 m away from the radar and the blue plot corresponds to the trolley located 28 m down the passage.

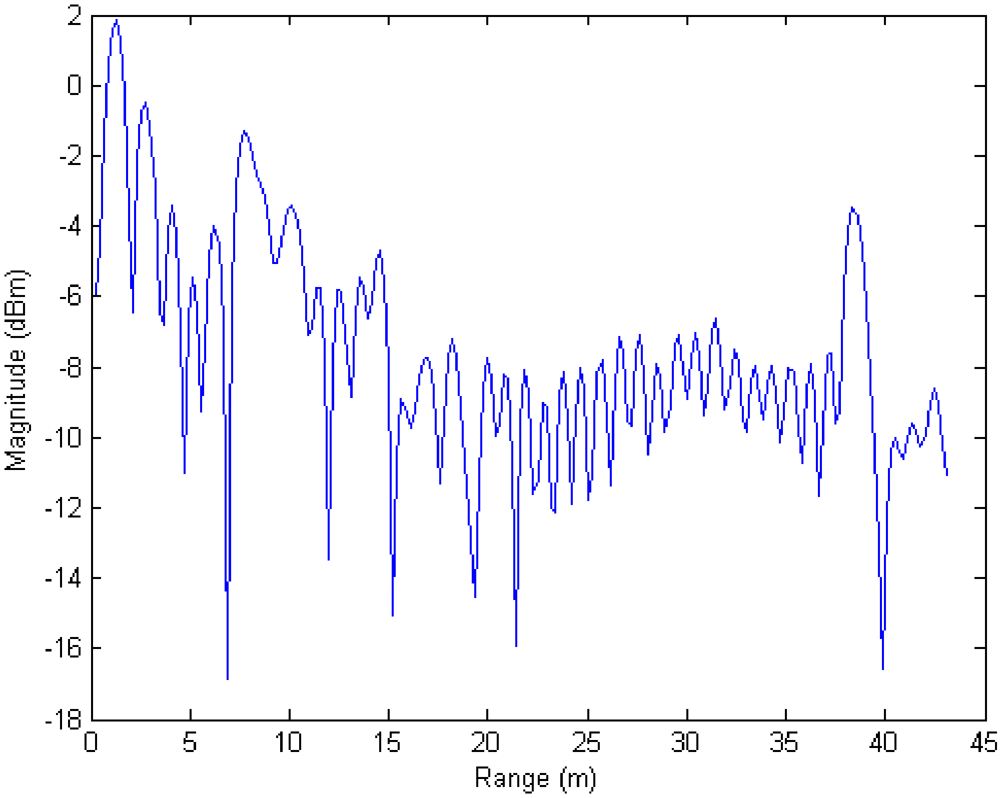

Figure 5.13: Receiver main channel Magnitude-Range plot

In most cases, unless the target is located very close to the radar the feed-through component is the most prominent signal in the spectrum, in order to reduce it, the characteristics of the video amplifier can be utilised. Figure 5.16 demonstrates the amplification profile, the markers show that if a component is placed at 1 MHz, the signal level will be approximately 3 dB lower than the component at 1.3 MHz, hence operation mode one can be utilised and the feed-through component can be placed at 1 MHz by setting a 130 ns delay between the transmitted waveforms, with transmitter channel 2 leading channel 1.

The results of this operation can be seen in Figure 5.17, where the blue plot corresponds to the return signals if one places the components in the frequency band where video amplifier has a flat gain response and the red plot corresponds to the case when the feed-through is placed at 1 MHz.

The result of this manipulation also causes the nearby components to be attenuated, however, the overall effect results in a decrease in the dynamic range requirement, atleast by a factor of 4 dB. In an ideal case a highpass filter with a steep cut-off should be used, but due to the fact that such a filter was unavailable during testing, the amplifier response was adapted to demonstrate the concept of the feed-through removal using the two-channel approach.

Lastly, the Range-Time-Intensity (RTI) plot was produced, which consists of 100

Figure 5.14: The trolley with a reflector that was used as a target for testing the FMCW ranging mode

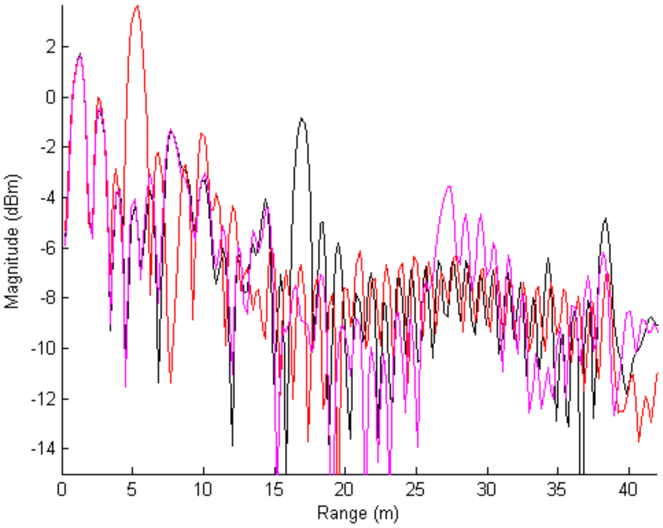

Figure 5.15: Overlay of returns that were collected from scenes with three different reflector locations

transmit-receive sessions, with approximately 1 second interval between each one, due to the fact that the Red Pitaya had to be reset after each session. Figure 5.18 shows the RTI plot, where no feed-through attenuation was carried out and Figure 5.19 demonstrates the case, where mode one was used to reduce the power level

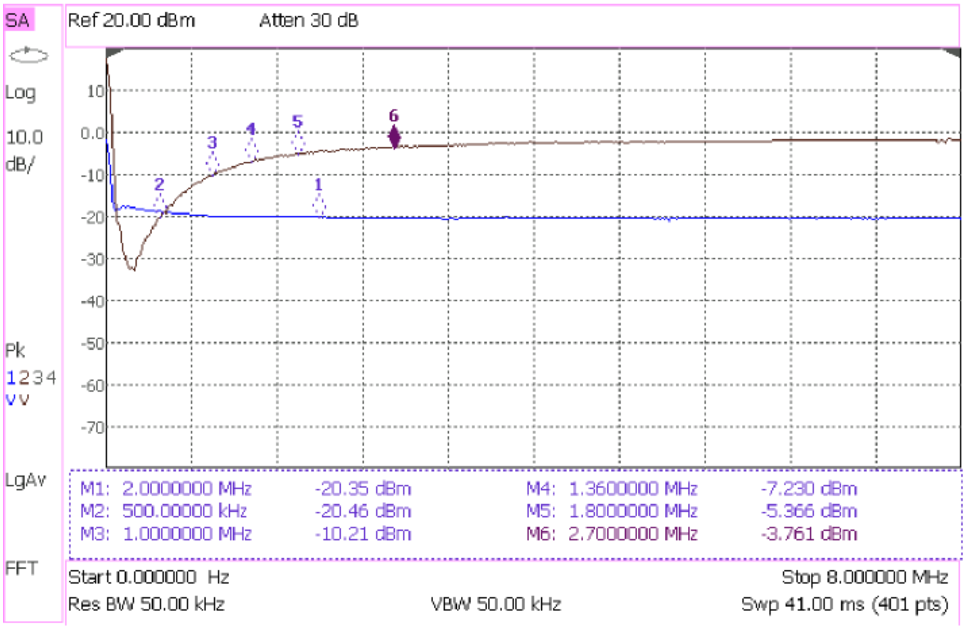

Ref 20.00 dBm Atten 30 dB

M1: 2.0000000 MHz -20.35 dBm
M2: 500.00000 kHz -20.46 dBm
M3: 1.0000000 MHz -10.21 dBm
M4: 1.3600000 MHz -7.230 dBm
M5: 1.8000000 MHz -5.366 dBm
M6: 2.7000000 MHz -3.761 dBm

Start 0.000000 Hz Stop 8.000000 MHz
Res BW 50.00 kHz VBW 50.00 kHz Swp 41.00 ms (401 pts)

Figure 5.16: The amplification response of the LMH6521 video amplifier, which demonstrates that the frequency range from DC to approximately 1 MHz, exhibits a decrease in gain, to the point where the signal is attenuated

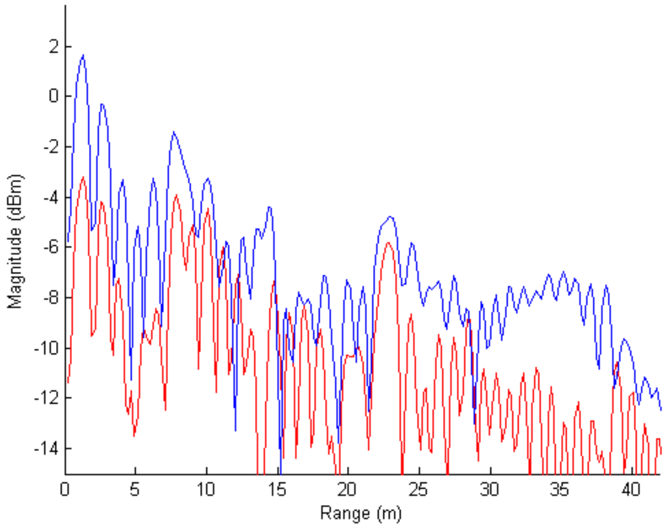

Figure 5.17: The feed-through component is attenuated by 4 dB in order to even out the spectrum and improve the requirements for dynamic range

of the feed-through signal.

It can be seen that there is an improvement in the dynamic range, based on the color intensity of the plots. To demonstrate the FMCW ranging that the radar is capable of, a reflector that was mounted on a trolley in the previous experiment, was picked up and shifted to the far wall of the corridor and back. Both plots show a

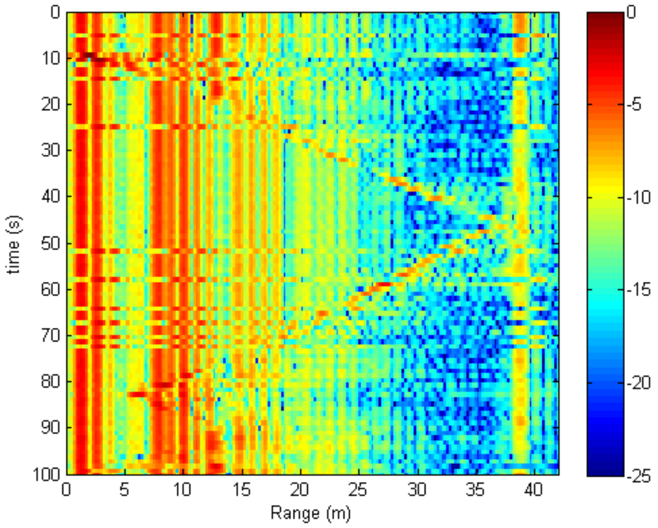

Figure 5.18: RTI plot where no feed-through attenuation is implemented

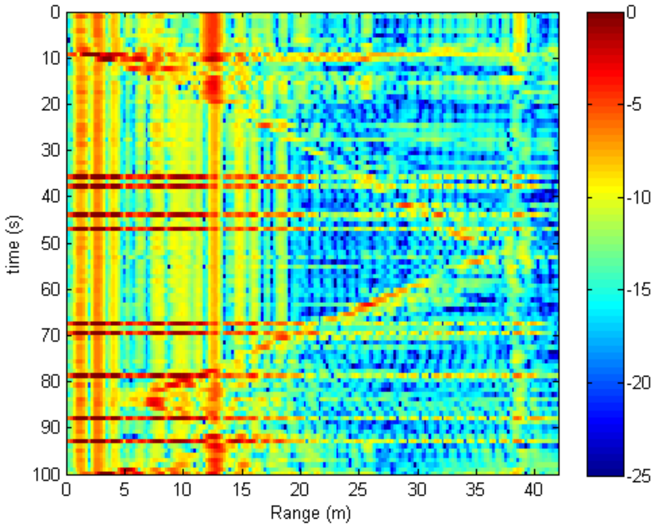

Figure 5.19: RTI of implementation of operation mode one

distinct detection pattern that start to move towards the far wall at approximately 10 seconds and reaches the end at 50 seconds. This is followed by the movement of the reflector back in the direction of the radar, where it is placed on the trolley that is found standing 10 m away from the radar.

Furthermore, interference can be seen in both plots, which manifests itself as dark horizontal lines that stretch across the plot. This could be caused by a Wi-Fi transmission, as the radar operates at 2.4125 GHz center frequency, which falls in the same band as Wi-Fi signals

5.5 Summary

The RadioCamera-S power levels along the transmitter and receiver modules were verified by comparing them to the projected values, which were obtained from the component datasheets. Then the system tests were carried out that entail delay-line testing, as well as complete system integration tests.

The delay-line tests were aimed at analysing the requirements for waveform sampling, as well as demonstrating the result of utilising operational mode one, where an offset between the two generated waveforms was introduced.

The system integration tests showed that the radar was able to detect the presence of a reflector in the test scene. The effect of using the reference channel in conjunction with the main receiver channel in order to determine the true range was also shown.

Operational mode one was utilised to shift the feed-through into the region where the video amplifier attenuated the signal and resulted in the reduction of amplitude, which, in turn, lead to the decrease of the dynamic range requirements.

Finally, RTI plots were demonstrated where a single moving target was observed. Two RTI plots of the same scenario were shown, with the only difference being the feed-through attenuation in the second case, which improved the dynamic range.

Chapter 6

Conclusions and Recommendations

6.1 Conclusions

In the context of hardware implementation, the RadioCamera-S prototype achieved the following objectives:

- Operates in S-Band
- LMX2492EVM was used to generate custom L-FMCW waveforms
- Successfully implemented the LMH6521 IF amplifier in the main channel of the receiver
- Red Pitaya was used to trigger the waveform generator boards
- Red Pitaya was used to acquire data while using an external trigger to start acquisition
- Low-cost antennas were made and tested

Hence, it can be said that the hardware requirements were fulfilled.

The proposed airborne system geometry was analysed and the effect on the design parameters was discussed and a waveform type was proposed for the implementation in the airborne scenario. However, due to the many discrepancies between the future airborne implementation which will operate in C-band, it was found problematic to relate the current prototype specification to the airborne scenario.

This resulted in a specification being developed for the ground based system only. The refined version of that specification can be seen in Table 6.1. Additional parameters, which come as a result of testing, are added to the existing specification.

Table 6.1: RadioCamera-S ground based system refined specifications

Radar Parameters	
Frequency Band	S-Band
Tx Central Frequency	2.4125 GHz
Tx Power	12.5 dBm
PRI_{min}	75 μs
PRI_{max}	1.05 ms
Bandwidth_{min}	175 MHz
Dimensions	420×500×220 mm
Receiver Noise Figure	5.14 dB
Chirp Generation	VCO
Modulation	Modified triangular

Antenna Parameters	
Antenna Type	Circular Waveguide
Elevation Beamwidth	72°
Antenna Gain	7.2 dBi
Centre Frequency	2.4 GHz
Antenna Isolation	-44 dB

Operating Specifications	
Range Resolution	0.89 m
Sampling Rate	125 MHz
Nominal Platform Elevation	0 m

In the context of the two-channel filtering technique that was proposed, the practical implementation was not realised completely due to the lack of suitable filters during the testing phase. However, Mode One was implemented by utilising the gain response of the LMH6521, which resembles a high pass filter at lower frequencies and the feed-through signal component was reduced in magnitude, to the same level as the near by echo returns, this was shown in Figure 5.17.

6.2 Recommendations for Future Work

Based on the issues that were encountered during the design procedure and the results of tests the following recommendations can be made.

6.2.1 RadioCamera System

In the current configuration when the system is operated in either Mode One or Mode Two of operation, the reference receiver channel is used to determine the frequency associated with zero range. This frequency depends on the time offset between the two ramp signals that are produced by the two waveform generators. Since the time offset is determined by the radar operator, there is no need to record this channel given that the two waveforms are triggered at the exact time that the operator specified.

RadioCamera-S prototype was used to investigate the operation of the Red Pitaya, as well as the LMX2492 ramp generator module and the time delays that were associated with triggering the ramp generators. Therefore, the reference signal was sampled for verification of the zero range and to ensure that the Red Pitaya platform could sample the two channels at the same time without a time delay between the two.

The future revisions of the RadioCamera system, could utilise the second channel to:

- Record a copy of the signal at the transmitter antenna to determine the time delay due to the transmit antenna cable
- Interferometry, where by an additional receiver antenna will be added to the setup. The de-ramped return of which could be sampled by the second channel

6.2.2 Transmitter

LMX2492EVM

The two waveform generators are currently synchronised using a single-ended 100 MHz Oscillator. As the Red Pitaya requires a differential clock signal that utilises the LVDS standard and the waveform generator boards also can be clocked using a differential clock source, it might be of interest to switch from the single-ended oscillator to a differential source that can provide a clock signal to all three devices, thereby keeping them synchronised.

Amplification stage

During the design process of RadioCamera-S, it was found that a single ZX60-272LN+ amplifier was not sufficient and as a result, two amplifiers were cascaded to provide sufficient gain. In order to improve on this a single amplifier can be utilised.

The amplifier is required to have a gain of approximately 21 dB. Additional constraints are that the current setup operates from a 5 Volt PSU, should an amplifier that has more gain and requires more power be chosen, the PSU that powers the RadioCamera-S prototype will have to be redesigned.

6.2.3 Antenna

The isolation between the two antennas was measured to be approximately -44 dB when a maximum probe-to-probe separation was utilised. The methods of improving the isolation through the use of Radar Absorbing Material (RAM) between the antennas or alternatively the use of choke rings around the antennas could be investigated.

The antenna isolation determine the level of the feed-through signal, which the current study aims to filter, if the isolation could be improved and the level of the signal attenuated, the problem of filtering could be simplified.

6.2.4 Receiver

Filters

During the testing phase of this research project, low pass filters with a steep cut-off and a cut-off frequency in the order of 20 to 30 MHz, were unavailable. Hence, Mode Two for feed-through signal filtering was not implemented.

Furthermore, an actual high pass filter could also be tested and the two modes of filtering the signals out compared. The gain response of the video amplifier that was used to demonstrate the operation of Mode One filtering technique, did demonstrate, the attenuation of the feed-through signal by 4 dB, however, this has to be implemented with a stand alone filter in order to see if the feed-through can be filtered completely.

Red Pitaya

If the Red Pitaya will be used on future revisions of the RadioCamera radars it will need to be able to:

- Program and send control signals to the LMX2492 ramp generator
- Store data on the SD card or on an alternative source
- Store data continuously (more than 16384 samples at a time)
- Control the gain on the LMH6521 video amplifier

Hence, the development of any of those aspects will be beneficial to the final design of the airborne FMCW imaging sensor.

Bibliography

[1] R. Smith, "Micro Synthetic Aperture Radar Using FM/CW Technology," Master's thesis, Brigham Young University, 2002.

[2] M. Duersch, "BYU Micro-SAR: A Very Small, Low-Power LFM-CW Synthetic Aperture Radar," Master's thesis, Brigham Young University, December 2004.

[3] E. Zaugg, D. Hudson, and D. Long, "The BYU microSAR: A Small, Student-Built SAR for UAV Operation," in *Proceedings of the International Geoscience and Remote Sensing Symposium*, August 2006.

[4] M. Edwards *et al.*, "MicroASAR: A Small, Robust LFM-CW SAR for Operation on UAVs and Small Aircraft," in *Proceedings of the International Geoscience and Remote Sensing Symposium*, July 2008.

[5] G. Charvat, *Small and Short-Range Radar Systems.* CRC Press, 2014.

[6] H. Griffiths, "New ideas in FM radar," *Electronics Communication Engineering Journal*, vol. 2, pp. 185–194, Oct 1990.

[7] E. Murphy and C. Slattery, "All About Direct Digital Synthesis," August 2004.

[8] Mini-Circuits, "Amplifier Terms Defined." [Online]. http://www.minicircuits.com/app/AN60-038.pdf [Accessed: 8 February 2015], October 2010.

[9] M. Inggs and R. Lord, "Applications of Satellite Imaging Radar," in *South African Institute of Electrical Engineering*, 2000.

[10] M. Inggs and R. Lord, "Current Applications of Imaging Radar," in *International Conference on Advanced Remote Sensing for Earth Observation Systems, Techniques and Applications*, vol. XXXVI-1/w12, May 2005.

[11] G. Charvat, A. Fenn, and B. Perry, "The MIT IAP radar course: Build a Small Radar System Capable of Sensing Range, Doppler, and Synthetic Aperture (SAR) Imaging," in *IEEE Radar Conference, 2012*, May 2012.

[12] D. Thompson, D. Arnold, and D. Long, "YINSAR: a compact, low-cost interferometric synthetic aperture radar," in *Geoscience and Remote Sensing Symposium, 1999. IGARSS '99 Proceedings. IEEE 1999 International*, vol. 1, pp. 598–600 vol.1, 1999.

[13] M. Skolnik, *Introduction to Radar Systems.* McGraw-Hill Kogakusha, LTD, second edition ed., 1980.

[14] G. Charvat, “A Unique Approach to Frequency-modulated Continuous-wave Radar Design,” Master’s thesis, Michigan State University, 2003.

[15] G. Stimson, *Introduction to Airborne Radar.* SciTech Publishing Inc., 1998.

[16] Texas Instruments, “LMX2492 14 GHz Low Noise Fractional N PLL with Ramp/Chirp Generation.” [Online]. http://www.ti.com/lit/ds/symlink/lmx2492.pdf [Accessed: 16 February 2015].

[17] Texas Instruments, “LMH6521 High Performance Dual DVGA.” [Online]. http://www.ti.com/general/docs/lit/getliterature.tsp?genericPartNumberl̄mh6521&fileTypep̄d [Accessed: 23 March 2015].

[18] A. Meta, *Signal Processing of FMCW Synthetic Aperture Radar Data.* PhD thesis, Delft University of Technology, 2006.

[19] RFMD, “RFVC1843.” [Online]. http://www.rfmd.com/store/downloads/dl/file/id/28192/rfvc1843_-data_sheet.pdf [Accessed: 8 February 2015].

[20] Texas Instruments, “LMX2492 Evaluation Instructions.” [Online]. http://www.ti.com/lit/ug/snau160c/snau160c.pdf [Accessed: 8 February 2015].

[21] Mini-Circuits, “ZX60-272LN+ Low Noise Amplifier.” [Online]. http://www.minicircuits.com/pdfs/ZX60-272LN+.pdf [Accessed: 16 February 2015].

[22] Mini-Circuits, “ZVE-3W-83+ High Power Amplifier.” [Online]. http://www.minicircuits.com/pdfs/ZVE-3W-83+.pdf [Accessed: 16 February 2015].

[23] Mini-Circuits, “ZHL-30W-262+ High Power Amplifier .” [Online]. http://www.minicircuits.com/pdfs/ZHL-30W-262+.pdf [Accessed: 16 February 2015].

[24] Mini-Circuits, “ZVE-2W-272+ High Power Amplifier.” [Online]. http://www.minicircuits.com/pdfs/ZVE-2W-272+.pdf [Accessed: 16 February 2015].

[25] W. Lee and E. Yung, “The input impedance of a coaxial line fed probe in a cylindrical waveguide,” *Microwave Theory and Techniques, IEEE Transactions on*, vol. 42, pp. 1468–1473, Aug 1994.

[26] S. Paine, “Design and Implementation of Dual Polarised L-Band Antenna with 10 Degree Azimuth Beamwidth,” tech. rep., October 2014.

[27] Mini-Circuits, "ZX05-42MH+ Frequency Mixer." [Online]. http://www.minicircuits.com/pdfs/ZX05-43MH+.pdf [Accessed: 23 March 2015].

[28] H. Griffiths and B. Purseyyed, "A Radar Altimeter with Synthetic Aperture Processing," in *Microwave Conference, 1989. 19th European*, pp. 281–286, Sept 1989.

[29] M. Richards, *Fundamentals of Radar Signal Processing.* McGraw-Hill, first edition ed., 2005.

[30] M. Richards, J. Scheer, and W. Holm, *Principles of Modern Radar - Basic Principles.* SciTech Publishing Inc., first ed., 2010.

[31] E. Murphy and C. Slattery, "Direct Digital Synthesis Controls Waveforms in Test, Measurement, and Communications," August 2005.

[32] C. Balanis, *Antenna Theory Analysis and Design.* John Wiley I& Sons, Inc., third edition ed., 2005.

[33] Mini-Circuits, "ZHL-20W-13+ High Power Amplifier." [Online]. http://www.minicircuits.com/pdfs/ZHL-20W-13+.pdf [Accessed: 8 February 2015].

[34] S. Levy, H. Moalem, D. Ackerman, and H. Matzner, "Experiment 3 - High Frequency Amplifiers." [Online] http://www.hit.ac.il/.upload/engineering/microwave-experiment4-highfrequencyamplifiers.pdf [Accessed: 10 February 2015], February 2009.

[35] D. Pozar, *Microwave Engineering.* John Wiley I& Sons, Inc., third edition ed., 2005.

[36] W. Stutzman, *Antenna Theory and Design.* John Wiley I& Sons, Inc., third edition ed., 2014.

[37] C. Bowrick, *RF Circuit Design.* Elsevier Inc., second edition ed., 2008.

[38] C. Slattery and M. McCarthy, "Oversampled ADC and PGA Combine to Provide 127-dB Dynamic Range." [Online]http://www.analog.com/library/analogDialogue/archives/45-12/dynamicrange.pdf[Accessed: 10 February 2015], December 2011.

Appendix A

FMCW Radar and SAR Background

Despite the fact that a more conventional approach dictates the use of a pulsed radar for SAR systems, recent research has shown that FMCW radar can also be used [1]. FMCW radar demonstrates a number of advantages over pulsed radar when presented with an application that requires low power and low cost. These advantages have been discussed in [6] and as a result, will be omitted in this report. Instead, Section A.1 will focus on the principles of operation of FMCW radar by introducing the reader to the nature of the waveforms that are associated with this approach, as well as explain how a simple FMCW system operates. Then, Section A.2 will illustrate the basic principles behind a SAR system, by addressing the system geometry and how it can be used to achieve an improvement in azimuth resolution [18].

A.1 FMCW Radar Principles

As the FMCW acronym suggests, the radar sensor transmits a signal continuously with varying frequency and at constant amplitude. The change in frequency during transmission is known as Frequency Modulation(FM), which makes it possible to extract range information from the received signal [13]. There are various types of FM techniques but for the purpose of this dissertations a Linear-FMCW (L-FMCW) *saw-tooth* and *triangular* waveforms will be used. A triangular modulation scheme essentially resembles the saw-tooth modulation in that the range data can be obtained from the up ramp, however, it also makes it possible to determine the Doppler frequency of the target by only using a single sweep. Meanwhile a single sweep of a saw-tooth waveform can only provide the range information. To obtain the Doppler frequency multiple sweeps will have to be analyzed.

The time domain representation of the saw-tooth and the triangular waveforms can be seen in Figure A.1(a) and A.1(b) respectively. The frequency change with time for both cases is demonstrated in Figure A.2(a) and A.2(b).

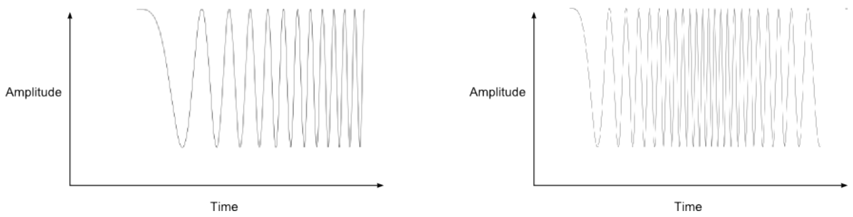

(a) Magnitude-Time plot of a saw-tooth waveform

(b) Magnitude-Time plot of the triangular waveform

Figure A.1: Typical FMCW waveforms in magnitude-time representation

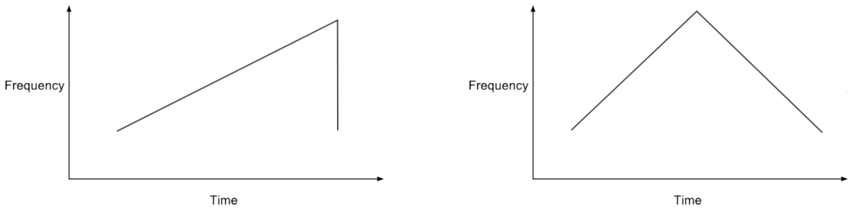

(a) Frequency-Time plot of a saw-tooth waveform

(b) Frequency-Time plot of the triangular waveform

Figure A.2: Typical FMCW waveforms in frequency-time representation

A typical FMCW radar front-end, that produces the L-FMCW signal, is shown in Figure A.3(a) and consists of a homodyne or direct-conversion receiver(DCR) and transmitter block. This is a mono-static system, which means that a single antenna is used to transmit and receive signals. The circulator performs the function of isolating the transmitter from the receiver. The isolation of the two blocks is required as the transmitter produces a signal that is significantly higher in power than the received signal. Therefore, if sufficient isolation is not provided, the receiver could be either damaged or contaminated by the higher power - transmitter signal. An alternative to using a circulator would be to use a bi-static arrangement, as shown in Figure A.3(b), where a dedicated antenna is used for the transmitter and the receiver channels [13].

In the two provided configurations, the transmitter consists of a chirp generator block, which produces an L-FMCW signal that is then transmitted from the antenna. Once the transmitted signal encounters a target, it gets reflected back to the antenna, resulting in a time delayed and scaled version of the transmitted signal at the receiver. The time delay, t_{delay}, is proportional to the distance, r from the antenna to the target. The relationship is as follows:

$$r = \frac{c \times t_{delay}}{2}, \tag{A.1}$$

where c is the velocity of electromagnetic wave propagation in free space and is equal to approximately 3×10^8 m/s. In order to be able to detect the time delay, a process of de-chirping, also known as deramping or stretch processing, takes place. This process requires the use of a mixer. A mixer is a non-linear device that is typically used to convert Radio Frequency(RF) energy to Intermediate Frequency(IF) energy,

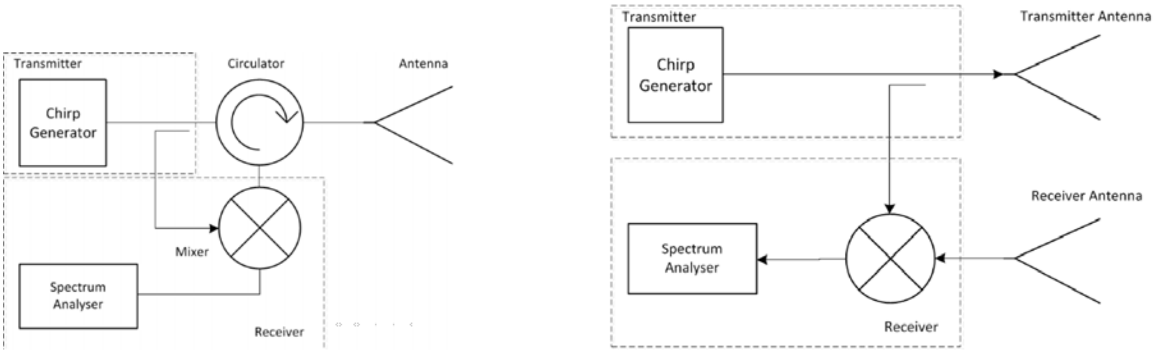

(a) Mono-static setup (b) Bi-static setup

Figure A.3: FMCW Radar front-end - high level representation

Equation A.2 shows what the output of the mixer is, given the input RF signal at frequency f_{RF} and Local Oscillator (LO) input signal at frequency f_{LO}.

$$f_{IF} = \begin{cases} f_{RF} + f_{LO} \\ f_{RF} - f_{LO}. \end{cases} \tag{A.2}$$

As Equation A.2 shows, there are two frequency components in the ideal case, hence a filter is required to select the component of interest. In the FMCW radar system case, the inputs to the mixer are the replica of the original transmitted signal and the received signal. The output of the mixer is known as the beat frequency signal. The process of mixing the two signals in the FMCW radar receiver is demonstrated in Figure A.4(a). First, the transmitted and received waveforms are shown, which are offset by a time delay, t_{delay}. Each of the signals has a bandwidth of Δf Hertz and a period of Δt seconds. The beat-frequency signal is shown in the Frequency-Time plot and then again in the Magnitude-Frequency plot (Figure A.4(b)) in order to better illustrate the two frequency components associated with it. In most cases t_{delay} is much smaller than Δt, hence the frequency component f_{b2} is much smaller in magnitude than f_{b1} and can thus be excluded from further calculations for the sake of simplification.

The range resolution, as shown in [6], refers to the minimum distance between two targets that can be distinguished by the radar and depends on the width of the main lobe of the sinc function centered at frequency f_{b1}. The width of the main lobe is inversely proportional to the duration of the signal, as shown in Figure A.4(b). Hence, the resolution in the frequency domain is $\frac{1}{\Delta t}$ (provided that $\Delta t >> t_{delay}$), which corresponds to the range resolution being

$$\delta r = \frac{c}{2\Delta f}. \tag{A.3}$$

From the equation above, one can see that the range resolution of the L-FMCW radar depends on the bandwidth of the signal, therefore the higher the bandwidth, the better the range resolution. A more detailed derivation of the above can be

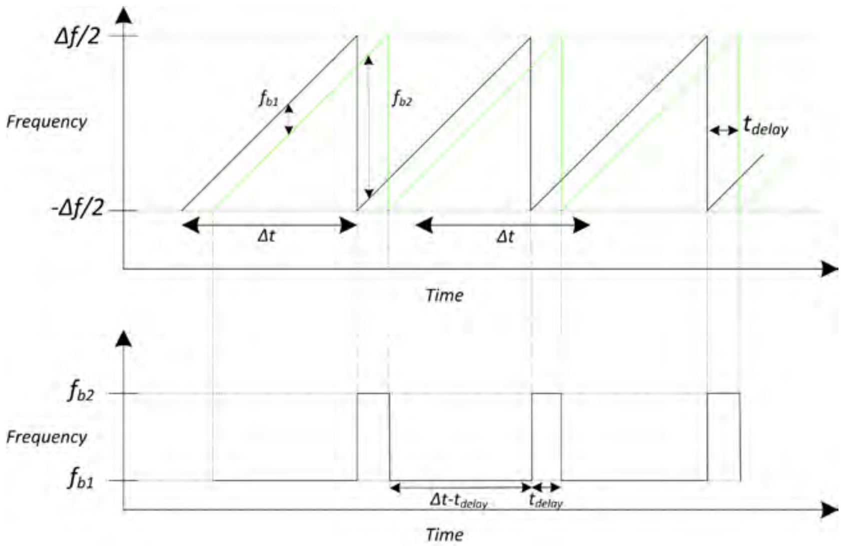

(a) Shows the mixing process of the transmitted and received signals to produce a beat frequency signal

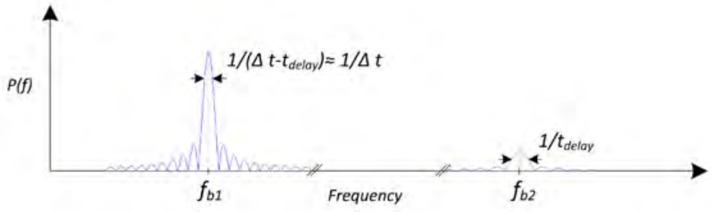

(b) Magnitude frequency plot of the beat frequency signal

Figure A.4: Mixing process in the FMCW radar front end[6]

seen in [1] and [18], which also provides some insight on how moving targets and the associated Doppler frequency component influence the received signal.

A.2 Synthetic Aperture Radar Overview

The main limiting factor of Real Aperture Radar (RAR) is the azimuth resolution which depends on the antenna aperture length and the range. As was shown in [2] the azimuth resolution δx of a RAR is:

$$\delta x \approx r\theta_{az} \approx \frac{r\lambda}{D_{az}}, \tag{A.4}$$

where r is the range to target, θ_{az} is the 3-dB beamwidth of the antenna in azimuth, λ is the wavelength and D_{az} is the antenna length in azimuth. Therefore, if one is required to have a compact system the azimuth resolution will be limited by the size of the antenna. In addition to this, the azimuth resolution will also degrade with range. Hence, a different approach needs to be utilized in order to achieve higher resolution.

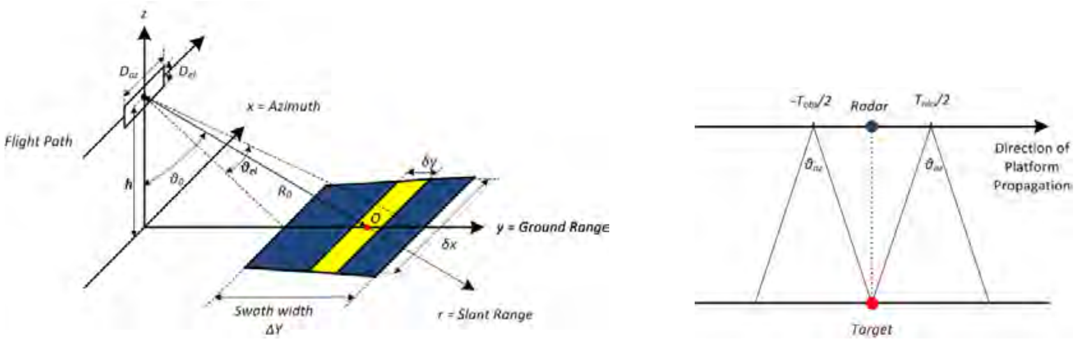

(a) Side View (b) Top View

Figure A.5: SAR Geometry

The use of synthetic aperture addresses those problems [28]. SAR approach relies on platform motion, and can mainly operate in strip-map or spotlight mode, a closer look at those methods can be found in [29], however, for the purpose of this dissertation only the strip-map mode will be used.

Stripmap SAR mode involves the platform moving along a fixed path with the radar positioned perpendicularly to the direction of platform motion, as shown in Figure A.5(a). The radar is pointed down towards the ground and depending on the angle of depression and the height, the width of the swath can be adjusted. The return echos are collected during time T_{obs}, as shown in Figure A.5(b), which demonstrates that the maximum time of observation is determined by the azimuth beamwidth, θ_{az}, of the antenna. As the main principle of SAR operation is based on observing a target from different angles as the platform moves past it. Therefore, it is ideal to have a wider beamwidth, which can be achieved by using an antenna with a narrow aperture. This bears a direct relation to the azimuth resolution, δx, which is

$$\delta x = \frac{D_{az}}{2} \tag{A.5}$$

and shows that the smaller the aperture the better the resultant resolution. However, there is a trade off when an antenna with a narrow aperture is used, as the gain of it also decreases, resulting in a decrease in range. A more detailed derivation of the azimuth resolution can be found in [18], [29] and [2].

Once the return echos for a scene were collected they are integrated coherently, which means that the phase of the signals is used during integration, in order to synthesize a big aperture that yields a higher azimuth resolution according to Equation A.4. It must be mentioned that most SAR azimuth compression algorithms operate on the stop and go premise, which as [18] shows, does not always hold for a FMCW SAR approach. Furthermore, in order to achieve the maximum azimuth resolution possible, additional processing is carried out in order to mitigate the effects of platform motion and range cell migration. This can be done in the radar backend, as can be seen in Figure A.6, using a time-domain backprojection algorithm [30].

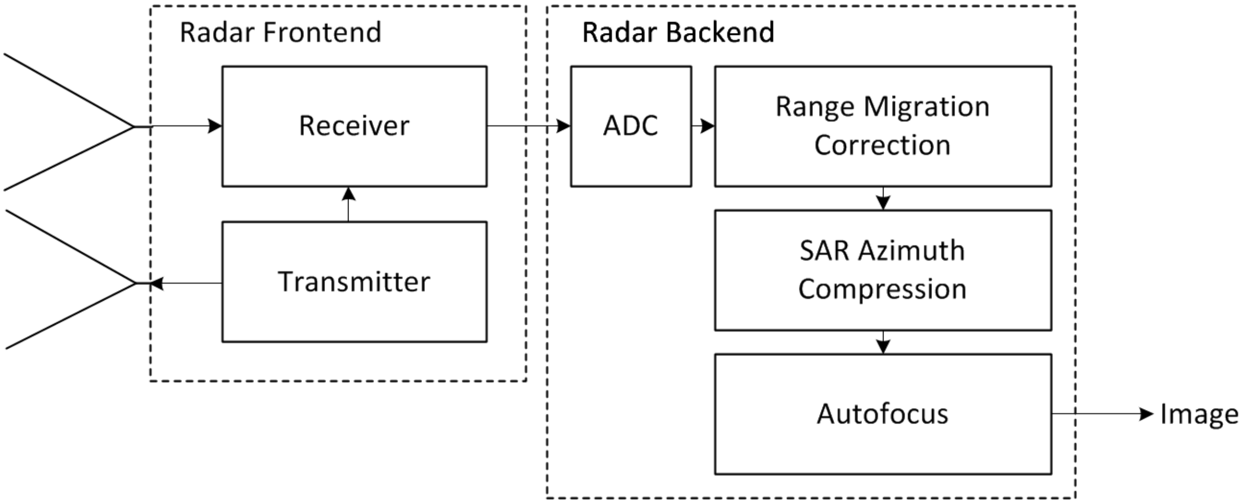

Figure A.6: SAR image chain

Appendix B

FMCW Radar Design Considerations

In its most basic form an FMCW radar consists of a transmitter, antenna and the receiver. As Figure B.1 suggests each of the three subsystems can be further divided into their respective components. The characteristics of those components have a direct effect on the performance of the radar. Hence, in order to be able to design a system to a particular specification one must understand how the component parameters effect the performance. This appendix provides the analysis of each of the subsystems.

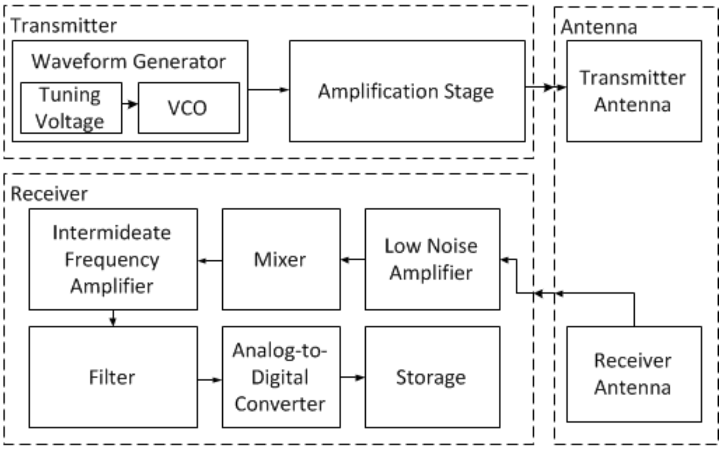

Figure B.1: FMCW imaging radar system diagram

B.1 Transmitter

An FMCW transmitter is a device that produces a signal that has frequency varying over a set time interval, upon the expiration of which, the cycle repeats. This repetition produces a continuous waveform that is amplified to a power level that is defined by the desired range of the radar. The higher the signal power, the further the theoretical range of detection of the radar. One can distinguish two processes that occur in the transmitter, which are: waveform generation and signal amplification. However, prior to discussing those two processes, one needs to address the parameters that define the waveform.

B.1.1 Waveform Design

During the waveform design phase one must consider a number of parameters that define an L-FMCW waveform. Those parameters are:

- Pulse Repetition Interval (PRI) and Pulse Repetition Frequency (PRF)
- Bandwidth
- Waveform non-linearity
- Chirp rate
- Doppler ambiguity
- Waveform type

PRI and PRF

The waveform can be characterized by the duration of a single cycle, referred to as the Pulse Repetition Interval (PRI), and the number of these cycles over a one second interval, known as the Pulse Repetition Frequency (PRF). The terms PRI and PRF are usually associated with the pulsed radar architecture, however, here they are applied to a continuous wave system. Therefore, the duty cycle of the pulse in an FMCW system is said to be set to 100%. Figure B.2(a)and B.2(b), demonstrate these characteristics of the FMCW waveforms using the saw-tooth and the triangular waveforms as an example and Equation B.1 shows the relationship between the two parameters.

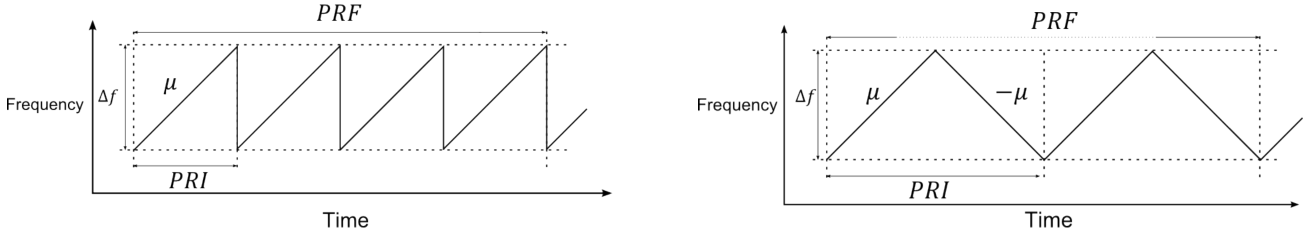

(a) Saw-tooth waveform

(b) Triangular waveform

Figure B.2: FMCW waveform design parameters

$$PRF = \frac{1}{PRI}. \tag{B.1}$$

In the FMCW radar, the received and transmitted waveforms are offset by a two-way propagation delay, which corresponds to the distance to target. Therefore, the maximum range from which a target return may be received without the observed range being ambiguous [15], also known as the maximum unambiguous range of the radar, will depend on the two-way propagation delay being equal to the length of the PRI. This can be expressed as follows:

$$R_u = \frac{c \times PRI}{2} \tag{B.2}$$

If the two-way propagation delay is greater than the duration of the PRI, then the received signal will be mixed together with the next repetition of the transmitted wave and result in the radar falsely detecting a target at close range, as opposed to its true position. This is shown in Figure B.3. It should be noted that if the two-way propagation delay will make up a significant portion of the PRI, then the signal return will be much weaker due to the fact that the overlap between the transmitted and received signals becomes smaller. This will not be a problem in a short-range imaging application, but should one increase the range of the radar, the PRI will also have to be adjusted accordingly.

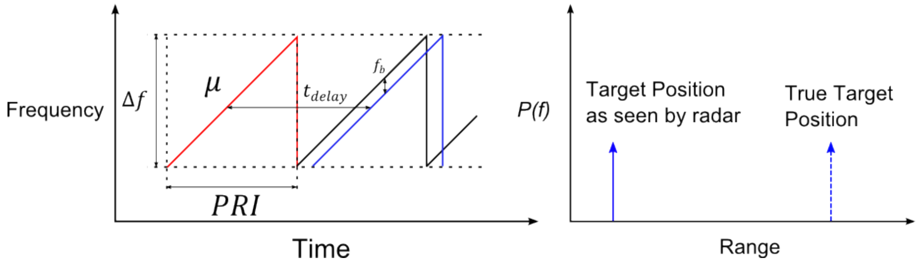

Figure B.3: Range ambiguity in FMCW radar

Using the above derivation, it follows that during the design of the waveform one must ensure that the duration of the PRI is sufficiently long in order to accommodate the range requirements of the system.

Bandwidth

The bandwidth, Δf, corresponds to the frequency excursion that the waveform performs during each repetition of the transmitted waveform. It is indicated in Figure B.2(a) and B.2(b). As was shown in Section A.1, the bandwidth of the waveform determines the range resolution of the system. The relationship was defined to be inverse, demonstrated by Equation A.3. Hence, the wider the bandwidth of the transmitted waveform, the finer the range resolution of the radar. The increase in the bandwidth also places requirements on the transmitter and the receiver hardware, as the transmitter and receiver components must be able to cater for the chosen frequency range.

In order to achieve the range resolution that is calculated by using Equation A.3 the duration of the PRI must be significantly greater than the two-way propagation delay [14]:

$$PRI \gg t_{delay} = \frac{2 \times r}{c}, \tag{B.3}$$

where t_{delay} is the two-way propagation delay and r is the distance to target.

Waveform non-linearity

According to the above definitions one needs to select a suitable duration (PRI) and bandwidth of a single repetition of the waveform in order to determine the maximum unambiguous range and the range resolution. However, this would only apply if the waveform is perfectly linear. In a practical case the linearity of the waveform would deviate. This will depend on the quality of the hardware that is employed.

To account for the expected non-linearity one can use the following relationship [14]:

$$\frac{\delta f}{\Delta f} = \frac{\delta r}{R_u} = \text{Waveform non}-\text{linearity}, \tag{B.4}$$

where δf is the deviation from the linear waveform. Hence, if the non-linearity factor is exceeded the radar performance that is derived using Equations A.3 and B.2 can not be expected.

Chirp rate

The chirp rate of the waveform is the ratio of the change in frequency ,Δf, to the change in time, Δt, and can be expressed as:

$$\mu = \frac{\Delta f}{\Delta t}, \tag{B.5}$$

where μ is the chirp rate. This essentially represents the slope of the up ramp of the waveform. The slope of the up ramp determines the relationship between the beat frequency signal and the two-way propagation delay. This can be expressed as:

$$f_b = \mu t_{delay} \tag{B.6}$$

In turn, the propagation delay is related to the range to target according to equation A.1. Using this relationship the beat frequency can be related to the range:

$$f_b = \frac{2\mu r}{c}, \tag{B.7}$$

where r is the range to target. It follows that if the chirp rate is high the targets that are at shorter range will correspond to a higher beat frequency and if the chirp rate is low the targets will correspond to a lower beat frequency signal.

The principle of varying the chirp rate can be used to shift the targets to a desired location in the beat frequency spectrum. This essentially forms the basis for the methods that are employed in this dissertation for the purpose of signal filtering.

Doppler ambiguity

Since radar imaging is the application of interest in this dissertation, one must consider the limitations that the SAR geometry imposes on the waveform, namely, the limitations on the PRF. The analysis of those limitation is most commonly carried out for the pulsed radar systems and utilizes the stop-and-go approximation.

After referring to the literature on FMCW SAR implementations, [1] and [2] showed that the stop-and-go approximation could also be employed. Although, [18] demonstrated that due to the continuous nature of the signal and the platform motion, the image quality may be effected and a suitable algorithm may need to be implemented to mitigate such effects. For the purpose of this dissertation the stop-and-go approximation will be used when determining the minimum PRF, as the development of the algorithm to mitigate the effects of platform motion falls outside the scope of the project.

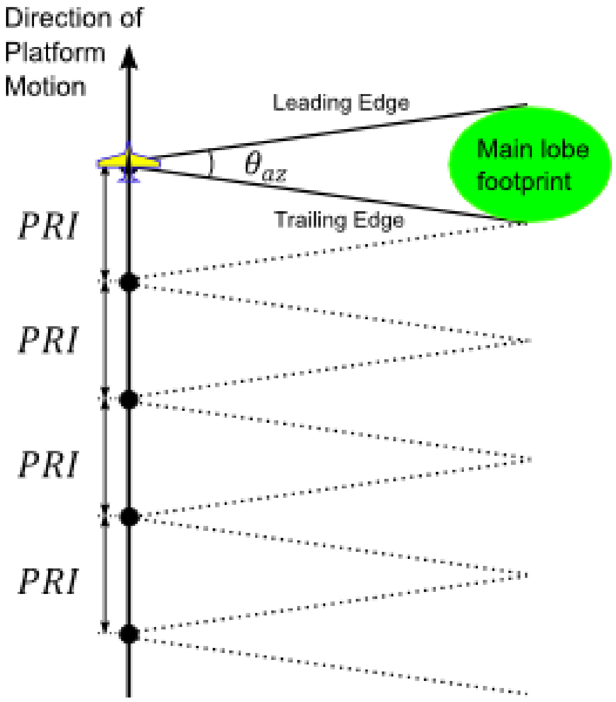

Figure B.4: Imaging radar geomeotry demonstrating real antenna mainlobe footprints

The stop-and-go approximation assumes that the radar stops and transmits a single pulse at constant intervals (equal to the PRI) along the flight trajectory. This is shown in Figure B.4. The area that the transmitted signal covers is defined by the dimensions of the real antenna. If one knows the characteristics of the antenna's main-lobe in azimuth, specifically the difference between the leading and trailing edges of the antenna beam, one can determine the minimum PRF that can be set in order to avoid ambiguity in the azimuth direction. This ambiguity is known as the *Doppler ambiguity*.

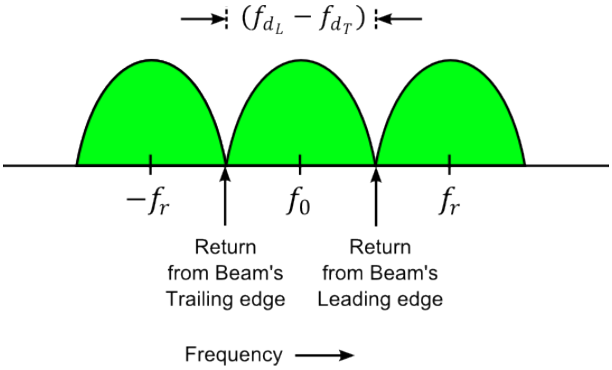

Figure B.5: In order to avoid Doppler ambiguities the PRF must exceed the difference between the Doppler shifts at the leading and trailing edges of the real antenna's mainlobe [15]

The leading and trailing edges of the main-lobe of the real antenna are demonstrated in Figure B.4. The case where a suitable PRF was chosen in order to avoid overlap of the main-lobes is shown in Figure B.5. If the antenna main-lobe footprints will overlap, Doppler ambiguity will occur. Hence, the minimum PRF that can be chosen must abide by the following expression:

$$PRF_{min} = f_{d_L} - f_{d_T}, \tag{B.8}$$

where f_{d_L} and f_{d_T} are the Doppler frequencies at the main-lobe's leading and trailing edges [15].

In a case where the real antenna has a narrow azimuth beamwidth, the minimum PRF can be calculated by using the following expression:

$$PRF_{min} = \frac{2v\theta_{NN_a}}{\lambda}, \tag{B.9}$$

where v is the velocity of the radar, θ_{NN_a} is the null-to-null azimuth beamwidth of the real antenna in radians and λ is the wavelength of the transmitted signal. Equation B.9 makes the assumption that the radar is perpendicular to the direction of platform motion.

Waveform type

The two types of waveforms that have been used in the above design discussion are the saw-tooth and the triangular modulated waveforms. They are widely used in practice, however they are not the only modulations that can be used.

The saw-tooth waveform has an advantage over the triangular waveform, in that one can achieve a higher PRF. This is apparent if one compares Figure B.2(a) and Figure B.2(b), the chirp rates are the same for both cases, but since the triangular waveform also has a down ramp of the same duration the PRI is effectively doubled.

As was mentioned in Section A.1, the down ramp of the triangular waveform allows one to determine the Doppler frequency shift, as well as the range information from a single sweep. In addition to that an advantage of the triangular waveform is that the return from a high frequency to the lower frequency occurs smoothly due to the fact that there is a up ramp and down ramp. The saw-tooth waveform modulation technique might result in an undershoot between repetition as the change from the high frequency to low frequency occurs in a very short period of time.

B.1.2 Waveform Generation

The waveform generator is the part of the transmitter that is responsible for generating the frequency modulated continuous waveform. The waveform that is produced also has to be centred at the desired carrier frequency. Two methods of waveform generation have been encountered in the literature:

- Direct Digital Synthesizer (DDS)
- Voltage Controlled Oscillator (VCO) driven by a tuning voltage

Direct Digital Synthesizer (DDS) approach

The DDS approach entails generating a frequency modulated signal at baseband and then stepping up the frequency to the desired carrier frequency. This approach was utilizes in Brigham Young University's (BYU) μSAR [3] and microASAR [4] systems.

The DDS generates a discrete-time signal, which it then converts to its analog form by using the Digital-to-analog converter (DAC). The output frequency of the DDS depends on the reference clock of the system and the binary number or tuning word [7]. Basic components of a DDS device can be seen in Figure B.6 and they are the phase accumulator, phase-to-amplitude converter and the DAC.

The tuning word is typically stored in a frequency register and can be seen at the input of the phase accumulator. The phase accumulator computes a phase address for the look-up table and the corresponding phase is converted to an amplitude

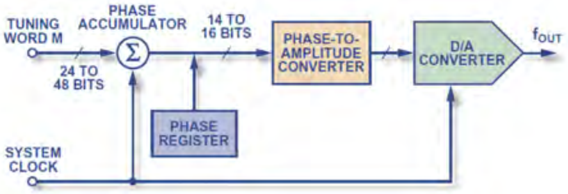

Figure B.6: Components of a direct digital synthesizer [7]

in the phase-to-amplitude converter. This amplitude is a digital value, which is then converted to an analog signal using the DAC. The rate at which the phase accumulator steps through the phase look-up table determines the frequency of the output signal. If a slow rate is chosen to step through the look-up table, a sinusoidal wave at a low frequency is produced. In a case where a fast rate is used, a higher frequency sinusoidal wave is produced. Finally, if the rate at which the phase accumulator steps through the look-up table is varied, a frequency modulated signal can be produced.

The advantage of the DDS approach lies in the fact that they operate at low power, can provide fast switching between output frequencies, fine frequency resolution and are available at a low cost [31]. Furthermore, the output waveform can be reprogrammed and the properties of the output waveform can be easily changed. This was employed in BYU microASAR, where the PRF of the output waveform was variable in order to account for the altitude of the platform.

Possible disadvantages of the DDS approach include the fact that since a DAC is used to produce the analog output, Nyquist images are also produced and therefor a reconstruction lowpass filter needs to be added to the system. Another disadvantage is the fact that the output frequency is limited to baseband and needs to be stepped up to the desired carrier frequency.

Voltage Controlled Oscillator (VCO) approach

Voltage Controlled Oscillator (VCO) outputs a frequency in linear proportion to its input control voltage. This method of producing the modulated waveform was used in the rail SAR setup in [1], TU Delft's demonstrator system [18] and the Massachusetts Institute of Technology (MIT) Independent Activity Period (IAP) radar setup [11].

The main issue with this approach is the fact that the VCOs tend to have a non-linear response to a linear tuning voltage. This can be illustrated by Figure B.7(a), where a linear tuning voltage would result in the demonstrated non-linear response of the VCO. To solve this problem, a tuning voltage profile that is shown in Figure B.7(b) will be required to compensate for the VCO non-linearity.

The linearity of the output waveform determines the performance of the radar, as was shown in Section B.1.1, therefore the above mentioned voltage profile that compensates the non-linearity is required. This can be done using a feedback system, where the output of the VCO is compared to the expected frequency as determined by the tuning voltage.

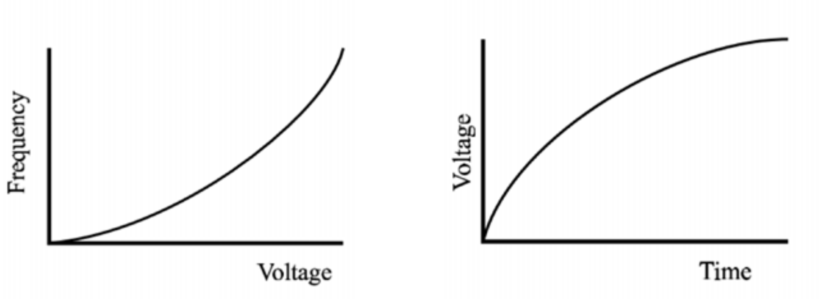

(a) VCO response (b) Compensation tuning voltage

Figure B.7: An exaggerated non-linear response of the VCO with the corresponding tuning voltage that is required for compensations [1]

For example, if a DAC is used to produce a tuning voltage, an output of the VCO can be fed back to the micro-controller or the computer that is responsible for producing the waveform and determine the disparity between the expected and the actual output of the VCO. After that the tuning voltage profile is changed to account for the non-linearities and fixed to that tuning profile for all the subsequent waveforms, as was done in [1]. Alternatively, the algorithm can carry out the adjustment on a pulse to pulse basis, continually improving the profile of the tuning voltage, as was done in [18].

Recently, complete systems on a chip that in conjunction with a VCO can carry out high frequency ramp generation started to emerge. A PLL that can be frequency modulated by varying the feedback signal from the VCO is one of them. This provides an alternative to the above mentioned approach, where the non-linearity of the VCO output is compensated using a predetermined algorithm that is executed on the micro-controller or any other processing unit.

The advantage of the VCO approach lies in the fact that a VCO that operates in the frequency range of interest can be chosen and the waveform can be produced at the carrier frequency, with out the need to step it up to the carrier frequency as is required when using a DDS.

B.1.3 Signal Amplification

The methods of generation that were explained in the previous section produce a modulated waveform at a relatively low power level. The Friis transmission equation, which is used to estimate the performance of radio communication and broadcast stations [32], shows that the power of the transmitted signal influences the expected range of signal propagation. The relationship is expressed as follows:

$$P_{rx} = P_{tx}\left(\frac{\lambda}{4\pi R}\right)^2 G_{tx}G_{rx}, \tag{B.10}$$

where, P_{rx} is the power received at the receiver antenna and P_{tx} is the power transmitted. G_{tx} and G_{rx} are the transmitter and receiver antenna gains and R is the range between the antennas.

The relationship between transmitted and received power demonstrates that if the transmitted power is increased, so will the power at the receiver antenna. However, if the range between antennas increases, the power at the receiver decreases.

Despite the fact that in the case of radar, the range of interest is typically double the range in the above equation, as the signal needs to travel to the target and return back to the radar. The relationship between transmitter and receiver power levels is directly proportional, as in Equation B.10. Therefore, given a specified range that the radar must operate in, one needs to ensure that the transmitter power is sufficiently high in order to receive a satisfactory power level at the receiver antenna.

To accomplish this the output of the waveform generator is fed into a power amplifier, which can be characterized by the following parameters:

- Operating frequency range
- Gain and gain flatness
- Output power at 1 dB compression point
- Output third-order intercept point (OIP3)

Operating frequency range

When choosing an amplifier for a particular application one needs to ensure that it is able to operate in the frequency range of interest. Given the imaging application of the radar, the bandwidth of the transmitted signal is desired to be wide due to the fact that it is responsible for determining range resolution. Hence, one needs to ensure that the amplifier of choice can operate predictably across the wide frequency range. This means that the parameters, such as gain, gain flatness and output third-order intercept points should be stable across the desired range.

Amplifier gain and gain flatness

The gain of the amplifier is the ratio of output power to the input power, specified in small-signal linear gain region [8]. It is measured in decibels (dB) and is relatively constant across the frequency range of the amplifier. The variance in the gain of the amplifier across the frequency range of operation is characterized by the gain flatness parameter.

For example, given a ZHL-20W-13+ amplifier with a 50 dB gain, maximum gain flatness of ± 1.8 dB and a frequency range of operation from 20 to 1000 MHz. The gain can vary from 48.2 to 51.8 dB across the frequency band. In an amplifier datasheet ([33]) this is typically demonstrated in graphical form, as shown by Figure B.8.

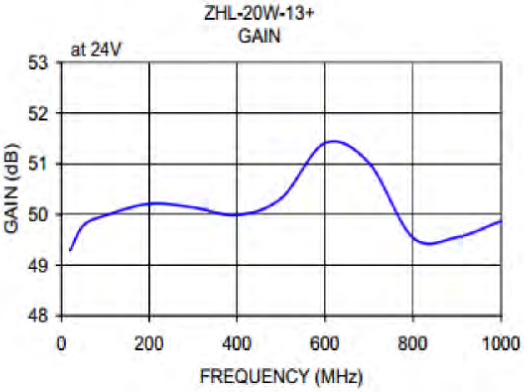

Figure B.8: Gain variance across the operational frequency range

It has to be noted that the gain of the amplifier is only linear in a particular region and as the input power increases, the gain exhibits a non-linear behavior, this is examined in the next section.

Output power at 1 dB compression point

One of the most critical aspects of amplifiers is the output power at 1 dB compression point. The 1 dB compression point defines the output level at which the amplifier's gain is 1 dB less than the small signal gain [8]. Figure B.9, shows the relationship between input power and the power at the output, the slope of the curve corresponds to the gain of the amplifier. As the power at the input of the amplifier is increased the output power also increases linearly. However, a point is reached where the gain becomes non-linear and starts to compress, which means that the gain starts to decrease. Eventually, the gain equals zero and the amplifier is said to be saturated.

In order to avoid saturating the amplifier one can ensure that the input power is less than the input power at 1 dB compression point. This can be computed:

$$P_{in}^{1dB} = P_{1dB} - G_{amp}, \tag{B.11}$$

where P_{1dB} is the 1 dB compression point, G_{amp} is the gain of the amplifier and P_{in}^{1dB} is the input power at 1 dB compression point.

If the amplifier is saturated, than the output power will not be increased and the effect of inter-modulation products will be more significant. This phenomenon is

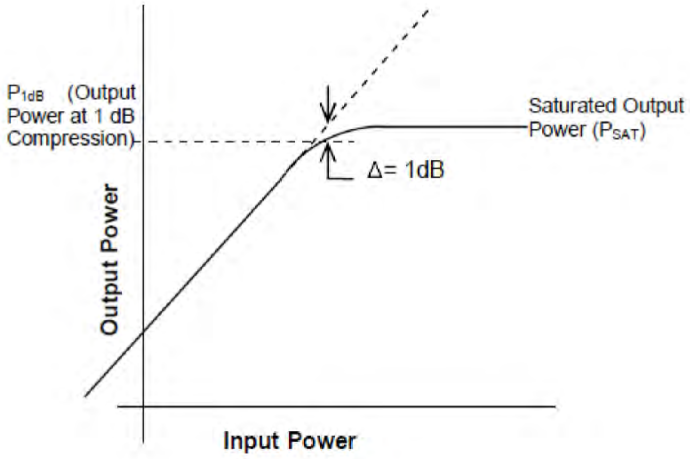

Figure B.9: 1 dB compression point of a typical amplifier [8]

addressed in the following section.

Output third-order intercept point

The non-linear behavior of a amplifier results in the formation of output harmonics [34]. The harmonic responses are undesired and need to be removed from the output signal. Given single frequency input at frequency f_1,the harmonics will be formed at $n \times f_1$, where n is the order of the harmonic. Figure B.10 demonstrates the presence of harmonics at a output of the amplifier that has an input signal located at 2.4 GHz. It can be seen that given a high frequency input signal, the harmonic responses are located relatively far from the original signal. Hence, a filter can be used to filter the unwanted harmonics out.

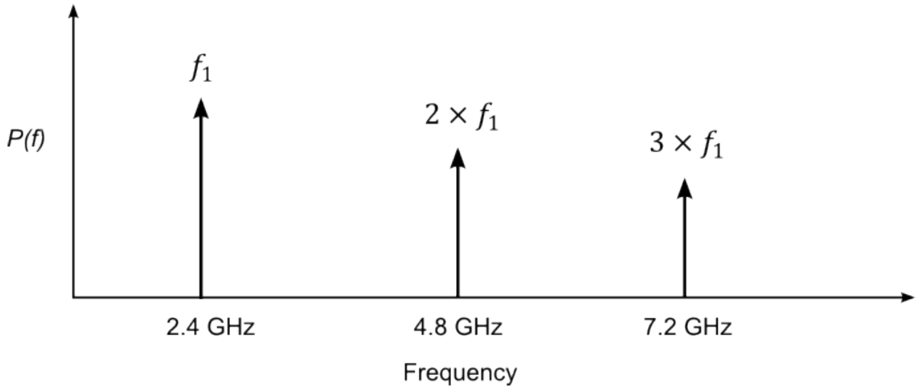

Figure B.10: n
First order harmonics of a 2.4 GHz signal at the output of the amplifier

In the case where there are two signals at the input of the amplifier located at frequencies f_1 and f_2 within the operational range of the amplifier, the harmonics will appear at $m \times f_1 + n \times f_2$, with the order of the harmonics equal to the sum of integers m and n. Figure B.11, shows a output of an amplifier that has two different frequency components at frequencies 2.35 GHz and 2.45 GHz at the input.

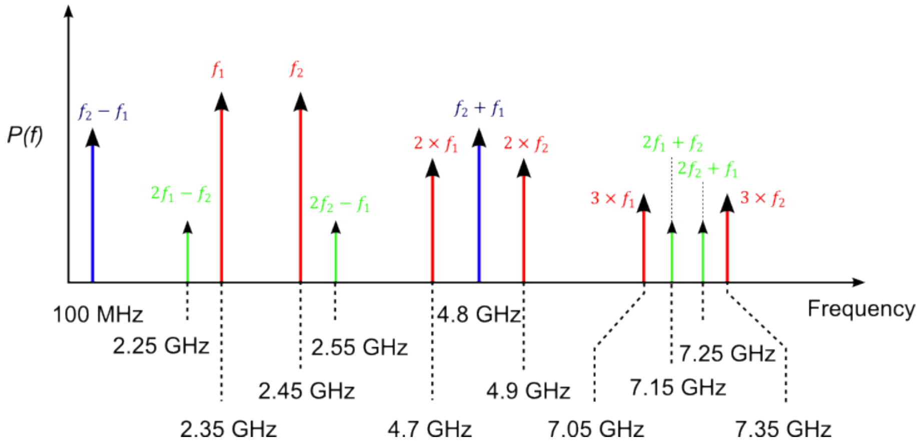

Figure B.11: First, Second and Third order harmonics of a 2.4 GHz signal at the output of the amplifier

It can be seen that third order harmonics, also known as inter-modulation products, are located close to the signals of interest and will be very difficult to filter out. Hence, one needs to ensure that the level of those harmonics is low enough not to interfere with the main component response.

The level of the third order harmonics can be estimated using the third order intercept point of the amplifier. This is the point where the linear gain of the amplifier intercepts the gain of the third order harmonics. Figure B.12 demonstrates the relationship. The relationship means that as one increases the input power the output power will increase linearly with a ratio of 1:1, whereas the power level of the third order harmonics will increase with a ratio of 3:1.

As a result, the increase in input power results in the third order harmonic level increasing at a faster rate than the main frequency components. If considered together with the fact that at a certain input power level the output of the amplifier saturates and results in zero gain, the third order harmonics can increase to the same level as the main frequency components and distort the output signal of the amplifier. Therefore, when designing the amplification stage for the transmitter and the receiver, one must ensure that the power level of the frequency components at the input of the amplifier will not result in a high level third order harmonic products.

B.2 Antenna

An antenna can be viewed as a device that converts a guided electromagnetic wave on a transmission line to a plane wave propagating in free space [35]. Antennas are inherently bi-directional and can be divided into directional and omni-directional types. Directional antennas focus the radiation over a narrow field of view where most of the gain is in only one direction [5]. In order to illustrate this a simulated

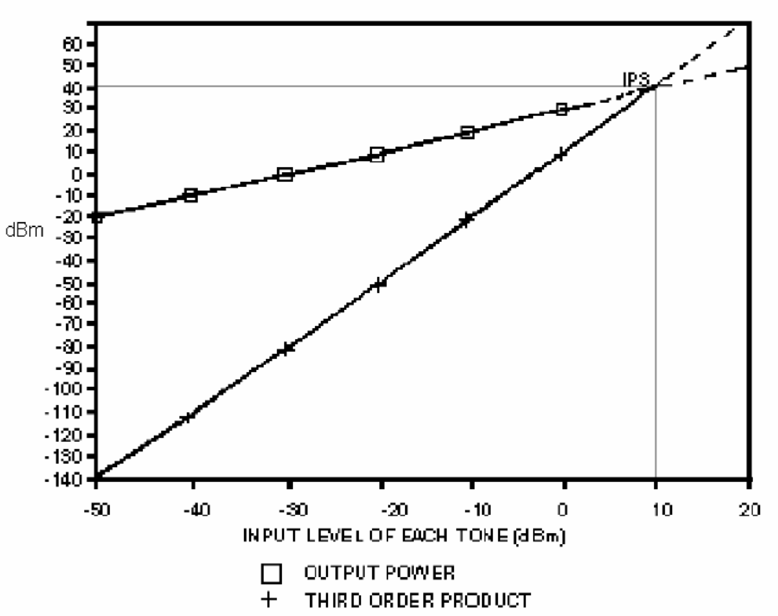

Figure B.12: Linear gain of the amplifier vs. the gain of the third order intermodulation products [8]

pattern of a main beam can be seen in Figure B.14. This figure demonstrates the 3-dimensional antenna pattern for a horn antenna and shows that most of the power is focused in the direction of the z-axis.

In contrast to the directional antennas, omni-directional antennas radiate equally in all directions. An example of omni-directional antenna is the dipole antenna.

For the purpose of this dissertation only the directional type of antennas will be analyzed, as that is the type of antenna that is required for an imaging radar application. Furthermore, the details of electromagnetic theory will be omitted, instead the properties that directly relate to the operational aspects of the antennas will be examined, namely:

- Frequency of Operation
- Half-Power Beamwidth
- Gain
- Aperture Efficiency
- Bi-static radar and Imaging Application Design Considerations

B.2.1 Frequency of Operation

As the signal that is produced at the transmitter is centered at a particular carrier frequency, the antenna must be designed so that it is capable to radiate efficiently

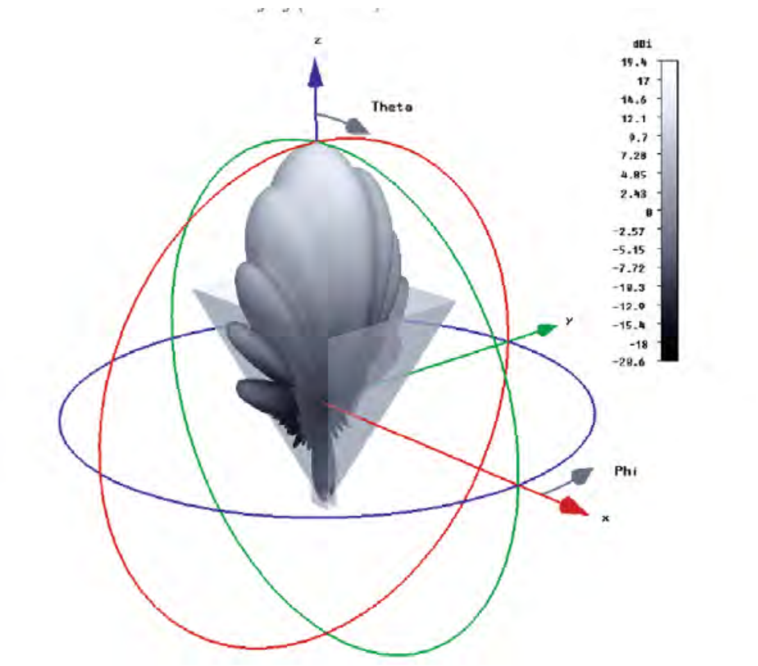

Figure B.13: 3D antenna pattern of a standard gain horn [5]

across the required signal bandwidth. The antenna bandwidth is the region where the key antenna parameters are within a desired range [26]. A parameter that is of particular interest, is the return loss, which is typically required to be below -10 dB. The -10 dB return loss implies that the power at that point is 90% of the maximum power of the main beam [26].

The bandwidth of the antenna can be represented by a percentage, where the upper and lower cut-off frequencies correspond to a region where the return loss is -10 dB. The expression for the antenna bandwidth is as follows:

$$BW_{ant} = \frac{f_U - f_L}{f_o} \times 100[\%], \tag{B.12}$$

where BW_{ant} is the antenna bandwidth, f_U and f_L is the upper and lower cut-off frequencies and f_o is computed as:

$$f_o = \frac{f_U - f_L}{2}. \tag{B.13}$$

B.2.2 Half-Power Beamwidth

In order to define the half-power beamwidth or 3-dB beamwidth, the antenna pattern must be examined. This is shown in Figure B.14, where a 2-dimensional representation of a typical antenna pattern is demonstrated. The antenna pattern consists of a main beam (main lobe) and additional minor lobes (side lobes), the half power beamwidth of the antenna is defined as the angle in degrees between the points on the left and right side of the main beam where the transmitted power is decreased by half of its peak value.

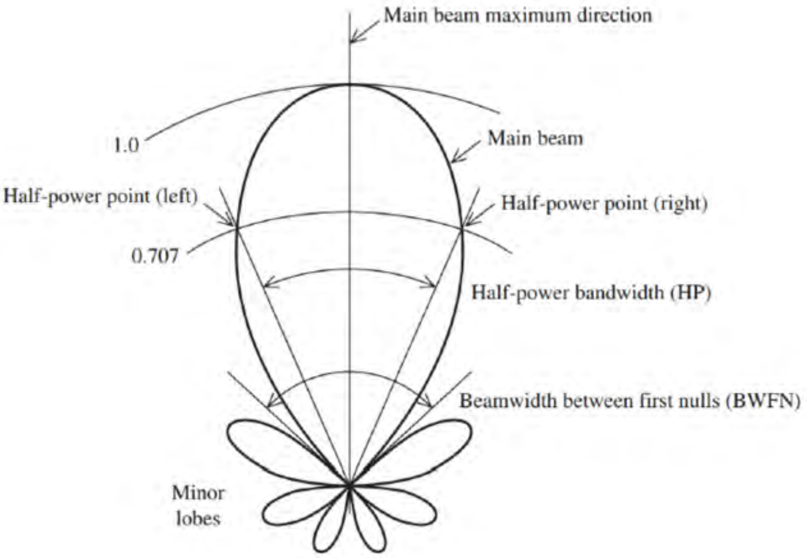

Figure B.14: Radiation pattern of a directional antenna indicating the left and right half-power points used to calculate the antenna beamwidth [36]

If one uses the decibel scale, the half-power beamwidth is called the 3-dB beamwidth, as a 3 decibel decrease in power level corresponds to decrease in power by a factor of 2.

Therefore, if the antenna is said to have a 3-dB beamwidth of 8 degrees, the power is reduced to half its maximum value 4 degrees to the left and right of the centre of the main lobe.

B.2.3 Gain

The gain of an antenna is defined as 4π times the ratio of maximum radiation intensity to the net input power into the antenna [26]. This can be expressed as:

$$G = \frac{4\pi U_{max}}{P_{max}}, \tag{B.14}$$

where U_{max} is the maximum radiation intensity and P_{max} is the antenna input power. A usefull approximation of this formula is found in [32] and can be used when the half-power beamwidth of the directional antenna are known:

$$G \simeq 10 \cdot log \left(\rho \frac{4\pi}{\Theta_H \Theta_E} \right), \tag{B.15}$$

where ρ is the antenna efficiency, Θ_H and Θ_E are the orthogonal half-power beamwidths corresponding to the magnetic and electric field planes [5].

Antenna efficiency is usually greater than 90% for the antennas that have a good impedance match. A good impedance match is responsible for efficient power transfer as is shown in [37], which in turn effect the antenna efficiency. Other factors, such as polarization mismatch with the receiver antenna can also effect the efficiency.

B.2.4 Aperture Efficiency

An antenna aperture largely determines the direction of propagation of the electromagnetic radiation in the antenna and is responsible for intercepting the incoming electromagnetic radiation when operating as a receiver. The effective cross-section of the antenna can be used to determine the antenna performance.

Aperture efficiency, which is the effective cross-section area of the antenna, is directly proportional to the gain of the antenna, therefore a higher gain will yield a larger effective aperture. The relationship between the two parameters is as follows:

$$A_{eff} = \frac{G\lambda^2}{4\pi}, \tag{B.16}$$

where G is measured in linear units and not decibels. This relationship was used in Section A.2 to explain the reason behind not employing an antenna with a small aperture to obtain a higher azimuth resolution in a SAR system, as the gain will also decrease and reduce the maximum range of the system.

B.3 Receiver

The receiver of a homodyne (direct conversion) type consists of a Low Noise Amplifier, a frequency mixer, an IF amplifier and a filter stage prior to the ADC that converts the analogue signal data into the digital domain for processing. The parameters that one should consider when specifying the receiver are:

- Noise Figure
- Receiver Sensitivity
- Dynamic Range
- ADC Sampling Frequency
- Storage Rate

B.3.1 Noise Figure

Noise figure is a measure of how much a given two-port device, such as an amplifier, degrades the signal-to-noise (SNR) of a given input signal. Sources of noise include thermal noise, shot noise and other effects due to the physics of various types of transistors, all of which are combined into the noise factor (F) [5].

The noise factor can be defined as the ratio between the SNR of the input signal(S_i/N_i) to the SNR of the output signal (S_o/N_o):

$$F = \frac{S_i/N_i}{S_o/N_o}. \tag{B.17}$$

The noise figure, which is the parameter that is typically used to characterize the noise associated with the LNA is equal to:

$$NF = 10 \times log_{10} F, \tag{B.18}$$

where NF is the noise figure in decibels [5].

To compute the noise figure for the receiver of the radar, one needs to consider the contributions of all the components in the chain and derive the cascaded noise figure.

The first element of the receiver is the LNA, which is designed to have a low noise figure. This is crucial, as it contributes the most to the overall noise figure of the receiver due to the fact that it is the first element of the receiver chain.

Other components in the receiver, apart from the IF amplifier, do not have a noise figure specification, instead their insertion loss parameter. As a result a receiver that consists of n elements will have the following cascaded noise figure [5]

$$NF_{sys} = 10 \times \left(F_1 + \frac{F_2 - 1}{G_1} + \frac{F_3 - 1}{G_1 G_2} + \frac{F_4 - 1}{G_1 G_2 G_3} ... \frac{F_n - 1}{G_1 G_2 G_3 ... G_{n-1}} \right), \tag{B.19}$$

where F_n is the noise factor and G_n is the gain of each stage of a receiver chain.

B.3.2 Receiver Sensitivity

Receiver sensitivity defines the weakest signal that can be detected by the radar setup. This is also known as the Minimum Detectable Signal (MDS) and is measured in dBm [13] [5]. The noise that is associated with the radar receiver essentially sets the limit on the MDS, as is shown by Equation B.20.

$$MDS = 10log_{10}\left(\frac{kT_0}{1mW}\right) + NF_{sys} + 10log(BW_{rec}) + SNR_{out}, \tag{B.20}$$

where k is the Boltzmann's constant (1.38×10^{-23} joules/Kelvin), BW_{rec} is the receiver bandwidth (Hz) and SNR_{out} is the minimum required SNR for detection.

B.3.3 Dynamic Range

The dynamic range of the receiver is defined as the ratio of the maximum signal that can be handled to the smallest signal capable of being detected. The smallest signal is the MDS as determined by the receiver noise and the maximum signal is that which causes a specified degree of intermodulation or a specified deviation from linearity of the output-vs.-input curve [13].

As was mentioned in Section B.1.3, an amplifier becomes saturated when the input power is higher than the difference between power at 1 dB compression and the amplifier gain (Equation B.11). When the amplifier is saturated the third-order intermodulation products can severely effect the signal at the output. Hence, the upper limited of the dynamic range can be said to be the input power level that is found just before the input amplifiers gain starts to compress.

Automatic gain control (AGC) can be used in a superheterodyne receiver to decrease the gain when strong signals can cause overload or distortion, although there may be trade-offs for the SNR performance [37].

B.3.4 ADC Sampling Frequency and Dynamic Range

The sampling frequency of the ADC essentially determines the frequency band that can be processed by the receiver. For example, if the sampling rate of the system is 125 Megasamples per second (Msps), then the highest frequency of a real signal that can be sampled is 62.5 MHz, according to the Nyquist sampling theorem.

Furthermore, the dynamic range of the ADC, which is defined to be the ratio of the rms value of the full scale to the rms noise. It indicates the range of signal amplitude that the ADC can resolve and can be calculated by using the following equation [38]:

$$DR = 6.021N + 1.763, \tag{B.21}$$

where N is the number of bits that the ADC uses to store the digitized analog signal.

B.3.5 System Storage Rate

If a radar system that is to be mounted on a small airborne platform is designed to operate on the “turn on and forget” basis, where the radar is switched on and the system records the data until the storage space is filled, the storage rate of the system can place a limitation on the other design parameters. This was the case in microASAR [4], where due to the high PRF, the amount of data that needed to be stored required a storage rate of 48 Mbytes/s. The hardware that was available to the designers was only capable of a storage rate of 5 MBytes/s. Hence, pre-summing of data that lead to a decrease in azimuth resolution had to be done.

One can calculate the required storage rate by considering the frequency range at the input to the ADC and doubling it in order to comply with the Nyquist sampling theorem, this will correspond to the number of samples per second that need to be stored.

$$\text{Sample Rate} = \text{Maximum Frequency} \times 2 \tag{B.22}$$

Then knowing that number of bits that the ADC uses to store the data, one can calculate the data rate in bits per second.

$$\text{Data Rate} = \text{Sample Rate} \times \text{Bits per Sample} \tag{B.23}$$

This corresponds to the storage rate that the system will require to store the incoming data.